

Regulation of Phosphoinositide 3-Kinase γ in Inflammation and Metabolism

Inauguraldissertation

Zur

Erlangung der Würde eines Doktors der Philosophie

vorgelegt der

Philosophisch-Naturwissenschaftlichen Fakultät

der Universität Basel

Von

Julie Ruili Jin

Basel, 2023

Genehmigt von der Philosophisch-Naturwissenschaftlichen Fakultät
auf Antrag von

Erstbetreuer: Prof. Matthias P. Wymann

Zweibetreuer: Prof. Gennaro De Libero

Externer Experte: Dr. Pius Lötscher

Basel, den 16.11.2021

Prof. Marcel Mayor
Dekan

Table of contents

1. Summary.....	4
2. Introduction.....	5
2.1. PI3Ks in clinical immunology.....	7
2.2. PI3K γ between inflammation and resolution.....	12
2.2.1. Leukocyte chemotaxis.....	12
2.2.2. Inflammatory mediator synthesis and release.....	14
2.2.3. T cell survival and maturation.....	16
2.3. PI3K γ structure and mode of activation.....	18
2.3.1. GPCR signaling and phospholipid generation.....	18
2.3.2. p110 γ as scaffolding protein.....	21
2.3.3. Non-redundant p84 and p101 adaptor subunits.....	22
3. Aims.....	24
4. References.....	26
5. Results	
5.1. Project 1: PI3K γ Regulatory Protein p84 Determines Mast Cell Sensitivity to Ras Inhibition – Moving towards Cell Specific PI3K Targeting?.....	32
5.2. Project 2: PI3K γ Adaptor Subunit p84 Controls Adipose Lipolysis and Hepatic Steatosis.....	57
5.3. Project 3: Targeting of PI3K γ Adaptor p101 Deteriorates Th2 Inflammation in Autoimmunity-Prone PI3K δ^{D910A} mice.....	95
6. Discussion and concluding remarks.....	119
7. Appendix.....	124
7.1. Protocols.....	124
7.2. Antibodies.....	143
7.3. Primers.....	145
7.4. Gene maps of transgenic mouse strains.....	150
7.5. Curriculum Vitae.....	156
8. Acknowledgments.....	159

1. Summary

Manipulation of Phosphoinositide 3-kinase γ (PI3K γ) attenuates inflammation, and ameliorates symptoms and progression of various inflammatory diseases. Activity of PI3K γ in leukocytes is determined by two regulatory proteins termed p84 and p101, but their detailed roles have only been rudimentarily studied yet. In the first study we investigated allergic inflammation characterized by IgE-mediated mast cell activation and the potential of Ras inhibitors to specifically attenuate p84-dependent PI3K γ activation. Pharmacologic Ras targeting using farnesyl-transferase inhibitors (FTIs), geranyl-geranyl-transferase inhibitors (GGTIs) and statins (inhibitors of 3-hydroxy-3-methyl-glutaryl-coenzyme A reductase) abolished p84-dependent mast cell outputs while p101-dependent macrophage activation remained unaffected. Therefore Ras inactivation could effectively inhibit mast cell -mediated allergic response without constraining monocyte and macrophage -dependent immunity in a cell culture-based model. However, current Ras inhibitors interfere with post-translational modification of many proteins and have pleiotropic effects on numerous critical signaling pathways, which disqualifies them as potential low side effect anti-allergic treatments.

Complementary to pharmacological inhibition, genetically modified mice devoid of p84 or p101 are powerful model systems to study the function of these signaling molecules in primary tissue, in bone marrow derived cultured cells and in live animal disease models. In the second study, a high fat diet (HFD) -dependent obesity model was used to provoke low-grade chronic inflammation leading to weight gain, hyperglycemia and hyperinsulinemia in p84^{-/-} and p101^{-/-} transgenic mice. p84 and p101- deficiency displayed distinct phenotypes from each other and from mice lacking p110 γ catalytical subunit of PI3K γ . p84 negatively regulates protein kinase A (PKA)-dependent hormone-sensitive lipase (HSL) activation but without net effect on body weight or fat mass. Despite adiposity p84^{-/-} animals are protected from hyperinsulinemia and

liver steatosis, proposing a change in insulin effects and/or in fatty acid flux from adipose compartment to liver. p101 null mice on HFD also become obese, yet they show improved fasting glucose and glycated hemoglobin (HbA1c) levels. p101 is responsible for chemokine-mediated signaling in myeloid leukocytes including macrophages. p101-dependent migration and activation of lymphocyte populations in white adipose tissue (WAT), and possibly other organs such as pancreas or liver, increase systemic glycemia, and accelerate the progression of adiposity-related type II diabetes. These findings disclose unexpected non-redundant roles of p84 and p101 in obesity and metabolic syndrome.

For the third project p84^{-/-}/p110δ^{D910A/D910A} and p101^{-/-}/p110δ^{D910A/D910A} double mutant mice were generated to study the consequences of disbalanced PI3Kγ and PI3Kδ signaling on innate and adaptive immunity. While p84^{-/-}/p110δ^{D910A/D910A} mice do not exert any gross anatomical or hematological phenotypes, p101^{-/-}/p110δ^{D910A/D910A} mice show thymus hypoplasia, impaired red and white zone differentiation of the spleen, neutrophilic and eosinophilic infiltrations in the gut mucosa, lymphopenia and eosinophilia, IgE class switch and Th2 cytokine elevation. The large discrepancy between p84^{-/-}/p110δ^{D910A/D910A} and p101^{-/-}/p110δ^{D910A/D910A} genotype implicates specific involvement of p101-dependent processes to maintain proper lymphocyte development and immune tolerance. On the other hand, blockage of the myeloid-restricted p84 subunit minimally impacts humoral immunity and preserves proper Th1/Th2 balance.

2. Introduction

Class I Phosphoinositide 3-kinases (PI3Ks) comprise four isoforms α,β,γ and δ. Although all PI3K family members catalyze the same reaction resulting in formation of the lipid messenger phosphatidylinositol(1,4,5)-trisphosphate (PtdIns(3,4,5)P3), the isoforms engage

highly contextual and distinctive functions in the immune system. Leukocytes express all four Class I PI3K isoforms, but PI3K γ and PI3K δ are more enriched in hematopoietic cells and thus have numerous immune-specific roles. The ubiquitous PI3K α and PI3K β provide basic cell functions such as survival, proliferation, migration and metabolism. As a consequence, systemic knockout mice for PI3K α and PI3K β are embryonically lethal, leaving their roles in immunology also underexplored. Transgenic mice lacking PI3K γ and PI3K δ or expressing a kinetically inactive mutated protein however are vital and show profound immunological abnormalities (1–5). Grouping into Class IA and IB is based on functional and structural characteristics and recognizes two definite modes of activation. The three protein tyrosine kinase-activated isoforms α , β and δ form the Class IA subfamily of PI3Ks. Their respective catalytic subunits p110 α , p110 β and p110 δ constitute heterodimeric complexes with a p85-like regulatory subunit (p85 α , p55 α , p50 α , p85 β or p55 γ). These regulatory proteins contain two Src homology 2 (SH2) domains that bind to phosphorylated tyrosine residues (pTyr-x-x-Met motifs) of activated receptor and non-receptor tyrosine kinases. SH2 domain engagement recruits the PI3K heterodimer to the plasma membrane and permits the p110 subunit to access and phosphorylate its substrate phosphatidylinositol(4,5)-bisphosphate (PtdIns(4,5)P₂) at the D3 position of the inositol ring (6, 7). PI3K γ is structurally distinct and the only member of Class IB PI3Ks. Its catalytic subunit p110 γ pairs with either p101 or p84 (also called p87) and integrates inputs from seven-transmembrane guanine nucleotide-binding protein (G protein)-coupled receptors (GPCRs) and small GTPases of the Ras family (8–10). This plausibly positions PI3K γ downstream of many G α i-coupled chemokine receptors and accounts for its prominent role in leukocyte chemotaxis. Furthermore, PI3K γ can be activated by PKC β upon stimulation of the high affinity IgE receptor, Fc ϵ RI on mast cells (11).

2.1. Class I PI3Ks in clinical immunology

The importance of Class IA PI3Ks and especially PI3K δ for adaptive immunity is manifested in a group of primary immunodeficiencies termed activated PI3K δ syndrome (APDS), also called p110 δ -activating mutation causing senescent T cells, lymphadenopathy and immunodeficiency (PASLI). Heterozygous gain-of-function mutations in the kinase domain of the catalytic p110 δ subunit or the p85 adaptor protein cause APDS. Importantly, homozygous loss-of-function mutations in the same genomic loci also instigate immunodeficiency, demonstrating that both overshooting as well as insufficient PI3K δ signaling leads to defects in the regulation of adaptive immune reactions. The human symptoms of APDS and homozygous loss-of p110 δ are variable and disease severity is gradual. A frequent clinical feature is immunoglobulin (Ig) deficiency (agammaglobulinemia) that manifests in recurrent chest infections due to defective B cell development and antibody production. Besides, patients often experience recurrent infections with herpes family viruses as a consequence of poor T cell and natural killer (NK) cell function. Etiology of irritable bowel syndrome in these patients is not completely understood and could result from both outgrowth of gut bacteria due to antibody deficiency or lack of T regulatory (Treg) cell activity to maintain tolerance towards normal microbiome (12). Of note, Cowden syndrome, also known as PTEN hamartoma tumor syndrome is frequently associated with immunological pathologies. PTEN dephosphorylates the PI3K product PtdIns(3,4,5)P3 at the D3 position, thus a PTEN loss-of-function mutation is equivalent to PI3K overactivation. In the report of Heindl and colleagues 43% of Cowden patients displayed immunological abnormalities, including autoimmunity, lymphoid and thymus hyperplasia, lymphopenia and reduced CD4/CD8 ratio (13).

Despite discrepancies between human and murine phenotypes (e.g. partial redundancy of PI3K α and δ in mouse but not human B cells) (12), it is now widely recognized that in man

and mouse PI3K δ is activated by CD19 co-receptor upon B cell receptor (BCR) stimulation, and is required for T cell independent antibody responses (14). Unrestrained PI3K δ signaling (e.g. loss of PTEN or mutant p85) furthermore interferes with activation-induced cytidine aminase (AID)- dependent immunoglobulin class switching and affinity maturation (14). T cell clonal expansion and differentiation is delayed upon PI3K δ inhibition in mice, which has consequences on T cell help for antibody production. PI3K δ is also required for regulatory T cells (Tregs) to maintain self- and microbiome tolerance. A presumable consequence of insufficient effector T cell suppression by Tregs is a susceptibility to autoimmune colitis in PI3K δ -deficient mice as well as in patients treated with PI3K δ - inhibitor Idelalisib (15–17).

Figure 1. Class I PI3K signaling in the immune system

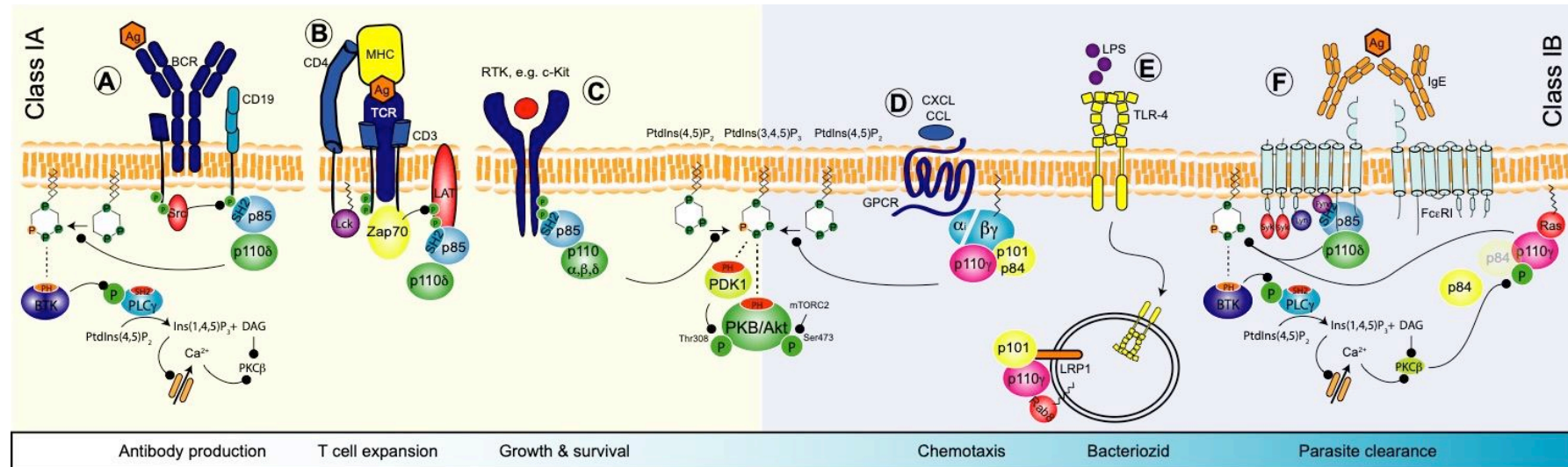


Figure 1. Class I PI3K signaling in immune cells. (A) BCR activation leads to CD19 co-receptor phosphorylation and recruitment of Class IA PI3Ks via SH2 domain interactions. Subsequently, p85 releases inhibitory action on catalytic p110 subunit and allows transformation of PtdIns(4,5)P₂ to PtdIns(3,4,5)P₃. (B) TCR-induced PI3K δ engagement is not fully clarified, though the process involves ZAP70 phosphorylating LAT. Accumulation of submembranous PtdIns(3,4,5)P₃ activates PH-domain containing Tec family enzymes such as BTK. This promotes hydrolysis of PtdIns(4,5)P₂ by PLC γ to form Ins(1,4,5)P₃ and DAG, both fueling intracellular calcium mobilization for signalosome formation in lymphocytes. (C) Growth factor receptors such as SCF receptor c-kit are receptor tyrosine kinases possess auto-phosphorylation capacity and intracellular SH2 domains to recruit PI3K. Local PtdIns(3,4,5)P₃ production further recruits Akt/PKB, which is modified at the T308 and S473 phosphorylation sites by PDK-1 and TORC2 respectively. (D) GPCR stimulation in many leukocyte types engages Class IB PI3K γ isoform through dissociation of the G $\beta\gamma$ subunit. (E) In phagocytic cells like macrophages, vesicle localized TLR signaling phosphorylates LRP1 and recruits Rab8 which binds and activates p101/p110 γ . (F) Crosslinking of mast cell IgE receptors Fc ϵ RI is able to mount PI3K δ -dependent calcium mobilization but requires PI3K γ for sustained signaling due to forward feeding loop involving calcium-dependent PKC β activating p110 γ .

PI3K γ is abundantly expressed in hematopoietic cells of the myeloid and lymphoid lineage (9, 18), and has been found in lower abundance in cardiomyocytes (19) and endothelial cells (20). In the last 20 years, transgenic mouse models lacking functional p110 γ considerably promoted the recognition of PI3K γ signaling as regulator of cell survival, motility and chemotaxis, as well as synthesis and release of inflammatory mediators (21–23). But only recently, the human inactivated PI3K γ syndrome (IPGS) following PI3K γ loss-of function mutation has been documented and provided valuable insight into PI3K γ -related inflammation and promotion of adaptive immunity in clinical disease (24, 25). Patient features such as antibody deficiency, lymphopenia, low Treg frequency and excessive myeloid activation were unexpected in light of previous murine models of PI3K γ deletion. However, the human phenotype could be partly reproduced in animals exposed to normal microbiota by co-housing with pet-store mice, accentuating the context dependent significance of PI3K γ signaling in healthy and aberrant immunity (24).

The first clinically approved PI3K drug Idealalisib (Zydelig, Cal101/GS1101) was a δ -selective inhibitor and entered the market in 2014 as second and third line treatment respectively for certain B cell leukemias and lymphomas. The PI3K $\gamma\delta$ dual inhibitor Duvelisib (IPI-145, Copiktra) obtained approval in 2018 and the most recent PI3K δ -targeting Umbralisib (TGR-1202) followed in 2020, both for hematological malignancies as well. To date, no PI3K γ or δ selective drugs have been authorized for non-oncological indications, although trials in airway inflammation (Asthma, COPD) and other inflammatory disorders (Sjörgeren syndrome) were initiated by several companies (26). High doses of PI3K δ inhibitors as cancer treatment are accompanied by significant side-effects that histologically resemble colitis and inflammatory bowel syndrome in PI3K δ kinase-inactive D910A mouse models, supporting

categorization as immune-related mechanism-based toxicity rather than general off-target effects. Due to their ubiquitous expression, all inhibitors diminishing PI3K α and β activity could also potentially exert immune-modulatory effects to some degree. Interestingly, when used against solid cancers, some PI3K α and pan-PI3K inhibitors seem to enhance immune-versus tumor responses, probably by modulating T cell infiltration, angiogenesis, cancer cell glucose metabolism and increasing nutrient availability to surrounding stroma and immune cells (26). The rationale behind PI3K γ inhibition in solid malignancies though is routed in mitigation of myeloid restraint on cytotoxic CD8 T cells to boost immune versus tumor reaction. The value of PI3K γ blockage in cancer therapy is subject of current clinical trials with IPI-549 (Eganelisib) and those outcomes might open new perspectives for use in non-malignant immune disorders as well (27, 28).

2.2. PI3K γ between inflammation and resolution

Successful host defense begins with adequate recognition of harmful pathogens and has to be succeeded by efficient removal of the threat by the innate and adaptive immune system. In order to prevent overshooting and long-lasting responses, resolution and healing mechanisms will normally limit destructive reactions against the self-tissues. In autoimmune and chronic inflammatory diseases one or several stages of this sensitive sequence are altered. PI3K γ has been recognized as a promising drug target against inappropriate inflammation because of its central role in leukocyte recruitment and activation. The following sections will dissect discoveries made in human and animal immune cells and the numerous murine disease models addressing the potential of PI3K γ inhibition to resolve inflammatory conditions.

2.2.1. Leukocyte chemotaxis

The physiological relevance of PI3K γ in chemotaxis was first discovered in isolated human and mouse neutrophilic granulocytes and mouse macrophages where PI3K γ mediates migration towards RANTES, MIP-5, SDF-1, C5a, fMLP and IL-8. Indicative for a role in chemotaxis, unchallenged transgenic mice lacking p110 γ catalytic subunit retain elevated numbers of neutrophils in the blood due to a defect in transmigration from circulation into peripheral tissues (29–31). Later, T cell migration (but not B cell homing) towards chemokines CCL-19, CCL-20, CCL-22 and CXCL-12 have also been shown to rely on PI3K γ (32, 33). Although motility of healthy B cells remain unaffected by p110 γ knockout, it has been reported that malignantly transformed leukemic cells become sensitive to PI3K γ blockage (34).

PI3K signaling is involved in several stages of the immune cell transmigration process from blood vessel lumen to site of inflammation. PI3K γ is thereby implicated in leukocyte migration as well as activation of the vascular endothelium. Capture of free floating blood

leukocytes via E-selectins as well as integrin-mediated firm attachment and subsequent extravasation involve PI3K γ and δ isoforms (35). Local PtdIns(3,4,5)P3 formation and F-actin accumulation at the leading edge of cells migrating towards the chemokine gradient correlate with directional movement. Correspondingly, instillation of MIP-2 and KC chemoattractants into mouse airways provoked neutrophil accumulation in a PI3K γ -dependent fashion (36). Furthermore, PI3K γ facilitates undirected motility or chemokinesis and acts as signal amplifier during chemokine gradient sensing of primed neutrophils (37).

Several mouse models confirm the chemotactic role of PI3K γ in inflammatory disease: In collagen-induced rheumatoid arthritis as well as joint inflammation caused by transgenic expression of TNF- α , p110 γ promotes accumulation of neutrophils in the synovia that damage cartilage and lead to destruction of the joint (38, 39). In a model of aseptic peritonitis p110 γ is required for neutrophil influx into the peritoneal cavity upon i.p. injection of thioglycolate (29). Neutrophil recruitment is furthermore reduced in murine cerulein-induced acute pancreatitis (40). Dextran sulfate sodium (DSS)-colitis is also attenuated in p110 γ ^{-/-} mice because they fail to recruit new leukocytes to the intestinal mucosa (41).

Relevant for IgE-dependent type I hypersensitivity, p110 γ -dependent mast cell rolling on TNF- α -activated blood vessels has been visualized by intra-vital microscopy (11). In ovalbumin (OVA)-induced pulmonary inflammation eosinophilic, neutrophilic and macrophage invasion are blocked upon genetic deletion of p110 γ (42). Another OVA-induced asthma trial found decreased lymphocyte and eosinophil numbers in broncho-alveolar lavage fluid of p110 γ -deficient mice. (43). In a model of contact dermatitis and delayed-type hypersensitivity dendritic cells (DC) lacking p110 γ fail to migrate from skin into the draining lymph node (44). The enhanced priming and survival of auto-reactive T cells in experimental

autoimmune encephalomyelitis (EAE) have also partly been attributed to reduced DC migration in p110 γ ^{-/-} mice during the immunization phase with central nervous antigens (45).

Arteriosclerotic plaque formation requires invasion of monocytes that transform into lipid-loaded macrophages termed foam cells. p110 γ ^{-/-} mice crossed to apo-lipoprotein E negative (ApoE^{-/-}) background show reduced foam cell activity inside plaques (46). Correspondingly, when p110 γ ^{-/-} bone marrow is transplanted into low density lipoprotein receptor deficient (LDLR^{-/-}) recipients, the arteriosclerotic lesions also contain fewer macrophages and T cells, suggesting that indeed p110 γ activity in leukocytes rather than the endothelium governs recruitment of cells from the circulation into the plaque (47).

Macrophages and neutrophils infiltrate expanding WAT in high fat diet (HFD) fed mice. There is evidence that neutrophils provide environmental factors to the WAT that direct macrophage polarization and promote insulin resistance, and that blockage of neutrophil recruitment in p110 γ ^{-/-} mice thus contributes to metabolic derailment in obesity (48).

2.2.2. Inflammatory mediator synthesis and release

Generation of reactive oxygen species (ROS) is a crucial ability of phagocytes that enables them to inactivate and digest engulfed pathogens. ROS formation is catalyzed by nicotinamide adenine dinucleotide phosphate (NADPH) oxidase in neutrophils and macrophages. Activation of formylmethionine-leucyl-phenylalanine (fMLP) receptor leads to PtdIns(3,4,5)P₃-dependent engagement of Rac and induces formation of an active NADPH oxidase complex, a process highly susceptible to p110 γ inhibition (29, 30, 49). ROS are also involved in vessel contractility in the context of hypertensive disease. Besides controlling L-type calcium channel current, PI3K γ also couples to angiotensin II receptors and activates Rac to stimulate NADPH oxidase in smooth muscle cells (50, 51).

Blood monocytes and their derivative tissue macrophages generate substantial cytokine amounts to communicate with local and systemic environment. In widely accepted cell culture models, stimulation with lipopolysaccharide (LPS) and Interferone γ (INF- γ) polarize macrophages towards a pro-inflammatory, so called M1 phenotype while IL-4 and IL-13 are classical inducers of anti-inflammatory M2 macrophages. LPS is a ligand for Toll-like receptor 4 (TLR-4) which is typically localized in the plasma membrane. However, PI3K γ is engaged in TLR signaling in endocytosed macropinosomes via the small GTPase Rab8 to bias M1/M2 cytokine expression profile in favor of anti-inflammatory IL-10 while lowering pro-inflammatory IL-6 and IL-12 (52). In tumor-associated myeloid cells an analogous bias towards M1 pro-inflammatory signature in p110 γ ^{-/-} genotype relieved tumor-protective signals and unleashed cytotoxic CD8⁺ T cell action (27). Likewise, in laboratory mice exposed to normal microbiota the lack of p110 γ led to over-activation of myeloid cell responses but blunted adaptive immunity (24). The details of macrophage polarization and cytokine profile skewing seem to be highly context dependent as other disease models propose a pro-inflammatory role of p110 γ . For instance, defective pro-inflammatory cytokine expression and therefore ineffective pathogen clearance and a deficit in IL-10 (and possibly other inflammation resolving factors) are likely responsible for susceptibility to lethal H1N1 influenza infection, even though the receptor/ligand relationship to PI3K γ has not yet been identified for viral infections (53). Adding more controversy, in subclinical metabolic inflammation adipose tissue macrophages (ATMs) are the dominant immune cell type in WAT. Still, the cytokine profile in epididymal fat of p110 γ ^{-/-} is biased towards decreased TNF- α and IL-6 levels (54). These findings were later confirmed in ob/ob mice that also shifted towards M2 biased macrophage polarization with increased Arginase-1 and low TNF- α expression (48). Also when p110 γ -deficient platelets were transferred to wild-type mice with ligated carotid vessels to mimic severe arteriosclerosis, cytokine expression in the lesion

showed reduced TNF- α and IL-6 (55). These discrepancies between disease milieus call for more clear-cut investigations of macrophage intrinsic PI3K γ -effects and environmental factors, e.g. neutrophil and stroma derived signals that secondarily bias macrophage polarization. Still, these examples undermine that context appropriate PI3K γ signaling is necessary to balance pathogen clearance, tumor immunity and resolution of inflammation.

Mast cell granules contain a plethora of preformed compounds including histamine, tryptase, chymase, heparin, β -hexosamidase, serotonin, TNF- α and more. Furthermore, de-novo synthesis of thromboxane, prostaglandins, platelet-activating factor, chemokines, cytokines and ROS among others can be stimulated upon high affinity IgE receptor (Fc ϵ RI) and GPCR engagement. Crosslinking of mast cell surface Fc ϵ RI for granule release requires PtdIns(3,4,5)P3 formation at the plasma membrane to recruit PH-domain containing Bruton's tyrosine kinase (BTK). BTK stimulates the degradation of PtdIns(4,5)P2 by PLC γ into Ins(1,4,5)P3 and diacylglycerol (DAG), both of which collectively stimulate rise of intracellular calcium. Calcium-dependent protein kinase C β (PKC β) phosphorylates and activates p110 γ , which demonstrates that the PI3K γ isoform is a critical source of PtdIns(3,4,5)P3 downstream of Fc ϵ RI (11). Autocrine/paracrine signaling by GPCR ligands such as adenosine and A3 adenosine receptor agonist IB-MECA, can potentiate degranulation capacity and de-novo mediator synthesis. As a consequence, p110 γ ^{-/-} mice are protected from systemic anaphylaxis and cutaneous edema formation upon IgE exposure (56).

2.2.3. T cell survival and maturation

The thymus of PI3K γ null mice is hypomorph with increased proportion of CD4⁻CD8⁻ double negative (DN) cells. Differentiation is halted in CD44⁻ CD25⁺ DN3 leading to

accumulation of incompletely matured thymocytes while total thymus cellularity is reduced by one third. Increased susceptibility to adenosine mediated apoptosis in $p110\gamma^{-/-}$ mice proposed A2A receptor coupling to $PI3K\gamma$ as a mechanism for increased cell death in neonatal thymus (30). Additional to its role in pre-TCR-dependent thymic survival and growth, $PI3K\gamma$ also regulates emigration of mature thymocytes to the periphery. Furthermore Class IA and IB $PI3K$ s seem to play complementary roles determining CD4/CD8 ratio, with Class IA overactivation favoring CD4 and $p110\gamma$ knockout favoring CD8 differentiation (57). While inactivation of $PI3K\delta$ leaves thymocyte maturation intact, combined $PI3K\gamma$ and $PI3K\delta$ deletion drastically reduces thymus cellularity by 27-fold (58, 59). Importance of the δ isoform for preTCR signaling added on the role of $PI3K\gamma$ for CXCR4/CXCL12 signaling during β -selection collectively account for disastrous failure of thymocyte development in $PI3K\gamma\delta$ double deficient mice (60). Such extreme lymphopenic conditions provoke homeostatic expansion of the remaining lymphocytes to countervail peripheral T cell deficiency. However, this compensatory mechanism is associated with autoimmunity due to limited TCR repertoire of Tregs and insufficient control of self-reactive effector T cells (59).

2.3. PI3K γ structure and mode of activation

2.3.1. GPCR signaling and phospholipid generation

Within the large family of PI3Ks, the γ isoform is categorized as Class 1B PI3K based on its activation by heterotrimeric G proteins. PI3K γ is composed of a catalytically active subunit, termed p110 γ , that dimerizes with a regulatory protein which can be either p84 or p101. p110 γ /p84 and p110 γ /p101 respectively forms the functional PI3K γ complex that catalyze the transformation of PtdIns(4,5)P₂ to PtdIns(3,4,5)P₃.

The canonical activation sequence of PI3K γ begins with extracellular ligand engagement of a transmembrane GPCR followed by submembranous dissociation of the G α i and G β γ subunits. p110 γ as well as p84 and p101 adaptor proteins contain G β γ -binding domains. The adaptor proteins direct localization of p110 γ in the cytosol and sub-membranous space, and sensitize the kinase to G β γ stimulation (61, 62). In vitro, p110 γ alone is able to engage with G β γ , however p101 and p84 stabilize G β γ binding and substantially potentiate PtdIns(3,4,5)P₃ generation. Although this effect has been demonstrated for both adaptors, p101 is the significantly more potent enhancer of G β γ -mediated p110 γ activation (9, 10, 63).

Since G β γ engagement is insufficient to fully stimulate p84/p110 γ , additional presence of GTP-loaded small GTPase Ras is required for maximal p84-mediated PI3K γ action (64). p101/p110 γ however is insensitive to disruption of Ras function. This important distinction between the two PI3K γ complexes provides an entry point for adaptor specific manipulation of PI3K γ activity via Ras targeting (65).

p101 and p84 interact with the helical domain of p110 γ (66). Phosphorylation of certain serine residues in the helical domain are able to dissociate adaptor binding and decouple PI3K γ from

GPCR stimulation. This not only emphasizes the functional importance of the helical domain to stabilize G β γ interaction but also demonstrates a cellular regulatory mechanism using adaptor proteins as molecular switches to associate PI3K γ signaling either to GPCR input or protein kinase activity (67).

Activated PI3K γ phosphorylates PtdIns(4,5)P₂ to rapidly and transiently form a local pool of PtdIns(3,4,5)P₃. The spatiotemporal localization and degradation dynamics of PtdIns(3,4,5)P₃ is determined by the adaptor protein. p84/p110 γ derived PtdIns(3,4,5)P₃ is found in distinct cholesterol-rich microdomains of the cell membrane called lipid rafts. p101/p110 γ derived PtdIns(3,4,5)P₃ is formed at the plasma membrane as well, but within 120 seconds forms speckles in the cytoplasm (68). The classical route to degrade membrane associated PtdIns(3,4,5)P₃ involves phosphatases such as PTEN or SH2 containing inositol 5-phosphatase (SHIP). The speckles seen with p101/p110 γ derived PtdIns(3,4,5)P₃ could represent an alternative PtdIns(3,4,5)P₃ elimination pathway via endocytosis into microtubule-associated vesicles. Yet, recent work indicates that PtdIns(3,4,5)P₃ formation by receptor-tyrosine kinase activated PI3K α is localized on endomembranes of microtubule-associated vesicles and activates endosomal rather than membrane localized PKB (69). A similar spatial-temporal organization is conceivable for GPCR-mediated PI3K activation, but has not been experimentally proven so far.

Timing and localization of PtdIns(3,4,5)P₃ formation and degradation translates into differences in cellular outputs. In general, the increase of the PtdIns(3,4,5)P₃ gradient at the plasma membrane recruits effector molecules containing a pleckstring-homology (PH)-domain, such as protein kinase B (PKB, Akt), Protein-dependent kinase 1 (PDK1), Bruton's tyrosine kinase (BTK), Interleukin-2 inducible T cell kinase (ITK) and various guanine exchange factors (GEFs) and GTPase activating proteins (GAPs) for small GTPases.

Recently, PI3K γ has been reported to bias PKB and mTor activation downstream of TLRs (52, 70). Luo et al. describe interaction of p101/p110 γ with the GTPase Rab8a inside of macropinosomes. Rab8a can be activated by low-density lipoprotein-receptor-related protein 1 (LRP1). In macrophages TLR-stimulation phosphorylates and activates LRP1, which provides a previously unrecognized mechanistic link between TLR signaling and PI3K γ -mediated PKB activation (52). In contrast to GPCR-dependent PI3K γ immune cell activation, the effects of TLR-dependent PI3K γ involvement seem to rather suppress macrophage pro-inflammatory cytokine production.

Figure 2. PI3K γ complexes can be composed with p84 or p101 adaptor protein

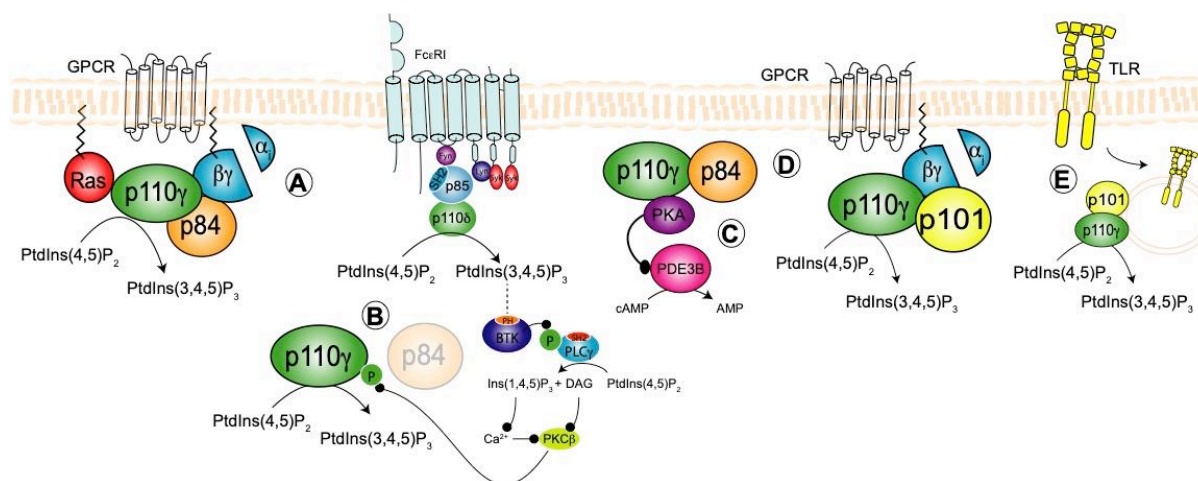


Figure 2. Activation of p84/p110 γ and p101/p110 γ heterodimers. (A) p84/p110 γ pairing requires activated GTP-loaded Ras for full functionality downstream GPCR stimulation, for instance during neutrophil oxidative burst or mast cell migration. **(B)** Fc ϵ RI crosslinking on mast cells induces calcium-dependent PKC β activation and phosphorylation of p110 γ . This induces dissociation of p84 adaptor and PtdIns(3,4,5)P₃ production. **(C)** A scaffolding structure containing p84, p110 γ , PKA and PDE3B and facilitates degradation of cAMP in cardiomyocytes to regulate contractility. **(D)** p101/p110 γ is activated by G-protein $\gamma\beta$ subunit independent from Ras involvement. p101 is best documented for its role in leukocyte migration towards chemokine gradients. **(E)** An additional activation mode downstream TLR-4 and Rab8 links p101 to macrophage cytokine production.

2.3.2. PI3K γ as scaffolding protein

The double identity of p110 γ as lipid kinase and scaffolding protein was first documented in cardiomyocytes in 2004 by Patrucco et al. (71). This important research was facilitated by the generation of transgenic mice harboring a targeted mutation that blunts the kinase activity of p110 γ (PI3K γ KI, kinase-inactive, K833R mutation) but still allows a full-length protein to be expressed. Only knockout cardiomyocytes but not PI3K γ KI mutants presented elevated levels of cyclic adenosinmonophosphate (cAMP) and increased contractility. It became evident that the p110 γ scaffold and not PtdIns(3,4,5)P3 generation was responsible for interaction with phosphodiesterase (PDE) 3B to degrade cAMP (21, 72).

p84 adaptor protein has been detected in healthy cardiomyocytes and was proposed to interact with PDE3B in conjunction with p110 γ to regulate cAMP levels (19). A later report described a direct negative feedback by PKA phosphorylating p110 γ blunting PI3K γ derived PtdIns(3,4,5)P3 (73). The authors concluded that under physiological conditions, PI3K γ has a minute signaling role, but primarily serves as docking site for PDE3B and PKA switch. Intriguingly, the same study discovered that cardiac p101 and p110 γ are upregulated during heart failure. High expression of p101/p110 γ leads to internalization of β -adrenoreceptors (β AR) in chronically pressured myocardium and decreases contractility. cAMP-mediated cardiac damage was coupled to generation of PtdIns(3,4,5) and could be restored by pharmacologic PI3K γ inhibition as well as KI mutation. Thus the scaffold function of p110 γ in healthy heart is substituted by lipid kinase activity in diseased myocardium (21, 72, 74).

In obesity, bone marrow transplantation experiments revealed that non-hematopoietic p110 γ is responsible for maintenance of lean body weight and therefore p110 γ -deficient mice preserve leanness when fed with HFD. Presence of p110 γ protein rather than PtdIns(3,4,5)P3

production restrains adaptive thermogenesis via cAMP-dependent lipolysis. In accordance with PDE3B-p110 γ association in cardiomyocytes, p110 γ -facilitated cAMP degradation has been postulated as underlying mechanism of kinase-independent action of p110 γ in body weight control (54).

2.3.3. Non-redundant p84 and p101 adaptor proteins

Although the function of the catalytic subunit p110 γ is well documented, only few studies so far have investigated the relevance of p101 and p84 adaptor proteins. As p101 and p84 are not equally distributed across tissues and cell types containing p110 γ , non-overlapping results from p101/p110 γ and p84/p110 γ manipulation are anticipated. Most cells of the myeloid lineage including macrophages and neutrophilic granulocytes express both p101 and p84 (65, 75, 76). Mast cells however, exclusively contain p84/p110 γ (10, 65, 68).

Lymphocyte-rich tissues such as thymus, spleen and lymph node predominantly express p101/p110 γ (60, 68, 77). Inhomogeneous tissue distribution will expectably have consequences on cellular networks of innate and adaptive immunity in health and disease. Still, the only *in vivo* demonstrations of adaptor protein function was attenuation of thioglycolate-induced sterile peritonitis in p101^{-/-} mice (75), and attenuation of peritonitis and ear-pouch inflammation in mice with disrupted G $\beta\gamma$ -p101 interaction (76).

Complementation experiments that introduced either p101/p110 γ or p84/p110 γ into PI3K γ null mast cells showed that both complexes are able to induce phosphorylation of PKB and cell migration towards chemokine gradients. However, mast cell degranulation was only enabled in cells expressing p84/p110 γ . These findings led to the conclusion, that cellular responses are not only dependent on PtdIns(3,4,5)P3 generation but that fine-tuned spatiotemporal control of the PtdIns(3,4,5)P3 pools have further consequences on downstream signaling. Degranulation

seems to require highly concentrated increases of PtdIns(3,4,5)P3 in lipid rafts while threshold concentrations to promote chemotaxis are less limited to distinct membrane compartments (68). More evidence that PtdIns(3,4,5)P3 derived from p101/p110 γ and p84/p110 γ exert separate cellular functions came from p101- and p84- deficient neutrophils (75). Chemoattractant-induced phosphorylation of PKB was blunted in the absence of either one adaptor protein, similarly to p110 γ null neutrophils. But cell migration was only reliant on p101/p110 γ , while p84/p110 γ was required for formation of reactive oxygen species (ROS).

3. Aims

The central theme of this thesis is to highlight differential regulation of PI3K γ action by p84 and p101 using novel transgenic mouse lines. Three projects were carried out to investigate the functional relevance of p84/p110 γ and p101/p110 γ pairings in immune and metabolic disorders:

The first project is a proof-of concept study to test the feasibility of mast cell specific PI3K γ inhibition by targeting small GTPase Ras. We cultured bone marrow derived mast cells (BMMC) and macrophages (BMDM) as model systems to investigate the FTI, GGTI and statin action on PI3K γ signaling. Since mast cells are a unique cell type that exclusively relies on p84/p110 γ dimer for degranulation and chemotaxis, p84 inhibition could be valuable in the treatment of mast cell-dependent type I hypersensitivity reactions. In the context of chronic conditions such as allergy, inhibition of mast cells without affecting p101-dependent macrophage functions in host defense is critical for treatment safety and long-term tolerability.

The second project aims to deconvolute the physiological role of PI3K γ regulatory proteins in glucose and lipid metabolism. Metabolic syndrome is a serious medical condition that connects PI3K γ -dependent thermogenesis and immune cell activation causing chronic low grade inflammation. Deciphering the energy balance and immunological aspects of obesity and type II diabetes is elemental for the understanding of the disease and acceleration of therapies targeted towards caloric expenditure and/or inflammation. This work presents the first *in vivo* demonstration of p84 and p101 action in a murine obesity model.

The third project documents non-redundancy of p84 and p101 in systemic regulation of adaptive immunity. An autoinflammation prone mouse line carrying kinase-inactive PI3K δ mutation (D910A) was crossed with mice lacking either p84 or p101. Side by side comparison

of p84^{-/-}/p110 δ ^{D910A/D910A} and p101^{-/-}/p110 δ ^{D910A/D910A} mouse lines aimed to identify possible myeloid contributions to lymphoid organ development, cytokine profile and antibody production.

4. References

1. Wymann, M. P., S. Sozzani, F. Altruda, A. Mantovani, and E. Hirsch. 2000. Lipids on the move: phosphoinositide 3-kinases in leukocyte function. *Immunol Today* 21: 260-264.
2. Okkenhaug, K., and B. Vanhaesebroeck. 2003. PI3K-signalling in B- and T-cells: insights from gene-targeted mice. *Biochem Soc Trans* 31: 270-274.
3. Hawkins, P. T., and L. R. Stephens. 2015. PI3K signalling in inflammation. *Biochim Biophys Acta* 1851: 882-897.
4. Vanhaesebroeck, B., L. Stephens, and P. Hawkins. 2012. PI3K signalling: the path to discovery and understanding. *Nat Rev Mol Cell Biol* 13: 195-203.
5. Fruman, D. A., H. Chiu, B. D. Hopkins, S. Bagrodia, L. C. Cantley, and R. T. Abraham. 2017. The PI3K Pathway in Human Disease. *Cell* 170: 605-635.
6. Whitman, M., C. P. Downes, M. Keeler, T. Keller, and L. Cantley. 1988. Type I phosphatidylinositol kinase makes a novel inositol phospholipid, phosphatidylinositol-3-phosphate. *Nature* 332: 644-646.
7. Stephens, L. R., T. R. Jackson, and P. T. Hawkins. 1993. Agonist-stimulated synthesis of phosphatidylinositol(3,4,5)-trisphosphate: a new intracellular signalling system. *Biochim Biophys Acta* 1179: 27-75.
8. Stoyanov, B., S. Volinia, T. Hanck, I. Rubio, M. Loubtchenkov, D. Malek, S. Stoyanova, B. Vanhaesebroeck, R. Dhand, and B. Nürnberg. 1995. Cloning and characterization of a G protein-activated human phosphoinositide-3 kinase. *Science* 269: 690-693.
9. Stephens, L. R., A. Eguinoa, H. Erdjument-Bromage, M. Lui, F. Cooke, J. Coadwell, A. S. Smrcka, M. Thelen, K. Cadwallader, P. Tempst, and P. T. Hawkins. 1997. The G beta gamma sensitivity of a PI3K is dependent upon a tightly associated adaptor, p101. *Cell* 89: 105-114.
10. Suire, S., J. Coadwell, G. J. Ferguson, K. Davidson, P. Hawkins, and L. Stephens. 2005. p84, a new Gbetagamma-activated regulatory subunit of the type IB phosphoinositide 3-kinase p110gamma. *Curr Biol* 15: 566-570.
11. Collmann, E., T. Bohnacker, R. Marone, J. Dawson, M. Rehberg, R. Stringer, F. Krombach, C. Burkhardt, E. Hirsch, G. J. Hollingworth, M. Thomas, and M. P. Wymann. 2013. Transient targeting of phosphoinositide 3-kinase acts as a roadblock in mast cells' route to allergy. *J Allergy Clin Immunol* 132: 959-968.
12. Lucas, C. L., A. Chandra, S. Nejentsev, A. M. Condliffe, and K. Okkenhaug. 2016. PI3K δ and primary immunodeficiencies. *Nat Rev Immunol* 16: 702-714.
13. Heindl, M., N. Händel, J. Ngeow, J. Kionke, C. Wittekind, M. Kamprad, A. Rensing-Ehl, S. Ehl, J. Reifenberger, C. Loddenkemper, J. Maul, A. Hoffmeister, S. Aretz, W. Kiess, C. Eng, and H. H. Uhlig. 2012. Autoimmunity, intestinal lymphoid hyperplasia, and defects in mucosal B-cell homeostasis in patients with PTEN hamartoma tumor syndrome. *Gastroenterology* 142: 1093-1096.e6.
14. Omori, S. A., M. H. Cato, A. Anzelon-Mills, K. D. Puri, M. Shapiro-Shelef, K. Calame, and R. C. Rickert. 2006. Regulation of class-switch recombination and plasma cell differentiation by phosphatidylinositol 3-kinase signaling. *Immunity* 25: 545-557.
15. Okkenhaug, K., A. Bilancio, G. Farjot, H. Priddle, S. Sancho, E. Peskett, W. Pearce, S. E. Meek, A. Salpekar, M. D. Waterfield, A. J. Smith, and B. Vanhaesebroeck. 2002. Impaired B and T cell antigen receptor signaling in p110delta PI 3-kinase mutant mice. *Science* 297: 1031-1034.

16. Patton, D. T., O. A. Garden, W. P. Pearce, L. E. Clough, C. R. Monk, E. Leung, W. C. Rowan, S. Sancho, L. S. Walker, B. Vanhaesebroeck, and K. Okkenhaug. 2006. Cutting edge: the phosphoinositide 3-kinase p110 delta is critical for the function of CD4+CD25+Foxp3+ regulatory T cells. *J Immunol* 177: 6598-6602.
17. Weidner, A. S., N. C. Panarelli, J. T. Geyer, E. B. Bhavsar, R. R. Furman, J. P. Leonard, J. Jessurun, and R. K. Yantiss. 2015. Idelalisib-associated Colitis: Histologic Findings in 14 Patients. *Am J Surg Pathol* 39: 1661-1667.
18. Shymanets, A., Prajwal, K. Bucher, S. Beer-Hammer, C. Harteneck, and B. Nürnberg. 2013. p87 and p101 subunits are distinct regulators determining class IB phosphoinositide 3-kinase (PI3K) specificity. *J Biol Chem* 288: 31059-31068.
19. Voigt, P., M. B. Dorner, and M. Schaefer. 2006. Characterization of p87PIKAP, a novel regulatory subunit of phosphoinositide 3-kinase gamma that is highly expressed in heart and interacts with PDE3B. *J Biol Chem* 281: 9977-9986.
20. Puri, K. D., T. A. Doggett, C. Y. Huang, J. Douangpanya, J. S. Hayflick, M. Turner, J. Penninger, and T. G. Diacovo. 2005. The role of endothelial PI3Kgamma activity in neutrophil trafficking. *Blood* 106: 150-157.
21. Wymann, M. P., and R. Marone. 2005. Phosphoinositide 3-kinase in disease: timing, location, and scaffolding. *Curr Opin Cell Biol* 17: 141-149.
22. Hirsch, E., G. Lembo, G. Montrucchio, C. Rommel, C. Costa, and L. Barberis. 2006. Signaling through PI3Kgamma: a common platform for leukocyte, platelet and cardiovascular stress sensing. *Thromb Haemost* 95: 29-35.
23. Rommel, C., M. Camps, and H. Ji. 2007. PI3K delta and PI3K gamma: partners in crime in inflammation in rheumatoid arthritis and beyond. *Nat Rev Immunol* 7: 191-201.
24. Takeda, A. J., T. J. Maher, Y. Zhang, S. M. Lanahan, M. L. Bucklin, S. R. Compton, P. M. Tyler, W. A. Comrie, M. Matsuda, K. N. Olivier, S. Pittaluga, J. J. McElwee, D. A. Long Priel, D. B. Kuhns, R. L. Williams, P. J. Mustillo, M. P. Wymann, V. Koneti Rao, and C. L. Lucas. 2019. Human PI3K γ deficiency and its microbiota-dependent mouse model reveal immunodeficiency and tissue immunopathology. *Nat Commun* 10: 4364.
25. Thian, M., B. Hoeger, A. Kamnev, F. Poyer, S. Köstel Bal, M. Caldera, R. Jiménez-Heredia, J. Huemer, W. F. Pickl, M. Groß, S. Ehl, C. L. Lucas, J. Menche, C. Hutter, A. Attarbaschi, L. Dupré, and K. Boztug. 2020. Germline biallelic PIK3CG mutations in a multifaceted immunodeficiency with immune dysregulation. *Haematologica* 105: e488.
26. Vanhaesebroeck, B., M. W. D. Perry, J. R. Brown, F. André, and K. Okkenhaug. 2021. PI3K inhibitors are finally coming of age. *Nat Rev Drug Discov*
27. Kaneda, M. M., K. S. Messer, N. Ralainirina, H. Li, C. J. Leem, S. Gorjestani, G. Woo, A. V. Nguyen, C. C. Figueiredo, P. Foubert, M. C. Schmid, M. Pink, D. G. Winkler, M. Rausch, V. J. Palombella, J. Kutok, K. McGovern, K. A. Frazer, X. Wu, M. Karin, R. Sasik, E. E. Cohen, and J. A. Varner. 2016. PI3K γ is a molecular switch that controls immune suppression. *Nature* 539: 437-442.
28. De Henau, O., M. Rausch, D. Winkler, L. F. Campesato, C. Liu, D. H. Cymerman, S. Budhu, A. Ghosh, M. Pink, J. Tchaicha, M. Douglas, T. Tibbitts, S. Sharma, J. Proctor, N. Kosmider, K. White, H. Stern, J. Soglia, J. Adams, V. J. Palombella, K. McGovern, J. L. Kutok, J. D. Wolchok, and T. Merghoub. 2016. Overcoming resistance to checkpoint blockade therapy by targeting PI3K γ in myeloid cells. *Nature* 539: 443-447.
29. Hirsch, E., V. L. Katanaev, C. Garlanda, O. Azzolino, L. Pirola, L. Silengo, S. Sozzani, A. Mantovani, F. Altruda, and M. P. Wymann. 2000. Central role for G protein-coupled phosphoinositide 3-kinase gamma in inflammation. *Science* 287: 1049-1053.
30. Sasaki, T., J. Irie-Sasaki, R. G. Jones, A. J. Oliveira-dos-Santos, W. L. Stanford, B. Bolon, A. Wakeham, A. Itie, D. Bouchard, I. Kozieradzki, N. Joza, T. W. Mak, P. S.

- Ohashi, A. Suzuki, and J. M. Penninger. 2000. Function of PI3K γ in thymocyte development, T cell activation, and neutrophil migration. *Science* 287: 1040-1046.
31. Li, Z., H. Jiang, W. Xie, Z. Zhang, A. V. Smrcka, and D. Wu. 2000. Roles of PLC-beta2 and -beta3 and PI3K γ in chemoattractant-mediated signal transduction. *Science* 287: 1046-1049.
 32. Reif, K., K. Okkenhaug, T. Sasaki, J. M. Penninger, B. Vanhaesebroeck, and J. G. Cyster. 2004. Cutting edge: differential roles for phosphoinositide 3-kinases, p110 γ and p110 δ , in lymphocyte chemotaxis and homing. *J Immunol* 173: 2236-2240.
 33. Thomas, M. S., J. S. Mitchell, C. C. DeNucci, A. L. Martin, and Y. Shimizu. 2008. The p110 γ isoform of phosphatidylinositol 3-kinase regulates migration of effector CD4 T lymphocytes into peripheral inflammatory sites. *J Leukoc Biol* 84: 814-823.
 34. Ali, A. Y., X. Wu, N. Eissa, S. Hou, J. E. Ghia, T. T. Murooka, V. Banerji, J. B. Johnston, F. Lin, S. B. Gibson, and A. J. Marshall. 2018. Distinct roles for phosphoinositide 3-kinases γ and δ in malignant B cell migration. *Leukemia* 32: 1958-1969.
 35. Ghigo, A., F. Damilano, L. Braccini, and E. Hirsch. 2010. PI3K inhibition in inflammation: Toward tailored therapies for specific diseases. *Bioessays* 32: 185-196.
 36. Thomas, M. J., A. Smith, D. H. Head, L. Milne, A. Nicholls, W. Pearce, B. Vanhaesebroeck, M. P. Wymann, E. Hirsch, A. Trifilieff, C. Walker, P. Finan, and J. Westwick. 2005. Airway inflammation: chemokine-induced neutrophilia and the class I phosphoinositide 3-kinases. *Eur J Immunol* 35: 1283-1291.
 37. Ferguson, G. J., L. Milne, S. Kulkarni, T. Sasaki, S. Walker, S. Andrews, T. Crabbe, P. Finan, G. Jones, S. Jackson, M. Camps, C. Rommel, M. Wymann, E. Hirsch, P. Hawkins, and L. Stephens. 2007. PI(3)K γ has an important context-dependent role in neutrophil chemokinesis. *Nat Cell Biol* 9: 86-91.
 38. Camps, M., T. Rückle, H. Ji, V. Ardisson, F. Rintelen, J. Shaw, C. Ferrandi, C. Chabert, C. Gillieron, B. Françon, T. Martin, D. Gretener, D. Perrin, D. Leroy, P. A. Vitte, E. Hirsch, M. P. Wymann, R. Cirillo, M. K. Schwarz, and C. Rommel. 2005. Blockade of PI3K γ suppresses joint inflammation and damage in mouse models of rheumatoid arthritis. *Nat Med* 11: 936-943.
 39. Hayer, S., N. Pundt, M. A. Peters, C. Wunrau, I. Kühnel, K. Neugebauer, S. Strietholt, J. Zwerina, A. Korb, J. Penninger, L. A. Joosten, S. Gay, T. Rückle, G. Schett, and T. Pap. 2009. PI3K γ regulates cartilage damage in chronic inflammatory arthritis. *FASEB J* 23: 4288-4298.
 40. Lupia, E., A. Goffi, P. De Giuli, O. Azzolino, O. Bosco, E. Patrucco, M. C. Vivaldo, M. Ricca, M. P. Wymann, E. Hirsch, G. Montrucchio, and G. Emanuelli. 2004. Ablation of phosphoinositide 3-kinase- γ reduces the severity of acute pancreatitis. *Am J Pathol* 165: 2003-2011.
 41. van Dop, W. A., S. Marengo, A. A. te Velde, E. Ciruolo, I. Franco, F. J. ten Kate, G. E. Boeckstaens, J. C. Hardwick, D. W. Hommes, E. Hirsch, and G. R. van den Brink. 2010. The absence of functional PI3K γ prevents leukocyte recruitment and ameliorates DSS-induced colitis in mice. *Immunol Lett* 131: 33-39.
 42. Thomas, M., M. J. Edwards, E. Sawicka, N. Duggan, E. Hirsch, M. P. Wymann, C. Owen, A. Trifilieff, C. Walker, J. Westwick, and P. Finan. 2009. Essential role of phosphoinositide 3-kinase γ in eosinophil chemotaxis within acute pulmonary inflammation. *Immunology* 126: 413-422.
 43. Takeda, M., W. Ito, M. Tanabe, S. Ueki, H. Kato, J. Kihara, T. Tanigai, T. Chiba, K. Yamaguchi, H. Kayaba, Y. Imai, K. Okuyama, I. Ohno, T. Sasaki, and J. Chihara. 2009. Allergic airway hyperresponsiveness, inflammation, and remodeling do not develop in

- phosphoinositide 3-kinase gamma-deficient mice. *J Allergy Clin Immunol* 123: 805-812.
44. Del Prete, A., W. Vermi, E. Dander, K. Otero, L. Barberis, W. Luini, S. Bernasconi, M. Sironi, A. Santoro, C. Garlanda, F. Facchetti, M. P. Wymann, A. Vecchi, E. Hirsch, A. Mantovani, and S. Sozzani. 2004. Defective dendritic cell migration and activation of adaptive immunity in PI3Kgamma-deficient mice. *EMBO J* 23: 3505-3515.
 45. Comerford, I., W. Litchfield, E. Kara, and S. R. McColl. 2012. PI3K γ drives priming and survival of autoreactive CD4(+) T cells during experimental autoimmune encephalomyelitis. *PLoS One* 7: e45095.
 46. Chang, J. D., G. K. Sukhova, P. Libby, E. Schwartz, A. H. Lichtenstein, S. J. Field, C. Kennedy, S. Madhavarapu, J. Luo, D. Wu, and L. C. Cantley. 2007. Deletion of the phosphoinositide 3-kinase p110gamma gene attenuates murine atherosclerosis. *Proc Natl Acad Sci U S A* 104: 8077-8082.
 47. Fougerat, A., S. Gayral, P. Gourdy, A. Schambourg, T. Rückle, M. K. Schwarz, C. Rommel, E. Hirsch, J. F. Arnal, J. P. Salles, B. Perret, M. Breton-Douillon, M. P. Wymann, and M. Laffargue. 2008. Genetic and pharmacological targeting of phosphoinositide 3-kinase-gamma reduces atherosclerosis and favors plaque stability by modulating inflammatory processes. *Circulation* 117: 1310-1317.
 48. Breasson, L., B. Becattini, C. Sardi, A. Molinaro, F. Zani, R. Marone, F. Botindari, M. Bousquenaud, C. Ruegg, M. P. Wymann, and G. Solinas. 2017. PI3K γ activity in leukocytes promotes adipose tissue inflammation and early-onset insulin resistance during obesity. *Sci Signal* 10:
 49. Hawkins, P. T., L. R. Stephens, S. Suire, and M. Wilson. 2010. PI3K signaling in neutrophils. *Curr Top Microbiol Immunol* 346: 183-202.
 50. Quignard, J. F., J. Mironneau, V. Carricaburu, B. Fournier, A. Babich, B. Nurnberg, C. Mironneau, and N. Macrez. 2001. Phosphoinositide 3-kinase gamma mediates angiotensin II-induced stimulation of L-type calcium channels in vascular myocytes. *J Biol Chem* 276: 32545-32551.
 51. Vecchione, C., E. Patrucco, G. Marino, L. Barberis, R. Poulet, A. Aretini, A. Maffei, M. T. Gentile, M. Storto, O. Azzolino, M. Brancaccio, G. L. Colussi, U. Bettarini, F. Altruda, L. Silengo, G. Tarone, M. P. Wymann, E. Hirsch, and G. Lembo. 2005. Protection from angiotensin II-mediated vasculotoxic and hypertensive response in mice lacking PI3Kgamma. *J Exp Med* 201: 1217-1228.
 52. Luo, L., A. A. Wall, S. J. Tong, Y. Hung, Z. Xiao, A. A. Tarique, P. D. Sly, E. Fantino, M. P. Marzolo, and J. L. Stow. 2018. TLR Crosstalk Activates LRP1 to Recruit Rab8a and PI3K γ for Suppression of Inflammatory Responses. *Cell Rep* 24: 3033-3044.
 53. Garcia, C. C., L. P. Tavares, A. C. F. Dias, F. Kehdy, L. E. Alvarado-Arnez, C. M. Queiroz-Junior, I. Galvão, B. H. Lima, A. R. Matos, A. P. F. Gonçalves, F. M. Soriani, M. O. Moraes, J. T. Marques, M. M. Siqueira, A. M. V. Machado, L. P. Sousa, R. C. Russo, and M. M. Teixeira. 2018. Phosphatidyl Inositol 3 Kinase-Gamma Balances Antiviral and Inflammatory Responses During Influenza A H1N1 Infection: From Murine Model to Genetic Association in Patients. *Front Immunol* 9: 975.
 54. Becattini, B., R. Marone, F. Zani, D. Arsenijevic, J. Seydoux, J. P. Montani, A. G. Dulloo, B. Thorens, F. Preitner, M. P. Wymann, and G. Solinas. 2011. PI3K γ within a nonhematopoietic cell type negatively regulates diet-induced thermogenesis and promotes obesity and insulin resistance. *Proc Natl Acad Sci U S A* 108: E854-63.
 55. Wang, C., R. Jin, A. Nanda, J. Yan, and G. Li. 2015. Platelet PI3K γ Contributes to Carotid Intima-Media Thickening under Severely Reduced Flow Conditions. *PLoS One* 10: e0129265.

56. Laffargue, M., R. Calvez, P. Finan, A. Trifilieff, M. Barbier, F. Altruda, E. Hirsch, and M. P. Wymann. 2002. Phosphoinositide 3-kinase gamma is an essential amplifier of mast cell function. *Immunity* 16: 441-451.
57. Rodríguez-Borlado, L., D. F. Barber, C. Hernández, M. A. Rodríguez-Marcos, A. Sánchez, E. Hirsch, M. Wymann, C. Martínez-A, and A. C. Carrera. 2003. Phosphatidylinositol 3-kinase regulates the CD4/CD8 T cell differentiation ratio. *J Immunol* 170: 4475-4482.
58. Swat, W., V. Montgrain, T. A. Doggett, J. Douangpanya, K. Puri, W. Vermi, and T. G. Diacovo. 2006. Essential role of PI3Kdelta and PI3Kgamma in thymocyte survival. *Blood* 107: 2415-2422.
59. Ji, H., F. Rintelen, C. Waltzinger, D. Bertschy Meier, A. Bilancio, W. Pearce, E. Hirsch, M. P. Wymann, T. Rückle, M. Camps, B. Vanhaesebroeck, K. Okkenhaug, and C. Rommel. 2007. Inactivation of PI3Kgamma and PI3Kdelta distorts T-cell development and causes multiple organ inflammation. *Blood* 110: 2940-2947.
60. Janas, M. L., G. Varano, K. Gudmundsson, M. Noda, T. Nagasawa, and M. Turner. 2010. Thymic development beyond beta-selection requires phosphatidylinositol 3-kinase activation by CXCR4. *J Exp Med* 207: 247-261.
61. Metjian, A., R. L. Roll, A. D. Ma, and C. S. Abrams. 1999. Agonists cause nuclear translocation of phosphatidylinositol 3-kinase gamma. A Gbetagamma-dependent pathway that requires the p110gamma amino terminus. *J Biol Chem* 274: 27943-27947.
62. Voigt, P., C. Brock, B. Nürnberg, and M. Schaefer. 2005. Assigning functional domains within the p101 regulatory subunit of phosphoinositide 3-kinase gamma. *J Biol Chem* 280: 5121-5127.
63. Maier, U., A. Babich, and B. Nürnberg. 1999. Roles of non-catalytic subunits in gbetagamma-induced activation of class I phosphoinositide 3-kinase isoforms beta and gamma. *J Biol Chem* 274: 29311-29317.
64. Kurig, B., A. Shymanets, T. Bohnacker, Prajwal, C. Brock, M. R. Ahmadian, M. Schaefer, A. Gohla, C. Harteneck, M. P. Wymann, E. Jeanclos, and B. Nürnberg. 2009. Ras is an indispensable coregulator of the class IB phosphoinositide 3-kinase p87/p110gamma. *Proc Natl Acad Sci U S A* 106: 20312-20317.
65. Jin, J. R., E. Gogvadze, A. R. Xavier, T. Bohnacker, J. Voelzmann, and M. P. Wymann. 2020. PI3K γ Regulatory Protein p84 Determines Mast Cell Sensitivity to Ras Inhibition—Moving Towards Cell Specific PI3K Targeting? *Front Immunol* 11: 585070.
66. Vadas, O., H. A. Dbouk, A. Shymanets, O. Perisic, J. E. Burke, W. F. Abi Saab, B. D. Khalil, C. Harteneck, A. R. Bresnick, B. Nürnberg, J. M. Backer, and R. L. Williams. 2013. Molecular determinants of PI3K γ -mediated activation downstream of G-protein-coupled receptors (GPCRs). *Proc Natl Acad Sci U S A* 110: 18862-18867.
67. Walser, R., J. E. Burke, E. Gogvadze, T. Bohnacker, X. Zhang, D. Hess, P. Küenzi, M. Leitges, E. Hirsch, R. L. Williams, M. Laffargue, and M. P. Wymann. 2013. PKC β phosphorylates PI3K γ to activate it and release it from GPCR control. *PLoS Biol* 11: e1001587.
68. Bohnacker, T., R. Marone, E. Collmann, R. Calvez, E. Hirsch, and M. P. Wymann. 2009. PI3Kgamma adaptor subunits define coupling to degranulation and cell motility by distinct PtdIns(3,4,5)P3 pools in mast cells. *Sci Signal* 2: ra27.
69. Thapa, N., M. Chen, H. T. Horn, S. Choi, T. Wen, and R. A. Anderson. 2020. Phosphatidylinositol-3-OH kinase signalling is spatially organized at endosomal compartments by microtubule-associated protein 4. *Nat Cell Biol* 22: 1357-1370.
70. Luo, L., A. A. Wall, J. C. Yeo, N. D. Condon, S. J. Norwood, S. Schoenwaelder, K. W. Chen, S. Jackson, B. J. Jenkins, E. L. Hartland, K. Schroder, B. M. Collins, M. J.

- Sweet, and J. L. Stow. 2014. Rab8a interacts directly with PI3K γ to modulate TLR4-driven PI3K and mTOR signalling. *Nat Commun* 5: 4407.
71. Patrucco, E., A. Notte, L. Barberis, G. Selvetella, A. Maffei, M. Brancaccio, S. Marengo, G. Russo, O. Azzolino, S. D. Rybalkin, L. Silengo, F. Altruda, R. Wetzker, M. P. Wymann, G. Lembo, and E. Hirsch. 2004. PI3K γ modulates the cardiac response to chronic pressure overload by distinct kinase-dependent and -independent effects. *Cell* 118: 375-387.
 72. Hirsch, E., L. Braccini, E. Ciraolo, F. Morello, and A. Perino. 2009. Twice upon a time: PI3K's secret double life exposed. *Trends Biochem Sci* 34: 244-248.
 73. Perino, A., A. Ghigo, E. Ferrero, F. Morello, G. Santulli, G. S. Baillie, F. Damilano, A. J. Dunlop, C. Pawson, R. Walser, R. Levi, F. Altruda, L. Silengo, L. K. Langeberg, G. Neubauer, S. Heymans, G. Lembo, M. P. Wymann, R. Wetzker, M. D. Houslay, G. Iaccarino, J. D. Scott, and E. Hirsch. 2011. Integrating cardiac PIP3 and cAMP signaling through a PKA anchoring function of p110 γ . *Mol Cell* 42: 84-95.
 74. Wymann, M. P., and G. Solinas. 2013. Inhibition of phosphoinositide 3-kinase γ attenuates inflammation, obesity, and cardiovascular risk factors. *Ann N Y Acad Sci* 1280: 44-47.
 75. Deladeriere, A., L. Gambardella, D. Pan, K. E. Anderson, P. T. Hawkins, and L. R. Stephens. 2015. The regulatory subunits of PI3K γ control distinct neutrophil responses. *Sci. Signal.* 8:
 76. Rynkiewicz, N. K., K. E. Anderson, S. Suire, D. M. Collins, E. Karanasios, O. Vadas, R. Williams, D. Oxley, J. Clark, L. R. Stephens, and P. T. Hawkins. 2020. G $\beta\gamma$ is a direct regulator of endogenous p101/p110 γ and p84/p110 γ PI3K γ complexes in mouse neutrophils. *Sci Signal* 13:
 77. Suire, S., A. M. Condliffe, G. J. Ferguson, C. D. Ellson, H. Guillou, K. Davidson, H. Welch, J. Coadwell, M. Turner, E. R. Chilvers, P. T. Hawkins, and L. Stephens. 2006. Gbetagammmas and the Ras binding domain of p110 γ are both important regulators of PI(3)K γ signalling in neutrophils. *Nat Cell Biol* 8: 1303-1309.

4. Results

4.1. Project 1: PI3K γ Regulatory Protein p84 Determines Mast Cell Sensitivity to Ras Inhibition – Moving towards Cell Specific PI3K Targeting?

An earlier version of this work before peer review and publication has been included in my dissertation to obtain the medical doctorate (MD) from the medical faculty of the university of Basel in 2020. The following section contains the final paper that was accepted for publication in September 2020.



PI3K γ Regulatory Protein p84 Determines Mast Cell Sensitivity to Ras Inhibition—Moving Towards Cell Specific PI3K Targeting?

Julie R. Jin[†], Elena Gogvadze[†], Ana R. Xavier[†], Thomas Bohnacker, Jan Voelzmann and Matthias P. Wymann^{*}

Department of Biomedicine, University of Basel, Basel, Switzerland

OPEN ACCESS

Edited by:

Paige Lacy,
University of Alberta, Canada

Reviewed by:

Edismauro Garcia Freitas Filho,
University of São Paulo, Brazil
Marianna Kulka,
National Research Council Canada
(NRC-CNRC), Canada
Gary Eitzen,
University of Alberta, Canada

*Correspondence:

Matthias P. Wymann
Matthias.Wymann@unibas.ch

[†]These authors have contributed
equally to this work

Specialty section:

This article was submitted to
Molecular Innate Immunity,
a section of the journal
Frontiers in Immunology

Received: 10 August 2020

Accepted: 30 September 2020

Published: 28 October 2020

Citation:

Jin JR, Gogvadze E, Xavier AR,
Bohnacker T, Voelzmann J and
Wymann MP (2020) PI3K γ Regulatory
Protein p84 Determines Mast Cell
Sensitivity to Ras Inhibition—Moving
Towards Cell Specific PI3K Targeting?
Front. Immunol. 11:585070.
doi: 10.3389/fimmu.2020.585070

Mast cells are the major effector cells in immunoglobulin E (IgE)-mediated allergy. The high affinity IgE receptor Fc ϵ RI, as well as G protein-coupled receptors (GPCRs) on the mast cell surface signals to phosphoinositide 3-kinase γ (PI3K γ) to initiate degranulation, cytokine release, and chemotaxis. PI3K γ is therefore considered as a target for treatment of allergic disorders. However, leukocyte PI3K γ is key to many functions in innate and adaptive immunity, and attenuation of host defense mechanisms is an expected adverse effect that complicates treatment of chronic illnesses. PI3K γ operates as a p110 γ /p84 or p110 γ /p101 complex, where p110 γ /p84 requires Ras activation. Here we investigated if modulation of Ras-isoprenylation could target PI3K γ activity to attenuate PI3K γ -dependent mast cell responses without impairment of macrophage functions. In murine bone marrow-derived mast cells, GPCR stimulation triggers activation of N-Ras and H-Ras isoforms, which is followed by the phosphorylation of protein kinase B (PKB/Akt) relayed through PI3K γ . Although K-Ras is normally not activated in Ras wild-type cells, it is able to compensate for genetically deleted N- and H-Ras isoforms. Inhibition of Ras isoprenylation with farnesyltransferase inhibitor FTI-277 leads to a significant reduction of mast cell degranulation, cytokine production, and migration. Complementation experiments expressing PI3K γ adaptor proteins p84 or p101 demonstrated a differential sensitivity towards Ras-inhibition depending on PI3K γ complex composition. Mast cell responses are exclusively p84-dependent and were effectively controlled by FTI-277. Similar results were obtained when GTP-Ras was inactivated by overexpression of the GAP-domain of Neurofibromin-1 (NF-1). Unlike mast cells, macrophages express p84 and p101 but are p101-dominated and thus remain functional under treatment with FTI-277. Our work demonstrates that p101 and p84 have distinct physiological roles, and that Ras dependence of PI3K γ signaling differs between cell types. FTI-277 reduces GPCR-activated PI3K γ responses in p84-expressing but not p101-containing bone marrow derived cells. However, prenylation inhibitors have pleiotropic effects beyond Ras and non-tolerable side-effects that disfavor further clinical validation. Statins are, however, clinically well-established drugs that have previously been proposed to block mast cell degranulation by interference with protein

prenylation. We show here that Simvastatin inhibits mast cell degranulation, but that this does not occur *via* Ras-PI3K γ pathway alterations.

Keywords: inflammation, allergy, phosphoinositide-3-kinase (PI3K), PIK3CG, Ras family proteins, p101, p84, IgE (Immunoglobulin E)

INTRODUCTION

Mast cells are key effector cells in the pathology of allergic disease and chronic inflammation and are thus target cells of novel therapeutic strategies (1). In sensitized mice and human patients, IgE binds to the high affinity IgE receptor (Fc ϵ RI) present on the surface of tissue mast cells (2). Multivalent antigen/IgE complexes cross-link Fc ϵ RI, and trigger a protein tyrosine kinase cascade involving Src family kinase activation and Syk (spleen tyrosine kinase) translocation. The subsequent relay of signals through Bruton tyrosine kinase (Btk) to phospholipase C γ (PLC γ) culminates in an extracellular calcium influx committing mast cells to release their histamine granule contents and initiate *de novo* synthesis of pro-inflammatory and immuno-modulatory mediators, including chemokines, cytokines, growth factors, vasoactive compounds, and more (3).

We have demonstrated earlier that G-protein coupled receptor (GPCR) ligands synergize with IgE/antigen to stimulate mast cell degranulation (4–6). IgE/antigen stimulated mast cells also release adenosine, which yields an autocrine augmentation of mast cell activation *via* the G α_i -coupled A3 adenosine receptor (7), triggering activation of phosphoinositide 3-kinase γ [PI3K γ (4–6)]. An alternative activation mechanism downstream of Fc ϵ RI involves the Ca²⁺-mediated activation of protein kinase C β (PKC β), which phosphorylates and activates PI3K γ (8).

An important aspect in anaphylaxis is recruitment of mast cell precursors to the tissue, which is also mediated by GPCRs engaging in PI3K γ activation (6, 9).

Mice lacking functional PI3K γ are thus resistant to IgE/antigen-induced anaphylaxis (4, 6), show a reduced IgE-mediated recruitment of mast cells to tissues (6), and display attenuated airway and pulmonary inflammation (10, 11), ventilator induced lung injury (12) and allergic asthma (13). PI3K γ therefore qualifies as a potential therapeutic target in allergic conditions.

Furthermore, PI3K γ is highly expressed in leukocytes of the myeloid and lymphoid lineage (14–17) and is involved in the transduction of innate and adaptive immune responses. Leukocyte chemotaxis, release of inflammatory mediators, and activation of the NADPH oxidase to release reactive oxygen species (ROS) represent crucial host defense mechanisms that require G protein-coupled receptor (GPCR) engagement and activated PI3K γ (4, 14–16, 18, 19). Early on, PI3K γ inhibition with AS-605240 has demonstrated protection against rheumatoid arthritis (20), pancreatitis (21), glomerulonephritis, and systemic lupus (22) in mouse models. Genetic and pharmacological targeting of PI3K γ attenuates macrophage/foam cell activation and atherosclerosis and supports plaque stability (23–25). Genetic inactivation of PI3K γ activity also attenuates heart failure during chronic pressure overload (26) and diet-induced obesity (27), partially reliant on kinase-

independent functions of PI3K γ as a scaffold protein for protein kinase A and phosphorylase 3B.

The flip-side to a broad action of PI3K γ inhibition in various animal disease models are potential associated adverse effects, including susceptibility to infections, as indicated by reduced neutrophil (14, 19), macrophage (14, 28, 29) and dendritic cell motility (17) in PI3K γ null cells and mice. Moreover, PI3K γ has been implicated in anti-viral response against Influenza A infection recently (30, 31). The possibility of cell type-specific PI3K γ targeting, allowing for alleviation of allergic inflammation without a general suppression of host immune defense would therefore be of great value.

PI3K γ acts as a heterodimer of a catalytic p110 γ subunit and one of two possible adaptor proteins—p84 (also called p87^{PIKAP}) (5, 32) or p101 (33). Both adaptor proteins take a role in the coupling of GPCR signaling to PI3K γ ; but p101 and p84 appear to have discrete physiological functions (5, 34). Distinct pools of PtdIns(3,4,5)P₃ at the plasma membrane emerging from the two PI3K γ /adaptor subunit complexes display a differential sensitivity to cholesterol depletion and capacity to promote mast cell granule release (5). Adaptor-specific responses were also described in neutrophils (34, 35), where p101 played a key role in cell migration, while p84 was essential for ROS production upon chemoattractant stimulation. Moreover, adaptor proteins are not equally distributed among hematopoietic cells. While lymphocytes express p101, mast cells express only the p84 adaptor subunit, but neutrophils and macrophages contain both p101 and p84 adaptors (5, 32).

Finally, a further distinction between adaptor subunits was revealed by analysis of the role of the small GTPase Ras in the activation of the PI3K γ complexes. Whereas p101/p110 γ is recruited and stimulated by G $\beta\gamma$ subunit of GPCRs and does not require Ras to be operational, Ras is indispensable for membrane recruitment and activation of the lipid kinase in the p84/p110 γ complex (5, 36). Differential involvement of Ras opens new opportunities for targeted regulation of the two PI3K γ complexes that could provide novel ways to specifically control distinct cell responses.

In the current study, we tested whether inhibition of Ras could attenuate mast cell activation due to its involvement in p84/p110 γ complex-dependent cell responses, and assessed if macrophages would be spared by Ras targeting.

MATERIALS AND METHODS

Mice

Transgenic mouse strains lacking H-Ras (37), N-Ras (38) and p110 γ (14) were previously described. Mice were backcrossed to a C57BL/6J background and housed according to the

institutional guidelines. In all experiments 8–12-week-old male and female animals were utilized. All animal experiments were carried out in accordance with the guidelines of the Swiss Federal Veterinary Office (SFVO) and the Cantonal Veterinary Office of Basel-Stadt (license number 2143).

Bone Marrow Derived Mast Cell (BMMC) and Macrophage (BMM ϕ) Culture

BMMC and BMM ϕ were cultured as previously described in (5). Briefly, bone marrow was isolated from femurs of wild-type and transgenic mice. To initiate differentiation of BMMCs, bone marrow cells were cultured in IMDM supplemented with 10% heat-inactivated fetal calf serum (HI-FCS), 2 mM L-Glutamine (Sigma, G7513), 100 U/ml Penicillin + 100 μ g/ml Streptomycin (Sigma, N109), 50 μ M β -mercaptoethanol (Sigma M6250) and 2 ng/ml murine interleukin-3 (IL-3, Peprotech 213-13). Recombinant murine SCF (5 ng/ml, Peprotech 250-03) was added only during the first passage. *c-kit*⁺*Fc ϵ RI*⁺ BMMCs were used for experiments after 4 weeks of culture. Culture medium was supplemented with IL-3 (2 ng/ml) every two days.

To generate BMM ϕ , bone marrow cells were cultured in bacterial petri dishes (Greiner bio-one 633180) in RPMI supplemented with 10% HI-FCS, 2 mM L-Glutamine, 1% Penicillin/Streptomycin, 50 μ M β -mercaptoethanol and 20% L929-conditioned medium. Non-adherent cells were collected after 5 days of culture to perform experiments.

For BMMC and BMM ϕ GPCR activation adenosine (Fluka Bio Chemika 01890), recombinant mouse C5a (R&D Systems #8085-C3-025) and platelet activating factor (PAF; Sigma, P7568) were used.

Ras Activation Assay and Western Blot Analysis

For pull-down of activated GTP-Ras 20×10^6 cells per experiment were starved in IMDM 2% HI-FCS (BMMC) or RPMI 1% HI-FCS (BMM ϕ) for 3 h. After starvation, cells were resuspended in Hank's Balanced Salt Solution (15 mM HEPES, 140 mM NaCl, 5 mM KCl, 2.8 mM NaHCO₃, 1.5 mM CaCl₂, 1 mM MgCl₂, 0.06 mM MgSO₄, pH = 7.4) supplemented with 1% BSA and 60 mM Glucose. Stimulation with 4 μ M adenosine (Sigma 01890) or 10 nM murine recombinant C5a (R&D Systems 2150-C5-025) was terminated after 2 min by placing tubes on ice, spinning down, and removing supernatant. Subsequently cells were incubated in 1 ml lysis buffer (50 mM Tris pH 7.5, 150 mM NaCl, 5 mM MgCl₂, 1 mM EGTA, 1% NP-40) supplemented with protease inhibitors (Leupeptin, Pepstatin, Aprotinin, PMSF, DTT, DFP) and containing GST-tagged Ras-binding domain of Raf1A (20 μ g/reaction) and 100 μ M GDP. After 10 min incubation on ice, lysates were centrifuged at 14,000 g for 15 min. For total lysis aliquots (input), 80 μ l of the lysate was mixed with 20 μ l 5 \times sample buffer (125 mM Tris-HCl (pH 6.8), 4% SDS, 10% β -mercaptoethanol, 20% glycerol and bromophenol blue) before denaturation (96°C, 7 min) and protein separation by SDS-PAGE, and transferred to a PDVF membrane (Immobilon FL, Millipore IPFL0010).

The remaining lysate was incubated with 40 μ l 50% Glutathione-Sepharose 4B bead slurry in lysis buffer (GE Healthcare, 17-0756-01) for 2 h at 4°C. Beads were resuspended in 20 μ l 2 \times sample buffer; denatured and pulled-down Ras protein was subjected to SDS-PAGE immunoblotting. The list of western blot antibodies is provided in the supplementary section (Table S3).

Recombinant p84 and p101 kindly provided by R. Williams were used as standards to quantify expression levels of PI3K γ adaptor proteins on western blots.

Mast Cell Degranulation Cytokine Expression and RT-qPCR

β -hexosaminidase assay to assess mast cell degranulation was performed as previously described in (5). For measurement of cytokine expression, BMMCs were pre-loaded with IgE anti-DNP-HSA (clone SPE-7, Sigma D8406) for 16 h, washed, and resuspended in fresh IMDM complete supplemented with IL-3 (2 ng/ml). Subsequently, cells were incubated with DNP-HSA (2 ng/ml, Sigma D8406) and adenosine (2 μ M) for 6 h at 37°C 5% CO₂, and RNA was extracted using RNeasy Mini Kit (Qiagen 74104).

2 μ g total RNA was used for reverse transcription with M-MVL RTase and oligo dT primers. Quantitative polymerase chain reaction (qPCR) was performed on StepOnePlus Real-Time PCR System (Applied Biosystems) with MESA Green qPCR MasterMix Plus for SYBR Assay (Eurogentech). qPCR results of Ras isoforms and farnesyltransferases (FTases) were normalized to GAPDH according to the following formulas

$$\% \text{ of GAPDH} = 2^{-\text{dCT}} \times 100 \text{ and } \text{dCT} = \text{CT}_{\text{target}} - \text{CT}_{\text{GAPDH}}$$

All primer sequences for qPCR are listed in the supplementary section (Table S1). Relative RNA expression was normalized to GAPDH as endogenous control and WT unstimulated cells as reference sample.

$$\text{Fold change} = 2^{-\text{ddCT}} \text{ and } \text{ddCT} = \text{dCT}_{\text{sample}} - \text{dCT}_{\text{reference}}$$

BMMC and HEK-293 Transfection

BMMCs were transfected with Amaxa Nucleofector kit T (VCA-1002) using 14 μ g of total plasmid per 10×10^6 cells. Medium was changed 5 h after transfection, and cells were cultured overnight in IMDM complete supplemented with IL-3 (2 ng/ml). Plasmids encoding for p101, p84, p110 γ , and NF1 were previously utilized in (5) and (36). Plasmid sequences of codon-optimized H-Ras, N-Ras, and K-Ras for transfection in human embryonic kidney 293 (HEK293) cells are provided in the supplementary section (Table S2). 24 h prior to the transfection, HEK293 cells cultured in DMEM supplemented with 10% HI-FCS, 2 mM L-glutamine (Sigma, G7513), 100 U/ml Penicillin/Streptomycin (Sigma, N109) were seeded on a 6 cm dish. The following day, 2.5 ml medium was replaced before addition of the mixture of 3 μ g total DNA and 6 μ l JetPEI transfection solution (Polyplus, 101B-010) in 100 μ l 150 mM NaCl. 6 h post-transfection, we added fresh medium and cultured cells overnight until lysis for protein

determination or imaging of Ras sub-cellular localization on a Leica DMI6000 microscope with Photometrics CoolSnap HQ2 camera.

Transwell Migration

250,000 cells were placed into fibronectin-coated Transwell chambers (0.5 μ m pores, Corning N32421) with migration assay medium (IMDM or RPMI, 2 mM L-Glutamine, 0.1% BSA low endotoxin, 1% Penicillin–Streptomycin, 50 μ M β -mercaptoethanol, 20 mM HEPES pH 7.4) containing 1 μ M adenosine (BMMC) or 10 nM C5a (BMM \emptyset) as chemoattractant in the lower well. After 6 h at 37°C and 5% CO₂ Transwell chambers and lower well compartments were fixed with Paraformaldehyde (PFA) 4% and stained with Hoechst nuclear stain (Invitrogen, H1399). Migrated cells were detected by fluorescence microscopy (Leica DMi8, DFC 9000 GT camera) and counted using the FIJI image analysis software. GFP fluorescence was used to detect transfected cells.

Statistics

All data is presented as mean \pm standard error of mean (SEM) of $n \geq 3$ biological replicates from independent experiments. The exact number of individual experiments is stated in the figure legends. Student's t-test or one-way ANOVA with Bonferroni's *post hoc* test (GraphPad prism) were used for calculation of p-values as indicated for each panel (ns: $p > 0.05$; *: $p \leq 0.05$, **: $p \leq 0.01$, ***: $p \leq 0.001$; ****: $p \leq 0.0001$).

RESULTS

N-Ras and H-Ras Are Activated Downstream of GPCRs in Mast Cells

First, we investigated which Ras isoforms would qualify for PI3K γ signaling in mast cells. Three Ras genes encode for four protein homologs N-Ras, H-Ras, K-Ras4A, and K-Ras4B (38). We found similar expression of N-Ras, K-Ras4B, H-Ras, and R-Ras (Ras-related protein) at the mRNA and protein level in mast cells and macrophages (Figures 1A, B). In order to estimate the relative ratio between these isoforms, we expressed codon-optimized 3 \times -HA tagged N-, K-, and H-Ras in HEK293 cells and used transfected HEK293 cell lysates as standards for protein quantification (Figures 1C, D). In BMMCs, K-Ras protein was the most abundant isoform, with expression levels twice as high as N-Ras and four times as high as H-Ras. In macrophages, N- and K-Ras levels were equal, while H-Ras was four times less abundant.

To determine which Ras isoform is activated downstream of GPCRs we performed GTP-Ras pull-down assays using the Ras-binding domain (RBD) of Raf. The C5a receptor [C5a anaphylatoxin chemotactic receptor 1 (C5AR1), CD88] expressed on macrophages responds to C5a stimulation and activates PI3K γ (14, 28). All three Ras isoforms (N-, K-, and H-Ras) were GTP-loaded after macrophage stimulation with C5a (Figures 1F, H). In mast cells, however, stimulation with adenosine activates PI3K γ downstream A3AR (4, 7).

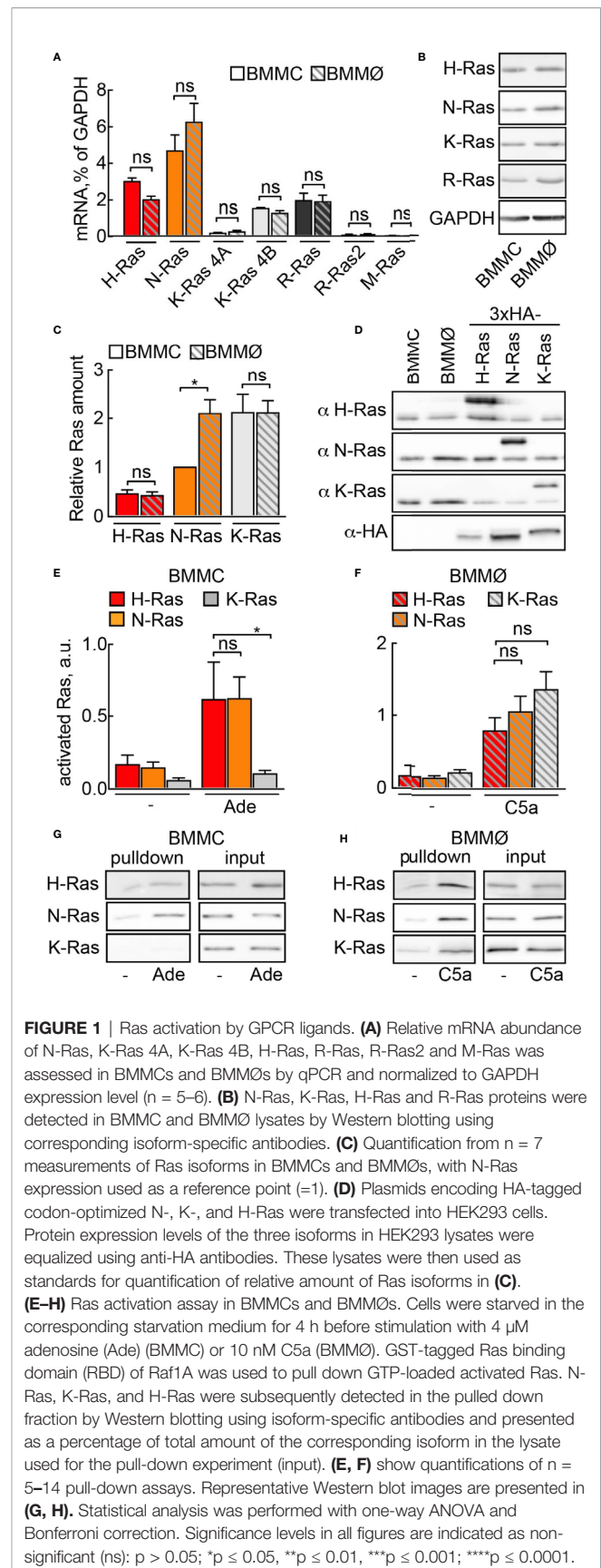


FIGURE 1 | Ras activation by GPCR ligands. (A) Relative mRNA abundance of N-Ras, K-Ras 4A, K-Ras 4B, H-Ras, R-Ras, R-Ras2 and M-Ras was assessed in BMMCs and BMM \emptyset s by qPCR and normalized to GAPDH expression level ($n = 5-6$). **(B)** N-Ras, K-Ras, H-Ras and R-Ras proteins were detected in BMMC and BMM \emptyset lysates by Western blotting using corresponding isoform-specific antibodies. **(C)** Quantification from $n = 7$ measurements of Ras isoforms in BMMCs and BMM \emptyset s, with N-Ras expression used as a reference point ($=1$). **(D)** Plasmids encoding HA-tagged codon-optimized N-, K-, and H-Ras were transfected into HEK293 cells. Protein expression levels of the three isoforms in HEK293 lysates were equalized using anti-HA antibodies. These lysates were then used as standards for quantification of relative amount of Ras isoforms in **(C)**. **(E-H)** Ras activation assay in BMMCs and BMM \emptyset s. Cells were starved in the corresponding starvation medium for 4 h before stimulation with 4 μ M adenosine (Ade) (BMMC) or 10 nM C5a (BMM \emptyset). GST-tagged Ras binding domain (RBD) of Raf1A was used to pull down GTP-loaded activated Ras. N-Ras, K-Ras, and H-Ras were subsequently detected in the pulled down fraction by Western blotting using isoform-specific antibodies and presented as a percentage of total amount of the corresponding isoform in the lysate used for the pull-down experiment (input). **(E, F)** show quantifications of $n = 5-14$ pull-down assays. Representative Western blot images are presented in **(G, H)**. Statistical analysis was performed with one-way ANOVA and Bonferroni correction. Significance levels in all figures are indicated as non-significant (ns): $p > 0.05$; * $p \leq 0.05$, ** $p \leq 0.01$, *** $p \leq 0.001$; **** $p \leq 0.0001$.

Adenosine led to the selective activation of N- and H-Ras, but not K-Ras (Figures 1E, G), suggesting that K-Ras is normally not involved in GPCR-mediated activation of PI3K γ in mast cells.

Loss of N- and H-Ras -Compensated by Upregulation of Substitute Ras Isoforms

To further study the physiologic importance of N-Ras and H-Ras isoforms for mast cell activity, we derived mast cells from N-Ras^{-/-} and H-Ras^{-/-} mouse bone marrow. Unexpectedly, neither adenosine-induced signaling to PKB/Akt (Figure 2A) nor PI3K γ -dependent migration (Figures 2B, C) or degranulation (Figure 2D) was affected in any of the analyzed genotypes.

However, quantification of Ras proteins revealed an upregulation of alternative Ras isoforms in the knock-out cells (Figure 2E). The level of K-Ras was elevated twice in N-Ras^{-/-} and H-Ras^{-/-} cells as compared to wild-type BMMCs. H-Ras showed approximately a 1.5-fold increase in N-Ras^{-/-} cells. Interestingly, N-Ras was not upregulated in H-Ras^{-/-} BMMCs. The fact that K-Ras activation occurs only significantly in the absence of N-Ras or H-Ras without any loss of cellular responsiveness illustrates the ability of K-Ras to compensate for absence of N-Ras or H-Ras (Figure 2F). Altogether this demonstrates that a major part of the GPCR signal is relayed via N-Ras and H-Ras, but that a dynamic compensatory redundancy of Ras isoforms exists in mast cells.

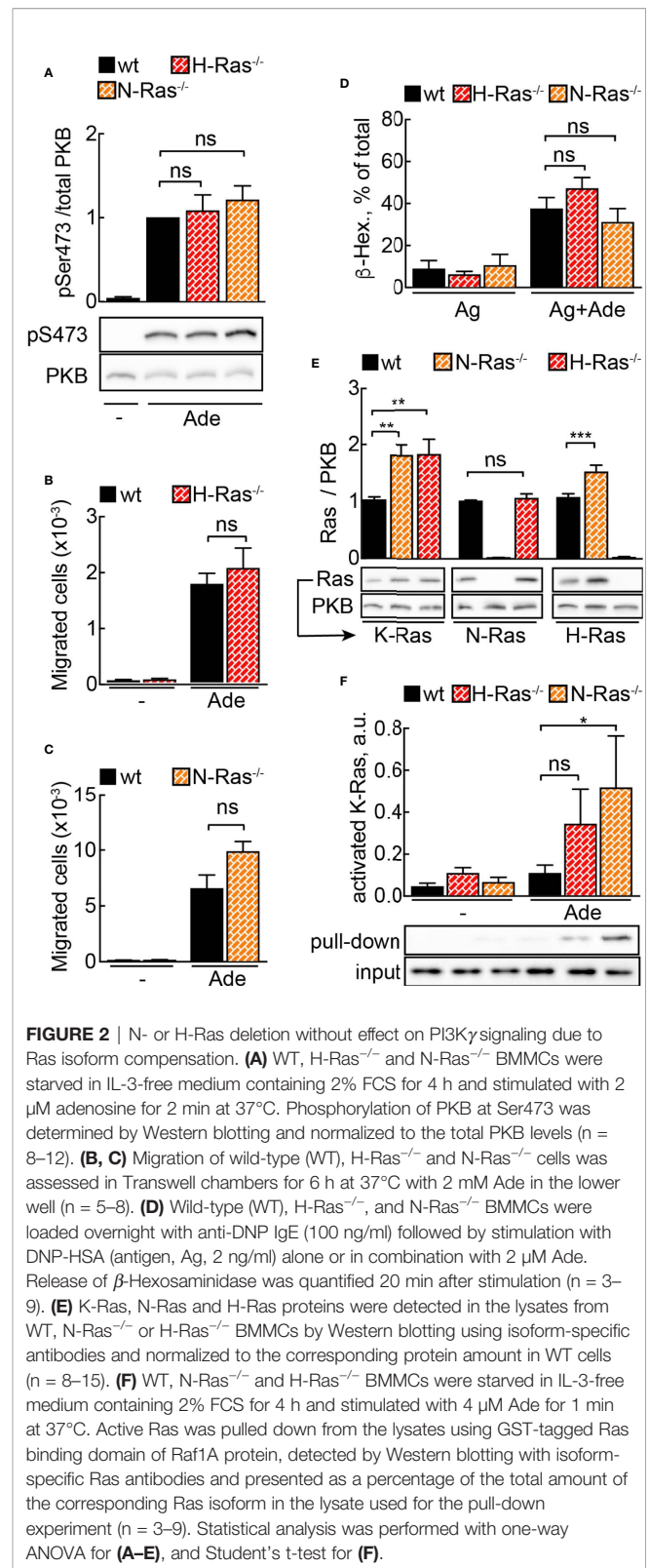
As all Ras proteins have to undergo post-translational isoprenylation to enable stable lipid membrane anchoring, the revealed redundancy between N-Ras, H-Ras, and K-Ras was not expected to interfere with the action of farnesyltransferase inhibitors (FTIs) to achieve a pharmacological Ras inhibition in mast cells.

Isoprenylation inhibitors prevent the addition of farnesyl (FTIs) or geranylgeranyl residues (GGTIs) to the CaaX box motif at the C-terminus of small GTPases, thus detaching these proteins from cell membranes (39–41). FTI-277 was used here because of its excellent selectivity for FTase over GGTase I (42).

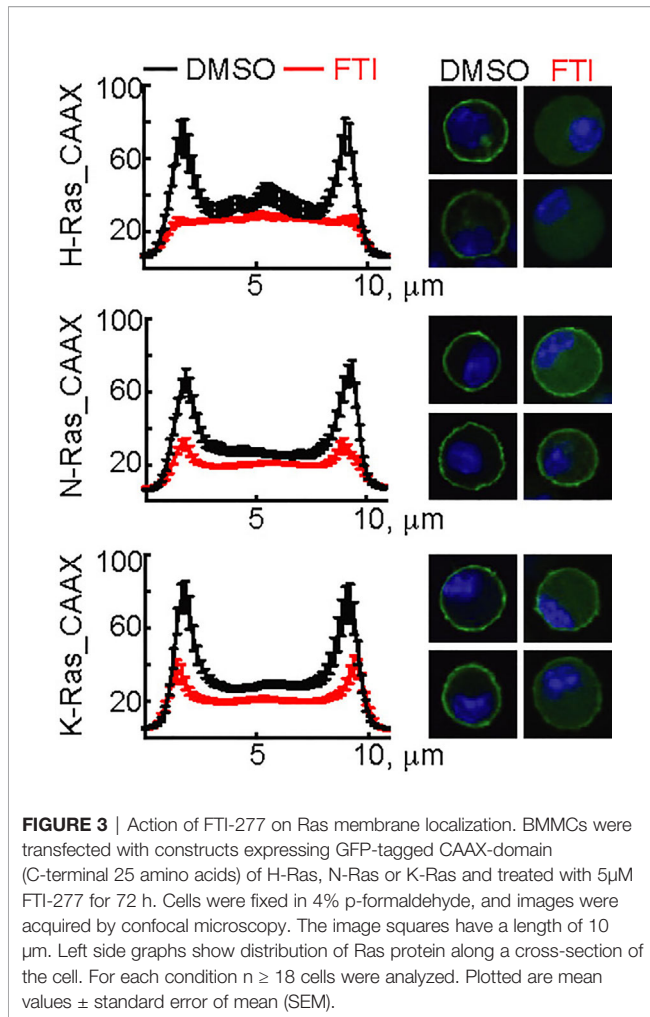
The three N-, H-, and K-Ras isoforms only differ in the 25 C-terminal amino acids containing the CaaX-box motif. To validate the action of FTI-277, GFP-constructs using the N-, H-, and K-Ras CaaX-box sequences were transfected into mast cells. FTI-277 caused delocalization of all GFP-CaaX constructs from the plasma membrane to the cytosol, resulting in complete displacement of H-Ras and reduction of N- and K-Ras in the cortical regions (Figure 3).

Subsequently, we assessed the effect of FTI-277 on Ras activation: in mast cells, adenosine-induced N-Ras activation was completely blocked, and H-Ras activation was decreased, although not statistically significant (Figures 4A, B). In macrophages, N-, H-, and K-Ras were activated upon stimulation with C5a, but here FTI-277 only inhibited activation of H-Ras (Figures 4C–E).

To determine why macrophages remained relatively insensitive towards FTI-277, expression levels of prenyltransferases before and after inhibitor exposure were determined. Treatment with FTI-277 did not cause, however, significant differences in the expression of prenyltransferases in neither macrophages nor mast cells (Figures



S2B, C). The accumulation of prelamin A confirmed that protein farnesylation was effectively blocked under the applied incubation conditions. The fact that FTI-277 had no effect on Rap1A geranyl-



geranylation, excludes that FTI-277 affected geranyl-geranylation in BMMC and BMM \emptyset (Figure S1).

Ras Inhibition With FTI-277 Leads to Reduced PI3K γ Signaling in Mast Cells

Mast cells are the main effector cells during acute IgE-dependent allergic reactions such as anaphylaxis. Activation of IgE-sensitized mast cells with allergen leads to release of inflammatory mediators from pre-formed granules. Simultaneously, *de-novo* synthesis of cytokines, chemokines, and other compounds is initiated. Importantly, secretion of TNF- α supports adhesion of rolling blood leukocytes to endothelia by upregulation of the adhesion molecule VCAM-1 (6). FTI-277 attenuated degranulation of IgE/antigen-activated mast cells upon co-stimulation with adenosine, but not with stem cell factor (SCF), which signals through c-kit and PI3K δ (Figure 5A). Furthermore, p110 γ -dependent expression of TNF- α and IL-6 was significantly decreased in mast cells co-stimulated with IgE/antigen and adenosine (Figure 5B).

Next, BMMCs and BMM \emptyset s were treated with FTI-277 (5 μ M for 72 h) to assess phosphorylation of the main PI3K downstream target PKB/Akt. To distinguish between Ras- and

Ras-independent PKB activation, BMMCs and BMM \emptyset s were stimulated with GPCR ligands after exposure to FTI-277: adenosine stimulation leads to PI3K γ activation *via* adenosine receptor A3 (A3AR, ARA3) in mast cells (4, 7), and C5a stimulates PI3K γ signaling *via* C5aR (CD88) in macrophages (14). Receptor tyrosine kinase (RTK) ligands such as SCF and macrophage colony-stimulating factor (M-CSF) served as reference for PI3K γ -independent signaling to PKB/Akt. In mast cells, FTI-277 led to a significant decrease in PKB/Akt phosphorylation at Ser473 upon activation with adenosine but had no effect on PKB/Akt activation upon stimulation with SCF. This demonstrates that the inhibitory action of FTI-277 is specific for the GPCR-mediated activation of PI3K γ (Figure 5C) but does not affect signaling through PI3K δ to PKB/Akt (43). In contrast to mast cells, Ras inhibition did not affect C5a-induced phosphorylation of PKB in macrophages (Figure 5D).

The IC₅₀ for inhibition of PKB phosphorylation by FTI-277 in adenosine-stimulated BMMCs was 1.65 μ M for pSer473 and 1.61 μ M for pThr308, and 4.76 μ M for phosphorylation of mitogen-activated protein kinase (MAPK, also known as ERK1 & 2; Figure S4). PKB phosphorylation downstream of PI3K γ is therefore more sensitive towards FTI-277 as compared to MAPK, which might be attributed to a proposed multi-step cascade activation of MAPK (44).

Chemoattractant-mediated leukocyte recruitment to inflamed tissues is initiated by GPCR engagement and PI3K γ activation. Here, we assessed the effect of Ras inhibition on mast cell and macrophage migration *in vitro* in a Transwell migration assay. In line with the results for PKB phosphorylation, only adenosine-stimulated migration of mast cells was significantly impaired by FTI-277 (Figure 5E). Meanwhile, macrophage migration toward GPCR agonist C5a, as well as the RTK ligand M-CSF remained intact (Figure 5F).

GGTI-298 Inhibits Mast Cell Activation

Other post-translational modifications such as geranyl-geranylation are known to provide lipid anchoring in membranes. Inhibition of geranyl-geranylation with GGTI-298 also interferes with PI3K γ signaling: interestingly, GGTI-298 blocked PKB phosphorylation in mast cells, but not macrophages (Figures 6A, B). Still, phosphorylation of mitogen-activated protein kinase (MAPK) was inhibited in adenosine-stimulated mast cells (Figure 6C) and macrophages exposed to C5a or M-CSF (Figure 6D). Although Ras proteins have previously not been reported to be geranyl-geranylated under normal conditions, we observed that GGTI-298 treatment causes re-localization of GFP-tagged H-Ras (Figure S3). N-Ras and K-Ras did not translocate to the cytosol under the same conditions. The specific action of GGTI-298 on geranyl-geranylation was confirmed by the accumulation of ungeranyl-geranylated Rap1A, while prelamin A did not accumulate in its non-farnesylated form in mast cells and macrophages (Figure S1).

Altogether, these results suggest that GGTI-298 does not affect PI3K γ signaling in mast cells by interference with Ras activation, but is likely to intercept upstream activation by

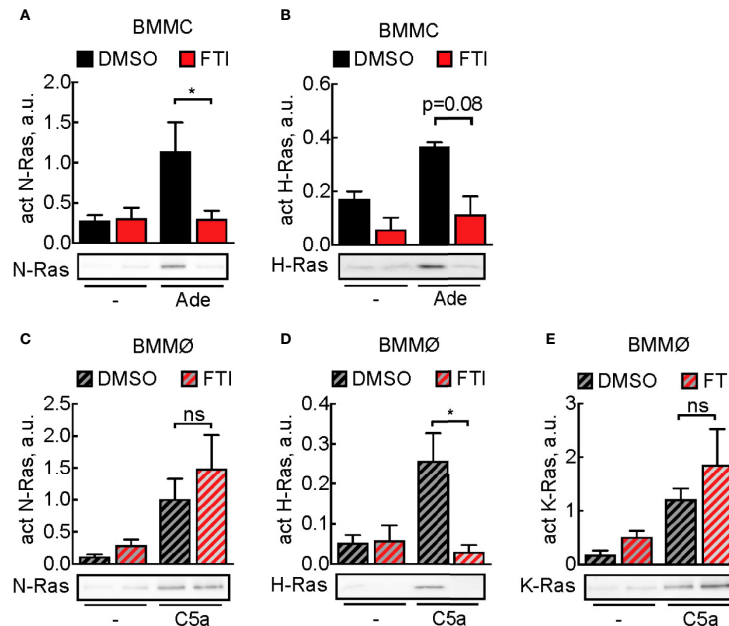


FIGURE 4 | Prevention of activation of Ras isoforms by FTI-277. **(A, B)** Effect of FTI-277 on N-Ras and H-Ras activation in BMMCs. Cells were treated with DMSO or 5 μ M FTI-277 for 72 h. Activated N-Ras and H-Ras was pulled down with GTP-Raf-RBD and normalized to Ras amount in complete cell lysate. **(C–E)** Effect of FTI-277 on N-Ras, K-Ras, and H-Ras activation in BMMØs. BMMØs cultured for 5 days were treated with DMSO or 5 μ M FTI-277 for 72 h. Every quantification contains $n = 3–6$ Ras activation assays, and one representative immunoblot is shown for each condition. Student's t-test was applied for statistical analysis.

geranyl-geranylated G γ subunit subtypes, which seems to be set up differently in macrophages.

Statins Inhibit Mast Cell Degranulation Independently of PI3K γ

Statins inhibit HMG-CoA reductase, the rate limiting enzyme of cholesterol biosynthesis, and deplete farnesyl pyrophosphate (FPP). The lack of substrate for FTase and GGTase then reduces protein farnesylation and geranyl-geranylation. It has been previously reported that statins inhibit mast cell cytokine production (45) and degranulation (46), but no mechanistic explanations are available. Recent studies have demonstrated that statins also reduce disease activity of rheumatoid arthritis (47–49), illustrating immunomodulatory effects of statins.

We therefore investigated, whether statins could interfere with the Ras-PI3K γ signal pathway and thereby elicit anti-inflammatory actions. Among the statins tested, Simvastatin and its active derivate Simvastatin Sodium Salt (Simvastatin-Na) had the most pronounced effect on mast cell degranulation (**Figure 7A**). Simvastatin-Na decreased IgE-antigen-mediated degranulation and IgE-antigen/adenosine co-stimulation in a concentration dependent fashion (**Figure 7B**). However, decreased degranulation did not correlate with changes in Ras or PI3K γ pathway activation since PKB and MAPK phosphorylation remained unaffected even at elevated concentrations of Simvastatin-Na (**Figures 7C, D**), suggesting

that Simvastatin blocks degranulation by pleiotropic action and not specific interference with PI3K γ .

Sensitivity to Ras Inhibition Is Largely Determined by PI3K γ Adaptor Subunit

PI3K γ adaptor subunits p84 and p101 are differentially expressed in various cell types of the myeloid and lymphoid lineages (5, 6, 32, 50). Mast cells express exclusively the p84 adaptor protein, while macrophages harbor both subunits. We measured messenger RNA by qPCR to compare expression of p101, p84, and p110 γ between BMMC and BMMØ (**Figure 8A**). According to qPCR data, while mast cells express only p84 subunit, p101 is the dominant adaptor protein in macrophages, with its expression level exceeding p84 by tenfold (**Figure 8A**). Next, we used recombinant p84/p110 γ and p101/p110 γ complexes to calibrate the quantification of the corresponding proteins (**Figure 8B**). BMMCs and BMMØs possess similar amounts of p110 γ ($\approx 33,000$ vs 35,000 molecules/cell). In BMMCs, the relation of p84 and p110 γ ($\approx 32,000$ and 33,000 molecules/cell) is nearly one to one, while p101 was undetectable. Meanwhile, in BMMØ the total of p101 molecules is seven times higher compared to p84 ($\approx 150,000$ vs 20,000 molecules/cell).

It was previously reported that Ras is indispensable for membrane recruitment and activation of p84/p110 γ ; but not for p101/p110 γ complexes (36). To assess if the observed difference in sensitivity to FTI-277 between mast cells and macrophages could be explained by the difference in the adaptor subunit content of

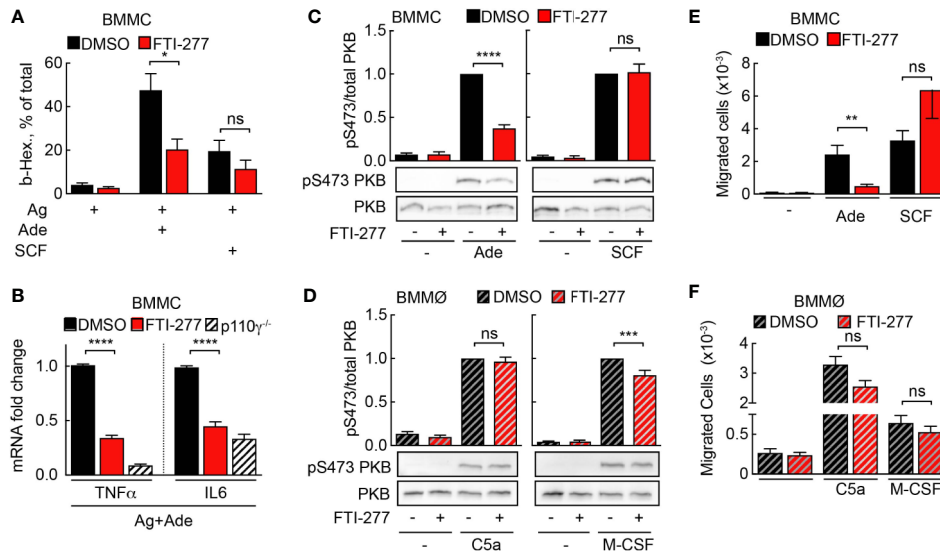


FIGURE 5 | Mast cell but not macrophage activation is affected by FTI-277-mediated Ras inhibition. **(A)** DMSO- or FTI-277-treated WT-BMMCs were loaded overnight with anti-DNP IgE (100 ng/ml) followed by stimulation with DNP-HSA (Ag, 2 ng/ml) alone or in combination with 2 μ M Ade or 10 ng/ml SCF. Release of β -Hexosaminidase was quantified 20 min after stimulation (n = 6–7). **(B)** DMSO- or FTI-277-treated WT-BMMCs as well as p110 γ ^{-/-} BMMCs were exposed overnight to anti-DNP IgE (100 ng/ml) followed by stimulation with DNP-HSA (Ag, 2 ng/ml) together with 1 μ M Ade for 6 h. TNF- α and IL-6 expressions were determined by qPCR and normalized to the level of GAPDH expression. Fold change of expression in FTI-277 treated or p110 γ ^{-/-} cells was quantified relative to DMSO-treated control (n = 6). **(C, D)** BMMCs and BMM \emptyset s were treated with either DMSO or 5 μ M FTI-277 for 72 h, starved for 4 h, and activated with 2 μ M Ade, 10 ng/ml SCF, 10 nM C5a, or 30 ng/ml M-CSF for 2 min at 37°C. Phosphorylation of PKB at Ser473 was determined by Western blot analysis of cell lysates with anti-PKB-Ser473 antibodies and normalized to the total level of PKB (n = 9–18). **(E, F)** Migration of BMMCs and BMM \emptyset s was assessed in Transwell chambers for 6 h at 37°C with indicated stimuli in the lower well, followed by quantification of migrated cells (n = 6–16). **(E, F)** were assessed with Student’s t-test and **(B–D)** were subjected to one-way ANOVA with Bonferroni’s *post hoc* test.

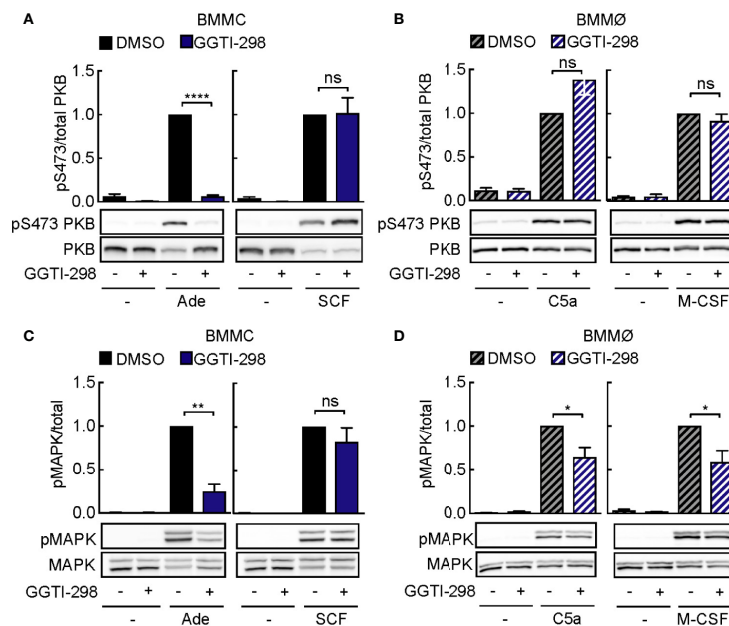


FIGURE 6 | GGTI-298 affects activation of mast cells, but not macrophages. BMMCs **(A, C)** and BMM \emptyset s **(B, D)** were treated with either DMSO or 5 μ M GGTI-298 for 24 h, starved for 4 h and activated with 2 μ M Ade, 10 ng/ml SCF, 10 nM C5a or 30 ng/ml M-CSF for 2 min at 37°C. Phosphorylation of PKB (Ser473) and MAPK was determined by immunoblot analysis of cell lysates and normalized to the total level of corresponding proteins (n = 4–10). Statistical significances were assessed by Student’s t-test.

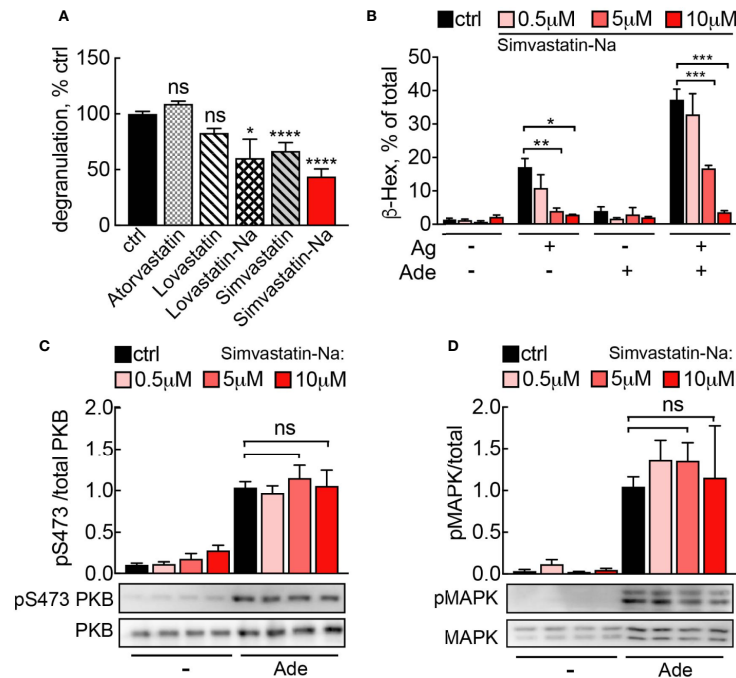


FIGURE 7 | (A) Simvastatin inhibits mast cell degranulation without interfering with PI3K γ signaling. BMDCs were treated with indicated statins at 5 μ M for 16 h and then loaded with anti-DNP IgE (100 ng/ml). The following day, cells were stimulated with DNP-HSA (Ag, 2 ng/ml) plus 2 μ M adenosine. Release of β -Hexosaminidase was quantified 20 min after stimulation and normalized to untreated control (ctrl=DMSO 0.05% for Lovastatin and Simvastatin; PBS 0.001% MetOH for Atorvastatin). Lovastatin (n = 4–7) and Simvastatin (n = 10–16) are pro-drugs, while Atorvastatin (n = 4), Simvastatin-Na (n = 10–16) and Lovastatin-Na (n = 4–7) are active drugs. **(B)** Dose dependency for Simvastatin-Na was tested in three independent experiments with total n = 9 biological replicates. Degranulation was assessed with IgE/antigen-stimulation alone (Ag, DNP-HSA 2 ng/ml) and IgE/antigen co-stimulation with adenosine (2 μ M). **(C, D)** Western blot analysis of BMDCs treated with 5 μ M Simvastatin-Na for 16 h and starved for 4 h. Adenosine (2 μ M) was used as stimulus. Phosphorylated PKB and MAPK was quantified from n = 3–9 experiments. Statistical significance was tested with one-way ANOVA applying Bonferroni correction.

these cells, we used a mast cell complementation technique described in (5): p110 γ null BMDCs lack both p110 γ and functional p84 and are ideal to complement either p84/p110 γ or p101/p110 γ complexes by nucleofection and to assess differences in signaling outputs of the two complexes in the same cellular context. We reconstituted p110 γ ^{-/-} BMDCs with p84/p110 γ or p101/p110 γ complexes and treated them with FTI-277 (**Figure 8D**). Only cells that expressed p84 as adaptor subunit exhibited significant reduction of phosphorylated PKB at Ser473. On the other hand, PI3K γ activation in cells expressing p101 adaptor protein remained insensitive to Ras inhibition. Remarkably, regardless of the adaptor protein, FTI-277 caused a significant decrease in the level of phosphorylated MAPK (**Figure 8E**). As a complementary approach for Ras inhibition, we overexpressed the GTPase-activating protein (GAP) domain of neurofibromin 1 (NF1) together with p84/p110 γ or p101/p110 γ in p110 γ ^{-/-} BMDCs. The ability of cells to migrate towards chemoattractant was then tested in a Transwell migration assay (**Figure 8C**). Like the effect of FTI-277 on PKB phosphorylation, only p84/p110 γ containing cells lost their migratory potential after NF1 overexpression, while migration of cells expressing p101 was insensitive to Ras inactivation.

Since FTI-277 potentially affects all farnesylated proteins and does not specifically target Ras, we further excluded the

possibility that the observed inhibitory action of FTI-277 on PI3K γ signaling is a result of impaired G-protein processing and functioning. Farnesylation of G γ and palmitoylation of G α subunits of heterotrimeric G-proteins are vital for proper GPCR signal transduction (51). In mast cells, only G α i-coupled GPCRs, such as adenosine A3 receptor (A3AR), have been reported to activate PI3K γ (4). G α q-coupled platelet-activating factor (PAF-) receptor triggers, however, calcium release from internal stores and phosphorylation of cyclic AMP-responsive element-binding protein (CREB) independent from PI3K γ (1). Treatment with FTI-277 had no effect on PAF-stimulated CREB phosphorylation in mast cells and macrophages (**Figure S5**), showing that trimeric G-protein activity remains intact upstream of PI3K γ .

DISCUSSION

RAS Isoforms Involved in Mast Cell Activation

The importance of Ras signaling in IgE-dependent mast cell activation has been demonstrated earlier, but the nature of downstream events has remained obscured: it has been observed that the deletion of RabGEF1 leads to the overactivation of Ras

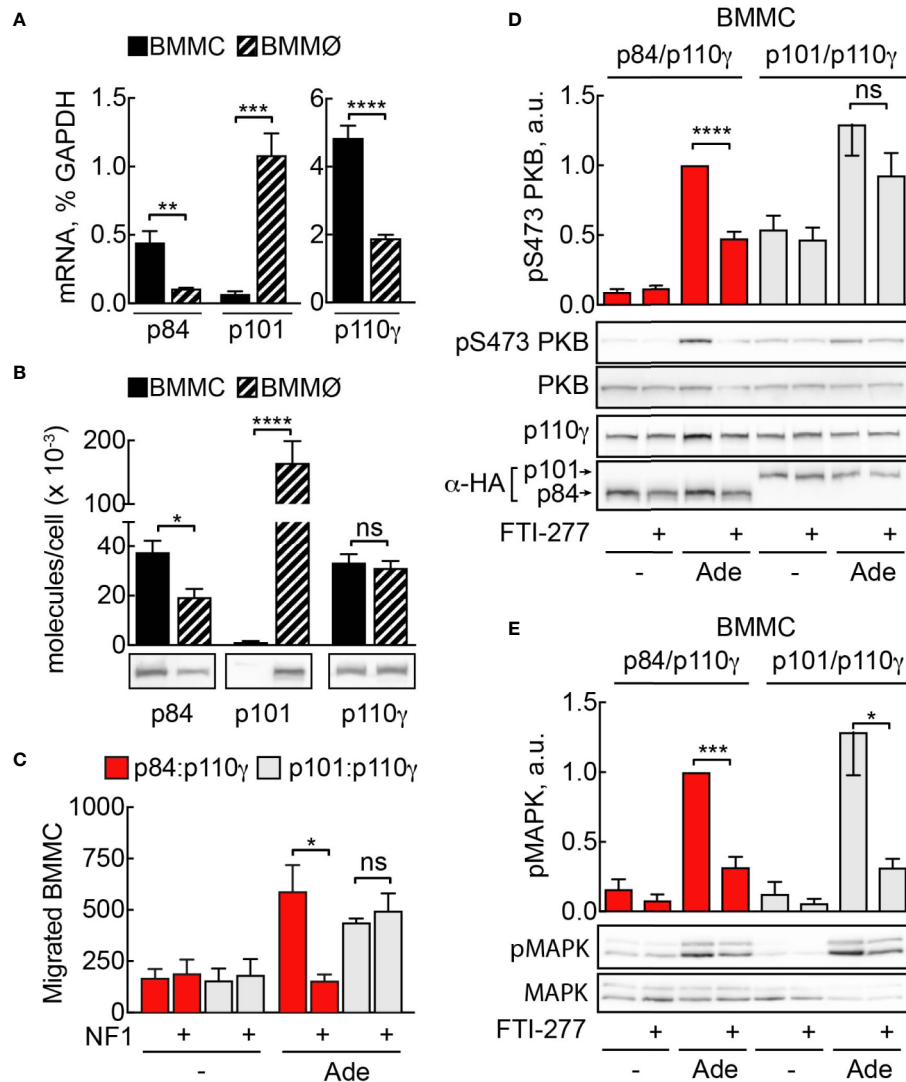


FIGURE 8 | Sensitivity to Ras inhibition is defined by PI3K γ adaptor subunit. **(A)** Expression of p110 γ , p84, and p101 in BMMCs and BMMØs was assessed by qPCR and normalized to GAPDH expression in BMMCs. **(B)** p84, p101, and p110 γ proteins were detected in BMMC and BMMØ lysates by Western blotting and quantified using recombinant p84/p110 γ and p101/p110 γ complexes with known protein concentration. **(C)** p110 γ and HA-p84 or HA-p101 were co-expressed with or without Flag-NF1 (GAP domain) in p110 γ ^{-/-} BMMCs; additionally, GFP-expressing plasmid was used to select for transfected cells. Migration of GFP-positive BMMCs was assayed in Transwell chambers for 6 h in the presence of 2 μ M Ade in the lower well. Subsequently, GFP-positive cells were quantified by fluorescence microscopy. The panel contains $n = 5$ biological replicates from two independent experiments. **(D, E)** p110 γ ^{-/-} BMMCs were transfected with plasmids encoding functional p110 γ and either HA-tagged p84 or p101. 5 h after transfection cells were put in fresh medium containing DMSO or 5 μ M FTI-277. The next day, cells were starved in IL-3-free medium containing 2% FCS and stimulated with 2 μ M Ade for 2 min at 37°C. Phosphorylation of PKB at Ser473 and MAPK was determined by Western blotting and normalized to the total PKB or MAPK levels, correspondingly. Transient expression of p110 γ was assessed with anti-p110 γ antibodies, while p84 and p101 were detected with anti-HA antibodies ($n = 5-6$). Student's t-test was performed to test for statistical relationships.

and thus causes mast cell hyperresponsiveness towards Fc ϵ RI stimulation and results in severe skin inflammation with an accumulation of tissue mast cells in mice (52). Constitutive Ras activation due to deficiency of neurofibromin 1 (NF1) on the other hand, leads to hyperproliferation of mast cell-rich neurofibromas, in a situation where RTK signaling seems to dominate Ras activation (53). The importance of GPCR-induced Ras activation in mast cells however, has barely been explored, despite the physiological implications for mast cell chemotaxis

and synergism with Fc ϵ RI activation during degranulation (9). PI3K γ in mast cells is a downstream effector of Ras and GPCRs. In the present study we exploited Ras-PI3K γ interactions as a proof-of-concept strategy for a cell-specific regulation of PI3K γ activity.

Among the seven Ras isoforms that were previously shown to interact and activate PI3Ks (N-, H-, K4A-, K4B-, R-, R1, and M-Ras (54), only N-Ras and H-Ras were found to be activated downstream of GPCRs in mast cells. N- and H-Ras, but not K-Ras, were previously reported to be associated with cholesterol-

rich lipid raft domains at the plasma membrane (55). Their activation downstream of the GPCR is, therefore, in line with the lipid-raft associated activation of p84/p110 γ complex (5). H-Ras has been proposed to be mainly localized to lipid rafts in inactive GDP-bound state and to be redistributed to non-raft microdomains of plasma membrane upon its activation (56, 57), making N-Ras the most probable candidate for p84/p110 γ activation at the plasma membrane. However, recent studies using artificial lipid bilayer models show that in the absence of scaffolding proteins also N-Ras relocates from rafts to disordered lipid domains when switching to a GTP-bound, active state (58). But naturally, the plasma membrane of intact cells provides a very different environment that potentially contains interacting scaffolds. One possibility is that p110 γ itself directs Ras to dedicated membrane microdomains. One could speculate that p110 γ /p84 complex formation induces a conformational change that favors Ras binding. Analogously, allosteric effects in p110 γ upon p101 binding have previously been proposed to increase G $\beta\gamma$ affinity (59), thus minimizing the need for Ras to achieve membrane recruitment of PI3K γ .

Nonetheless, altering p110 γ affinity towards Ras does not fully explain the isoform preference we observed in mast cells. Despite not being activated in wild-type mast cells, K-Ras has been activated and recruited in N-Ras^{-/-} and H-Ras^{-/-} BMMCs to restore PI3K γ signaling. Consequently, N-Ras^{-/-} and H-Ras^{-/-} BMMCs showed no impairment in PI3K γ dependent degranulation, migration, and phosphorylation of PKB. This observation clearly argues for overlapping functions of Ras isoforms present in mast cells. It remains uncertain how K-Ras is engaged only in the absence of H-Ras and N-Ras in mast cells, while in WT macrophages N-Ras, H-Ras, and K-Ras are all activated downstream of C5a stimulation.

Pharmacologic Inhibition of Ras With FTI, GGTI, and Statins

Pharmacologic Ras inhibition with FTI-277 diminished N-Ras activation in mast cells but did not impact N-Ras and K-Ras activation in macrophages. In the case of H-Ras, we observed reduced activation in both cell types (BMMC $p = 0.0863$, BMM \emptyset $p = 0.0241$). Alternative geranyl-geranylation of N-Ras and K-Ras in the presence of FTI-277 could have provided a hypothetical explanation for insensitivity of macrophages towards the inhibitor. According to our qPCR data, macrophages express less FTase, as well as GGTase compared to mast cells, and these expression levels were not influenced by FTI-277. This does not support the assumption that macrophages need higher dosage of FTI treatment to cope with higher amounts of FTase, neither that geranyl-geranylation is more efficient in macrophages than in mast cells. Another hypothesis is that varying half-life of Ras proteins in different cells might explain the differential susceptibility to farnesyltransferase inhibitors.

FTI-277 blocks protein farnesylation in macrophages as well as in mast cells, as controlled by accumulation of prelamin A. It is

expected that farnesylated proteins other than Ras are also malfunctioning under FTI-277 treatment. Three subtypes of G γ subunits, G γ 1, G γ 8, and G γ 11 of trimeric G-proteins are farnesylated (51). Phosphorylation of CREB in cells stimulated with platelet activating factor (PAF) however, was not attenuated (Figure S4). This demonstrates that G α q containing trimeric G-protein functions are intact. It is therefore unlikely that insufficient processing of G γ subunits in FTI-277 treated cells cause defective GPCR to PI3K γ signaling. Altogether, it appears that Ras functions are conserved more strictly in macrophages, ensuring proper host defense. Further mechanistic studies are needed to elucidate the mechanism behind the resistance of Ras proteins to FTIs in macrophages, and whether it could be used for developing strategies for cell-specific Ras targeting. Yet, a recent study by Bratt et al. (60) found that FTI-277 unexpectedly worsened asthmatic airway changes in mice instead of ameliorating them. The authors examined Ras localization in bronchial epithelial cells but did not see translocation from membrane-bound to cytosolic state. Instead, accumulation of farnesyl pyrophosphate (FPP) under FTI treatment turned out to exacerbate allergic asthma. Thus, *in vivo* FTI-277 does not act as cell-type specific agent and more importantly, did not show clinical benefits against allergic asthma.

Although Ras is not known to be geranyl-geranylated in the absence of FTIs, we observed reduced H-Ras membrane localization upon treatment with GGTI-298. We also found that inhibition of geranyl-geranylation with GGTI-298 impacted PI3K γ signaling. This indicates that non-Ras proteins likely affirm different sensitivity of mast cells and macrophages towards GGTIs (and FTIs) as well.

Rab proteins are geranyl-geranylated small GTPases. Rab5 in particular delivers H-Ras from the cell membrane to recycling endosomes (61, 62). Still, the di-cysteine motif in Rab5's C-terminus is modified by GGTase II (also known as Rab geranyl-geranyl transferase, RGGT) and is not expected to malfunction under treatment with the GGTase I-specific GGTI-298 (63). Several G γ subunit subtypes (G γ 2–5, 7, 9, 10, 12 and 13) are geranyl-geranylated by GGTase I and therefore likely fail to operate as relay from GPCR to PKB after GGTI-298 exposure. Despite the finding that macrophages are more resistant to GGTI-298 than mast cells, inhibition of the majority of G γ proteins is not a viable therapeutic approach for cell-selective PI3K γ inactivation.

Overall, clinical translation of prenylation inhibitors to mast cell targeted therapy is currently complicated by insufficient potency and side-effects of FTIs and GGTIs in clinical trials (64). However, inhibition of protein prenylation has previously also been postulated for statins, a class of clinically tolerable inhibitors that deplete FPP and thus lower protein prenylation. In an effort to translate our findings into therapeutic application we treated mast cells with Simvastatin, Lovastatin and Atorvastatin. Despite effective inhibition of mast cell degranulation by Simvastatin, PI3K γ signaling to PKB/Akt was preserved. Hence, the mast cell stabilizing effect of statins is of different nature than FTI-277 and GGTI-298 effects.

Mast Cell Specific PI3K γ Targeting via p84 and Ras

From the discovery of the second possible adaptor subunit for PI3K γ (32), the questions regarding the physiological importance of having two regulatory proteins for PI3K γ were arising. In the recent years it has become evident that p84 and p101 are non-redundant and confer specific properties to PI3K γ that result in diverse cellular responses. Different outputs triggered by two complexes are most likely explained by differences in the spatiotemporal distribution of PtdIns(3,4,5)P₃ derived from either p101/p110 γ or p84/p110 γ (5). Ras was shown to be indispensable for membrane recruitment and activation of p84/p110 γ , but not p101/p110 γ complexes (36). Ras, therefore, could contribute to the differential coupling of PI3K γ heterodimers to downstream responses by ensuring their distribution to dedicated membrane compartments.

The two regulatory proteins p84 and p101 are not equally distributed in PI3K γ expressing cells. The fact that p110 γ ^{-/-} mast cells reconstituted with p101/p110 γ were resistant to Ras inhibition, while p84/p110 γ mediated PI3K γ pathway was inhibited pharmacologically as well as by overexpression of GAP-domain of NF1, shows that PI3K γ adaptor subunit is a major factor explaining differential sensibility towards FTIs of p101 and p84 dominated cells. Consequently, macrophages/monocytes with an abundance of p101 adaptor protein (\approx 150,000 molecules/cell, \approx 90% of all adaptor protein) are spared by FTIs. On the other hand, in cells with a predominant expression of p84 adaptor subunit such as mast cells, PI3K γ -dependent responses are susceptible to modulation of Ras signaling.

It was suggested previously that free monomeric p101 is unstable and undergoes cytosolic degradation (65). Therefore, we were surprised to detect sixfold higher abundance of p101 compared to p110 γ in macrophages. Excess of p101 exogenously expressed was previously shown to localize to the nucleus (66). A surplus of p101 over p110 γ and p84 in macrophages might favor p101/p110 γ complex formation even in presence of p84.

Overall, the dominance of p84/p110 γ complex clearly renders mast cells Ras dependent. But the currently available pharmacological inhibitors, such as FTI-277 or statins, act pleiotropically and cannot be pursued as cell-specific targeting strategy. Cell type specific modulation of PI3K γ might be achieved by interference with p110 γ -adaptor protein complex formation in the future. The development of specific p84/p110 γ targeting strategies for mast cell-related diseases will presumably have limited effects on macrophages and other p101-dominated leukocytes, thus better preserving a proper host defense as compared to PI3K γ ATP-site inhibitors.

REFERENCES

1. Brown JM, Wilson TM, Metcalfe DD. The mast cell and allergic diseases: role in pathogenesis and implications for therapy. *Clin Exp Allergy* (2008) 38:4–18. doi: 10.1111/j.1365-2222.2008.03000.x
2. Kraft S, Kinet JP. New developments in Fc ϵ RI regulation, function and inhibition. *Nat Rev Immunol* (2007) 7:365–78. doi: 10.1038/nri2072
3. Mukai K, Tsai M, Saito H, Galli SJ. Mast cells as sources of cytokines, chemokines, and growth factors. *Immunol Rev* (2018) 282:121–50. doi: 10.1111/imr.12634

DATA AVAILABILITY STATEMENT

All datasets presented in this study are included in the article/**Supplementary Material**.

ETHICS STATEMENT

The animal study was reviewed and approved by Swiss Federal Veterinary Office (SFVO) and the Cantonal Veterinary Office of Basel-Stadt (license number 2143).

AUTHOR CONTRIBUTIONS

JJ, EG, AX, TB, and JV performed experiments. JJ, EG, AX, TB, and MW analyzed data, wrote the manuscript and contributed conceptually. All authors contributed to the article and approved the submitted version.

FUNDING

This work was funded by the Swiss National Science Foundation (SNF) grants 310030_153211 and 310030_189065. JJ received a Swiss Cancer Research Foundation grant (MD-PhD-3916-06-2016). EG was supported by a Marie Curie Fellowship 255070 PI3KACT and the Peter & Traudl Engelhorn Foundation.

ACKNOWLEDGMENTS

Preliminary conclusions and parts of the content of this manuscript have been published as part of the Ph.D. thesis of Fabrizio Botindari (67), and will be incorporated in a doctoral thesis of JJ (68) (not accessible in full text).

SUPPLEMENTARY MATERIAL

The Supplementary Material for this article can be found online at: <https://www.frontiersin.org/articles/10.3389/fimmu.2020.585070/full#supplementary-material>

4. Laffargue M, Calvez R, Finan P, Trifileff A, Barbier M, Altruda F, et al. Phosphoinositide 3-kinase gamma is an essential amplifier of mast cell function. *Immunity* (2002) 16:441–51. doi: 10.1016/S1074-7613(02)00282-0
5. Bohnacker T, Marone R, Collmann E, Calvez R, Hirsch E, Wymann MP. PI3Kgamma adaptor subunits define coupling to degranulation and cell motility by distinct PtdIns(3,4,5)P₃ pools in mast cells. *Sci Signal* (2009) 2:ra27. doi: 10.1126/scisignal.2000259
6. Collmann E, Bohnacker T, Marone R, Dawson J, Rehberg M, Stringer R, et al. Transient targeting of phosphoinositide 3-kinase acts as a roadblock in mast

- cells' route to allergy. *J Allergy Clin Immunol* (2013) 132:959–68. doi: 10.1016/j.jaci.2013.03.008
7. Tilley SL, Wagoner VA, Salvatore CA, Jacobson MA, Koller BH. Adenosine and inosine increase cutaneous vasopermeability by activating A(3) receptors on mast cells. *J Clin Invest* (2000) 105:361–7. doi: 10.1172/JCI8253
 8. Walser R, Burke JE, Gogvadze E, Bohnacker T, Zhang X, Hess D, et al. PKC β phosphorylates PI3K γ to activate it and release it from GPCR control. *PLoS Biol* (2013) 11:e1001587. doi: 10.1371/journal.pbio.1001587
 9. Kuehn HS, Gilfillan AM. G protein-coupled receptors and the modification of Fc ϵ RI-mediated mast cell activation. *Immunol Lett* (2007) 113:59–69. doi: 10.1016/j.imlet.2007.08.007
 10. Thomas MJ, Smith A, Head DH, Milne L, Nicholls A, Pearce W, et al. Airway inflammation: chemokine-induced neutrophilia and the class I phosphoinositide 3-kinases. *Eur J Immunol* (2005) 35:1283–91. doi: 10.1002/eji.200425634
 11. Thomas M, Edwards MJ, Sawicka E, Duggan N, Hirsch E, Wymann MP, et al. Essential role of phosphoinositide 3-kinase gamma in eosinophil chemotaxis within acute pulmonary inflammation. *Immunology* (2009) 126:413–22. doi: 10.1111/j.1365-2567.2008.02908.x
 12. Lionetti V, Lisi A, Patrucco E, De Giuli P, Milazzo MG, Ceci S, et al. Lack of phosphoinositide 3-kinase-gamma attenuates ventilator-induced lung injury. *Crit Care Med* (2006) 34:134–41. doi: 10.1097/01.CCM.0000190909.70601.2C
 13. Takeda M, Ito W, Tanabe M, Ueki S, Kato H, Kihara J, et al. Allergic airway hyperresponsiveness, inflammation, and remodeling do not develop in phosphoinositide 3-kinase gamma-deficient mice. *J Allergy Clin Immunol* (2009) 123:805–12. doi: 10.1016/j.jaci.2008.11.047
 14. Hirsch E, Katanaev VL, Garlanda C, Azzolino O, Pirola L, Silengo L, et al. Central role for G protein-coupled phosphoinositide 3-kinase gamma in inflammation. *Science* (2000) 287:1049–53. doi: 10.1126/science.287.5455.1049
 15. Sasaki T, Irie-Sasaki J, Jones RG, Oliveira-dos-Santos AJ, Stanford WL, Bolon B, et al. Function of PI3Kgamma in thymocyte development, T cell activation, and neutrophil migration. *Science* (2000) 287:1040–6. doi: 10.1126/science.287.5455.1040
 16. Li Z, Jiang H, Xie W, Zhang Z, Smrcka AV, Wu D. Roles of PLC-beta2 and -beta3 and PI3Kgamma in chemoattractant-mediated signal transduction. *Science* (2000) 287:1046–9. doi: 10.1126/science.287.5455.1046
 17. Del Prete A, Vermi W, Dander E, Otero K, Barberis L, Luini W, et al. Defective dendritic cell migration and activation of adaptive immunity in PI3Kgamma-deficient mice. *EMBO J* (2004) 23:3505–15. doi: 10.1038/sj.emboj.7600361
 18. Wymann MP, Sozzani S, Altruda F, Mantovani A, Hirsch E. Lipids on the move: phosphoinositide 3-kinases in leukocyte function. *Immunol Today* (2000) 21:260–4. doi: 10.1016/S0167-5699(00)01649-2
 19. Ferguson GJ, Milne L, Kulkarni S, Sasaki T, Walker S, Andrews S, et al. PI(3)Kgamma has an important context-dependent role in neutrophil chemokinesis. *Nat Cell Biol* (2007) 9:86–91. doi: 10.1038/ncb1517
 20. Camps M, Rückle T, Ji H, Ardisson V, Rintelen F, Shaw J, et al. Blockade of PI3Kgamma suppresses joint inflammation and damage in mouse models of rheumatoid arthritis. *Nat Med* (2005) 11:936–43. doi: 10.1038/nm1284
 21. Lupia E, Goffi A, De Giuli P, Azzolino O, Bosco O, Patrucco E, et al. Ablation of phosphoinositide 3-kinase-gamma reduces the severity of acute pancreatitis. *Am J Pathol* (2004) 165:2003–11. doi: 10.1016/S0002-9440(10)63251-8
 22. Barber DF, Bartolomé A, Hernandez C, Flores JM, Redondo C, Fernandez-Arias C, et al. PI3Kgamma inhibition blocks glomerulonephritis and extends lifespan in a mouse model of systemic lupus. *Nat Med* (2005) 11:933–5. doi: 10.1038/nm1291
 23. Chang JD, Sukhova GK, Libby P, Schwartz E, Lichtenstein AH, Field SJ, et al. Deletion of the phosphoinositide 3-kinase p110gamma gene attenuates murine atherosclerosis. *Proc Natl Acad Sci USA* (2007) 104:8077–82. doi: 10.1073/pnas.0702663104
 24. Fougerat A, Gayral S, Gourdy P, Schambourg A, Rückle T, Schwarz MK, et al. Genetic and pharmacological targeting of phosphoinositide 3-kinase-gamma reduces atherosclerosis and favors plaque stability by modulating inflammatory processes. *Circulation* (2008) 117:1310–7. doi: 10.1161/CIRCULATIONAHA.107.720466
 25. Gayral S, Garnotel R, Castaing-Berthou A, Blaise S, Fougerat A, Berge E, et al. Elastin-derived peptides potentiate atherosclerosis through the immune Neu1-PI3K pathway. *Cardiovasc Res* (2014) 102:118–27. doi: 10.1093/cvr/cvt336
 26. Patrucco E, Notte A, Barberis L, Selvetella G, Maffei A, Brancaccio M, et al. PI3Kgamma modulates the cardiac response to chronic pressure overload by distinct kinase-dependent and -independent effects. *Cell* (2004) 118:375–87. doi: 10.1016/j.cell.2004.07.017
 27. Becattini B, Marone R, Zani F, Arsenijevic D, Seydoux J, Montani JP, et al. PI3K γ within a nonhematopoietic cell type negatively regulates diet-induced thermogenesis and promotes obesity and insulin resistance. *Proc Natl Acad Sci USA* (2011) 108:E854–63. doi: 10.1073/pnas.1106698108
 28. Jones GE, Prigmore E, Calvez R, Hogan C, Dunn GA, Hirsch E, et al. Requirement for PI 3-kinase gamma in macrophage migration to MCP-1 and CSF-1. *Exp Cell Res* (2003) 290:120–31. doi: 10.1016/S0014-4827(03)00318-5
 29. Barberis L, Pasquali C, Bertschy-Meier D, Cuccurullo A, Costa C, Ambrogio C, et al. Leukocyte transmigration is modulated by chemokine-mediated PI3Kgamma-dependent phosphorylation of vimentin. *Eur J Immunol* (2009) 39:1136–46. doi: 10.1002/eji.200838884
 30. Garcia CC, Tavares LP, Dias ACF, Kehdy F, Alvarado-Arnez LE, Queiroz-Junior CM, et al. Phosphatidylinositol 3 Kinase-Gamma Balances Antiviral and Inflammatory Responses During Influenza A H1N1 Infection: From Murine Model to Genetic Association in Patients. *Front Immunol* (2018) 9:975. doi: 10.3389/fimmu.2018.00975
 31. Nobs SP, Schneider C, Heer AK, Huotari J, Helenius A, Kopf M. PI3K γ Is Critical for Dendritic Cell-Mediated CD8+ T Cell Priming and Viral Clearance during Influenza Virus Infection. *PLoS Pathog* (2016) 12:e1005508. doi: 10.1371/journal.ppat.1005508
 32. Suires S, Coadwell J, Ferguson GJ, Davidson K, Hawkins P, Stephens L. p84, a new Gbetagamma-activated regulatory subunit of the type IB phosphoinositide 3-kinase p110gamma. *Curr Biol* (2005) 15:566–70. doi: 10.1016/j.cub.2005.02.020
 33. Stephens LR, Eguinoa A, Erdjument-Bromage H, Lui M, Cooke F, Coadwell J, et al. The G beta gamma sensitivity of a PI3K is dependent upon a tightly associated adaptor, p101. *Cell* (1997) 89:105–14. doi: 10.1016/S0092-8674(00)80187-7
 34. Deladeriere A, Gambardella L, Pan D, Anderson KE, Hawkins PT, Stephens LR. The regulatory subunits of PI3K gamma control distinct neutrophil responses. *Sci Signal* (2015) 8:ra8. doi: 10.1126/scisignal.2005564
 35. Suires S, Condliffe AM, Ferguson GJ, Ellison CD, Guillou H, Davidson K, et al. Gbetagamma and the Ras binding domain of p110gamma are both important regulators of PI(3)Kgamma signalling in neutrophils. *Nat Cell Biol* (2006) 8:1303–9. doi: 10.1038/ncb1494
 36. Kurig B, Shymanets A, Bohnacker T, Prajwal, Brock C, Ahmadian MR, et al. Ras is an indispensable coregulator of the class IB phosphoinositide 3-kinase p87/p110gamma. *Proc Natl Acad Sci USA* (2009) 106:20312–7. doi: 10.1073/pnas.0905506106
 37. Ise K, Nakamura K, Nakao K, Shimizu S, Harada H, Ichise T, et al. Targeted deletion of the H-ras gene decreases tumor formation in mouse skin carcinogenesis. *Oncogene* (2000) 19:2951–6. doi: 10.1038/sj.onc.1203600
 38. Nakamura K, Ichise H, Nakao K, Hata T, Otani H, Sakagami H, et al. Partial functional overlap of the three ras genes in mouse embryonic development. *Oncogene* (2008) 27:2961–8. doi: 10.1038/sj.onc.1210956
 39. Gibbs JB, Oliff A. The potential of farnesyltransferase inhibitors as cancer chemotherapeutics. *Annu Rev Pharmacol Toxicol* (1997) 37:143–66. doi: 10.1146/annurev.pharmtox.37.1.143
 40. Baines AT, Xu D, Der CJ. Inhibition of Ras for cancer treatment: the search continues. *Future Med Chem* (2011) 3:1787–808. doi: 10.4155/fmc.11.121
 41. Cox AD, Der CJ, Philips MR. Targeting RAS Membrane Association: Back to the Future for Anti-RAS Drug Discovery. *Clin Cancer Res* (2015) 21:1819–27. doi: 10.1158/1078-0432.CCR-14-3214
 42. Lerner EC, Qian Y, Blaskovich MA, Fossum RD, Vogt A, Sun J, et al. Ras CAAX peptidomimetic FTI-277 selectively blocks oncogenic Ras signaling by inducing cytoplasmic accumulation of inactive Ras-Raf complexes. *J Biol Chem* (1995) 270:26802–6. doi: 10.1074/jbc.270.45.26802
 43. Ali K, Bilancio A, Thomas M, Pearce W, Gilfillan AM, Tkaczyk C, et al. Essential role for the p110delta phosphoinositide 3-kinase in the allergic response. *Nature* (2004) 431:1007–11. doi: 10.1038/nature02991
 44. Hirasawa N, Scharenberg A, Yamamura H, Beaven MA, Kinet JP. A requirement for Syk in the activation of the microtubule-associated protein kinase/

- phospholipase A2 pathway by Fc epsilon R1 is not shared by a G protein-coupled receptor. *J Biol Chem* (1995) 270:10960–7. doi: 10.1074/jbc.270.18.10960
45. Kagami S, Kanari H, Suto A, Fujiwara M, Ikeda K, Hirose K, et al. HMG-CoA reductase inhibitor simvastatin inhibits proinflammatory cytokine production from murine mast cells. *Int Arch Allergy Immunol* (2008) 146(Suppl 1):61–6. doi: 10.1159/000126063
 46. Krauth MT, Majlesi Y, Sonneck K, Samorapompichit P, Ghannadan M, Hauswirth AW, et al. Effects of various statins on cytokine-dependent growth and IgE-dependent release of histamine in human mast cells. *Allergy* (2006) 61:281–8. doi: 10.1111/j.1398-9995.2006.00997.x
 47. McCarey DW, McInnes IB, Madhok R, Hampson R, Scherbakov O, Ford I, et al. Trial of Atorvastatin in Rheumatoid Arthritis (TARA): double-blind, randomised placebo-controlled trial. *Lancet* (2004) 363:2015–21. doi: 10.1016/S0140-6736(04)16449-0
 48. Tikiz C, Utuk O, Pirildar T, Bayturan O, Bayindir P, Taneli F, et al. Effects of Angiotensin-converting enzyme inhibition and statin treatment on inflammatory markers and endothelial functions in patients with longterm rheumatoid arthritis. *J Rheumatol* (2005) 32:2095–101.
 49. Okamoto H, Koizumi K, Kamitsuji S, Inoue E, Hara M, Tomatsu T, et al. Beneficial action of statins in patients with rheumatoid arthritis in a large observational cohort. *J Rheumatol* (2007) 34:964–8.
 50. Shymanets A, Prajwal K, Bucher, Beer-Hammer S, Harteneck C, Nürnberg B. p87 and p101 subunits are distinct regulators determining class IB phosphoinositide 3-kinase (PI3K) specificity. *J Biol Chem* (2013) 288:31059–68. doi: 10.1074/jbc.M113.508234
 51. McCudden CR, Hains MD, Kimple RJ, Siderovski DP, Willard FS. G-protein signaling: back to the future. *Cell Mol Life Sci* (2005) 62:551–77. doi: 10.1007/s00018-004-4462-3
 52. Tam SY, Tsai M, Snouwaert JN, Kalesnikoff J, Scherrer D, Nakae S, et al. RabGEF1 is a negative regulator of mast cell activation and skin inflammation. *Nat Immunol* (2004) 5:844–52. doi: 10.1038/ni1093
 53. Ingram DA, Hiatt K, King AJ, Fisher L, Shivakumar R, Derstine C, et al. Hyperactivation of p21(ras) and the hematopoietic-specific Rho GTPase, Rac2, cooperate to alter the proliferation of neurofibromin-deficient mast cells in vivo and in vitro. *J Exp Med* (2001) 194:57–69. doi: 10.1084/jem.194.1.57
 54. Yang HW, Shin MG, Lee S, Kim JR, Park WS, Cho KH, et al. Cooperative activation of PI3K by Ras and Rho family small GTPases. *Mol Cell* (2012) 47:281–90. doi: 10.1016/j.molcel.2012.05.007
 55. Parker JA, Mattos C. The Ras-Membrane Interface: Isoform-specific Differences in The Catalytic Domain. *Mol Cancer Res* (2015) 13:595–603. doi: 10.1158/1541-7786.MCR-14-0535
 56. Rotblat B, Prior IA, Muncke C, Parton RG, Kloog Y, Henis YII, et al. Three separable domains regulate GTP-dependent association of H-ras with the plasma membrane. *Mol Cell Biol* (2004) 24:6799–810. doi: 10.1128/MCB.24.15.6799-6810.2004
 57. Prior IA, Muncke C, Parton RG, Hancock JF. Direct visualization of Ras proteins in spatially distinct cell surface microdomains. *J Cell Biol* (2003) 160:165–70. doi: 10.1083/jcb.200209091
 58. Shishina AK, Kovrigina EA, Galiakhmetov AR, Rathore R, Kovrigin EL. Study of Förster Resonance Energy Transfer to Lipid Domain Markers Ascertain Partitioning of Semisynthetic Lipidated N-Ras in Lipid Raft Nanodomains. *Biochemistry* (2018) 57:872–81. doi: 10.1021/acs.biochem.7b01181
 59. Vadas O, Dbouk HA, Shymanets A, Perisic O, Burke JE, Abi Saab WF, et al. Molecular determinants of PI3K γ -mediated activation downstream of G-protein-coupled receptors (GPCRs). *Proc Natl Acad Sci USA* (2013) 110:18862–7. doi: 10.1073/pnas.1304801110
 60. Bratt JM, Chang KY, Rabowsky M, Franzi LM, Ott SP, Filosto S, et al. Farnesyltransferase Inhibition Exacerbates Eosinophilic Inflammation and Airway Hyperreactivity in Mice with Experimental Asthma: The Complex Roles of Ras GTPase and Farnesylpyrophosphate in Type 2 Allergic Inflammation. *J Immunol* (2018) 200:3840–56. doi: 10.4049/jimmunol.1601317
 61. Porat-Shliom N, Kloog Y, Donaldson JG. A unique platform for H-Ras signaling involving clathrin-independent endocytosis. *Mol Biol Cell* (2008) 19:765–75. doi: 10.1091/mbc.e07-08-0841
 62. Gomez GA, Daniotti JL. H-Ras dynamically interacts with recycling endosomes in CHO-K1 cells: involvement of Rab5 and Rab11 in the trafficking of H-Ras to this pericentriolar endocytic compartment. *J Biol Chem* (2005) 280:34997–5010. doi: 10.1074/jbc.M506256200
 63. Leung KF, Baron R, Seabra MC. Thematic review series: lipid posttranslational modifications. geranylgeranylation of Rab GTPases. *J Lipid Res* (2006) 47:467–75. doi: 10.1194/jlr.R500017-JLR200
 64. Cox AD, Fesik SW, Kimmelman AC, Luo J, Der CJ. Drugging the undruggable RAS: Mission possible. *Nat Rev Drug Discovery* (2014) 13:828–51. doi: 10.1038/nrd4389
 65. Brock C, Schaefer M, Reusch HP, Czupalla C, Michalke M, Spicher K, et al. Roles of G beta gamma in membrane recruitment and activation of p110 gamma/p101 phosphoinositide 3-kinase gamma. *J Cell Biol* (2003) 160:89–99. doi: 10.1083/jcb.200210115
 66. Voigt P, Brock C, Nürnberg B, Schaefer M. Assigning functional domains within the p101 regulatory subunit of phosphoinositide 3-kinase gamma. *J Biol Chem* (2005) 280:5121–7. doi: 10.1074/jbc.M413104200
 67. Botindari F. *Targeting SHIP1 and PI3K γ for a synergistic inhibition of mast cell activation* [Ph.D. thesis, published]. Faculty of Science, University of Basel (2016). Available at: http://edoc.unibas.ch/diss/DissB_11905.
 68. Jin RJ. *PI3K Regulatory Protein p84 Determines Mast Cell Sensitivity to Ras Inhibition - Moving Towards Cell Specific PI3K Targeting?* [Doctoral thesis, full text not accessible]. Faculty of Medicine, University of Basel (2020). Available at: <https://baselbern.swissbib.ch>.

Conflict of Interest: The authors declare that the research was conducted in the absence of any commercial or financial relationships that could be construed as a potential conflict of interest.

Copyright © 2020 Jin, Gogvadze, Xavier, Bohnacker, Voelzmann and Wymann. This is an open-access article distributed under the terms of the Creative Commons Attribution License (CC BY). The use, distribution or reproduction in other forums is permitted, provided the original author(s) and the copyright owner(s) are credited and that the original publication in this journal is cited, in accordance with accepted academic practice. No use, distribution or reproduction is permitted which does not comply with these terms.

Supplementary Information

Content	page
Figure S1. FTI-277 specifically inhibits protein farnesylation and GGTI-298 specifically inhibits protein geranyl-geranylation.	2
Figure S2. Expression of farnesyltransferase (FTase) and geranylgeranyltransferase (GGTase) in mast cells and macrophages.	2
Figure S3. GGTI-298 causes re-localization of H-Ras from the plasma membrane to the cytosol.	3
Figure S4. Time- and concentration-dependence of FTI-277 action on mast cells.	3-4
Figure S5. Neither FTI-277 nor GGTI-298 affect PAF-signaling in BMMC or BMMØ	4
Table S1. Primer Sequences used for qPCR	5-6
Table S2. Sequences of codon-optimized 3xHA-Ras, used for expression in HEK293 cells	7
Table S3. ORF sequences of GFP-tagged Ras isoforms used for cellular localization assays	8
Table S4. Antibodies used for immunoblotting	9-10

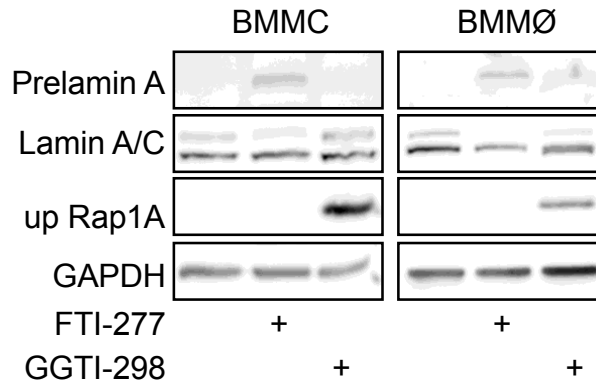


Figure S1. FTI-277 specifically inhibits protein farnesylation and GGTI-298 specifically inhibits protein geranyl-geranylation. BMMCs and BMMØ were treated with 5 μ M FTI-277 (72 h) or 5 μ M GGTI-298 (24 h). Levels of non-prenylated lamin (Prelamin A) and un-prenylated Rap1A (up Rap1A) were determined by Western blotting. Accumulation of Pre-lamin in FTI-277 incubated cells demonstrate inhibition of protein farnesylation. GGTI-298 had no effect on pre-lamin but abrogated geranyl-geranylation of Rap1A. Experiment was performed 3 times for each cell type and one representative Western blot image is shown.

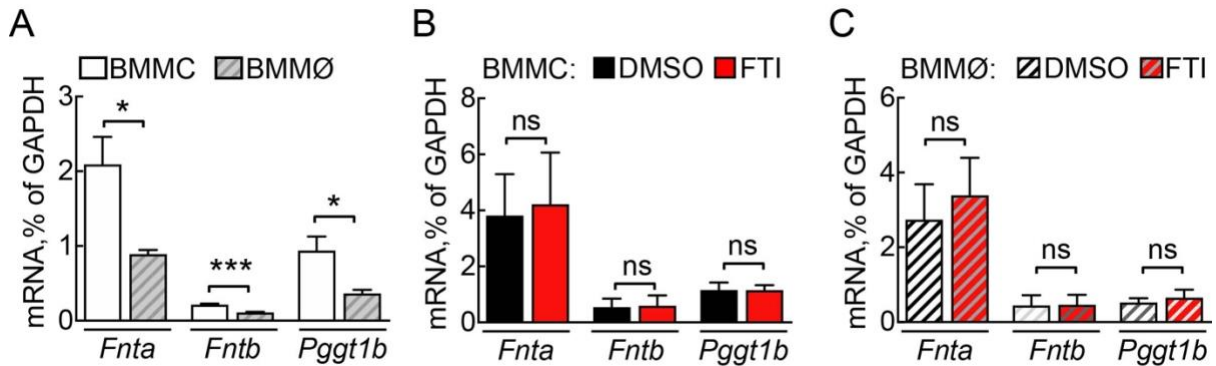


Figure S2. Expression of farnesyltransferase (FTase) and geranylgeranyltransferase (GGTase) in mast cells and macrophages. (A) mRNA abundance of *Fnta* (α subunit of FTase and GGTase), *Fntb* (β subunit of FTase) and *Pggt1b* (β subunit of GGTase) in BMMCs and BMMØ was assessed by qPCR and normalized to the corresponding level of GAPDH expression. Results from n=4 independent experiments are shown. (B and C) Effect of FTI-277 on FTase and GGTase expression. BMMCs (B) and BMMØ (C) were treated with DMSO or 5 μ M FTI-277 for 72 h. Expression of *Fnta*, *Fntb* and *Pggt1b* genes was assessed by qPCR and normalized to GAPDH. Experimental number is n=3 for BMMC and n=2 for BMMØ from independent experiments. Statistical significance was evaluated with Student T-test. ns: p>0.05; *: p \le 0.01, ***: p \le 0.001.

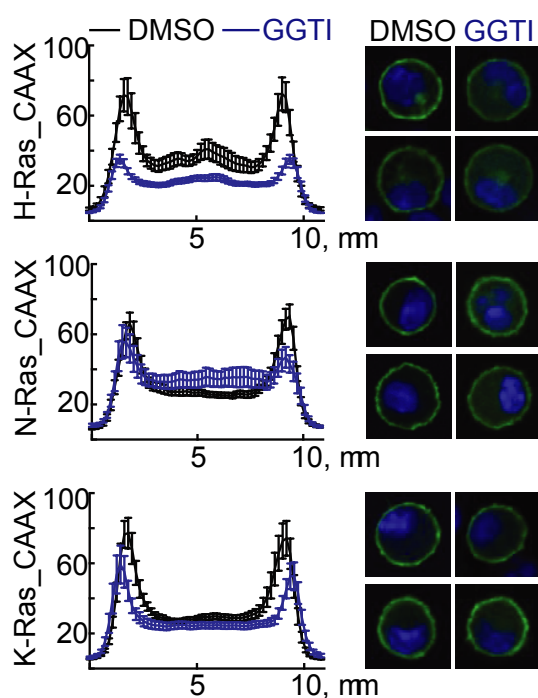


Figure S3. GGTI-298 causes re-localization of H-Ras from the plasma membrane to the cytosol. BMMCs were transfected with GFP-tagged C-terminal 25 amino acids (CAAX domain) of H-Ras, N-Ras or K-Ras. Afterwards we treated them with 5 μ M GGTI-298 for 24 h. Images of PFA-fixed cells were acquired by confocal microscopy. Plotted are GFP-intensity mean values \pm standard error of mean (SEM) of N>18 cells.

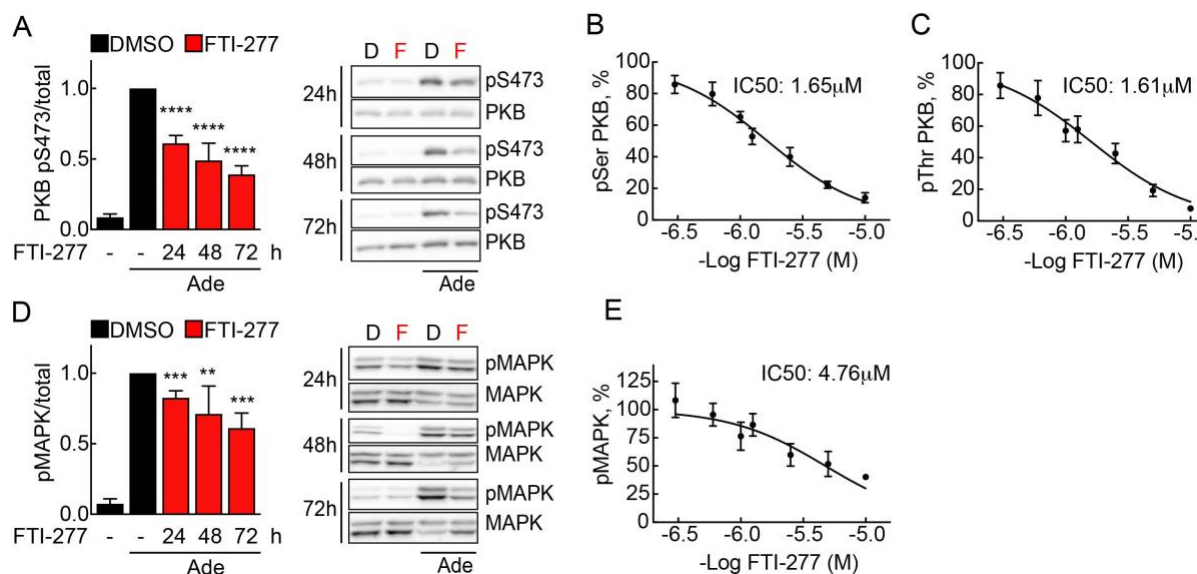


Figure S4 Time- and concentration-dependence of FTI-277 action on mast cells. BMMCs were treated with DMSO or 5 μ M FTI-277 for 24, 48 or 72 h. Cells were then starved for 4 h in IL3-free medium containing 2% FCS and either DMSO or 5 μ M FTI-277, followed by stimulation with 2 μ M adenosine. Phosphorylation of PKB at Ser473 (A) and pMAPK (D) were determined by Western blotting and normalized to the total PKB or MAPK levels, correspondingly. Each time point contains results from 3-7 experiments. (B, C, E) BMMCs were treated with increasing concentration of FTI-277 (0.3 μ M – 10 μ M) for 72 h, starved and stimulated as in (A). Levels of phosphorylation of PKB at Ser473 (B), pThr308 (C) and pMAPK (E) were quantified by western blotting, normalized to the total PKB or MAPK levels, and used to determine IC₅₀. Each dilution series was tested in n=5 experiments

and one-way ANOVA with Bonferroni's post hoc test was used to determine statistical significance. **: $p \leq 0.01$, ***: $p \leq 0.001$; ****: $p \leq 0.0001$. D=DMSO; F=FTI-277.

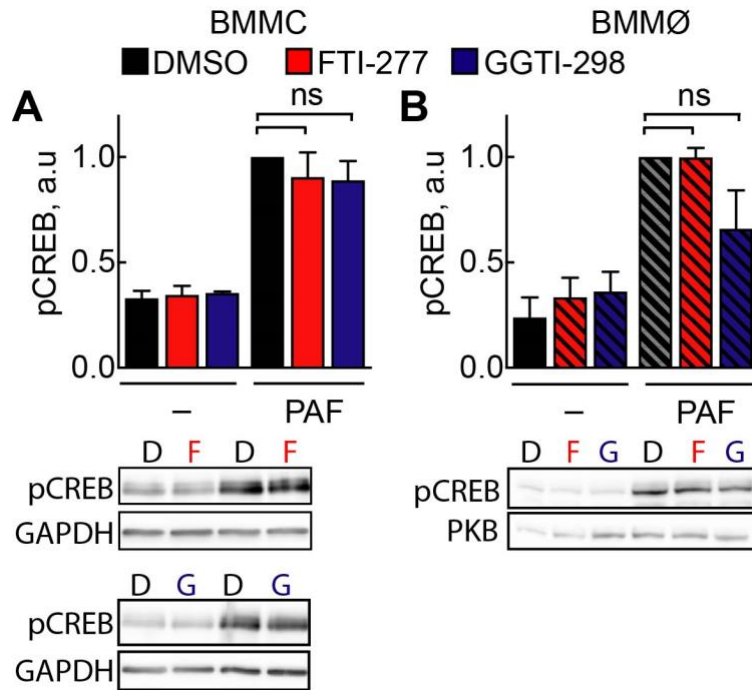


Figure S5. Neither FTI-277 nor GGTI-298 affect PAF-signaling in BMMC or BMMØ. BMMCs and BMMØ were treated with DMSO, 5 μ M FTI-277 (72 h) or 5 μ M GGTI (24 h), starved for 4 h and activated with 1 μ M PAF. Phosphorylation of cyclic AMP-responsive element-binding protein (CREB) at Ser133 was determined by Western blot analysis of cell lysates and normalized GAPDH (BMMC) or PKB (BMMØ). N=3-4 for each data point. Significant relationship was tested with one-way ANOVA with Bonferroni correction. ns: $p > 0.05$. D=DMSO; F=FTI-277; G=GGTI-298.

Table S1. Primer Sequences used for qPCR

Gene	Accession-No	Primer sequence 5' to 3'
Mm_GAPDH	NM_008084.3	F: CTGCACCACCAACTGCTTAG R: CCATCCACAGTCTTCTGGGTG
Mm_p84	AY753194.1	F: ATAGAGCAGGTGGCTAGCGA R: CAGAAGGTCACCGACACAGTG
Mm_p101	NM_177320.2	F: GACATCCTACAGGAAGTCCTTCTC R: TCAGCGCAATGCCTGTCCAT
Mm_p110g	NM_020272.2	F: CCCTGGTGATCGAGAAATGC R: GTCTTGGCGCAGATCATCAC
Mm_NRas	NM_010937.2	F: ATGAGGACAGGCGAAGGGTTC R: TCACACTTGTTGCCTACCAGCAC
Mm_KRas4A	XM_006506919.3	F: GATGTGCCTATGGTCCTGGTAGG R: GCATCCTCCACTCTCTGTCTTGTC
Mm_KRas4B	NM_021284.6	F: GATGTGCCTATGGTCCTGGTAGG R: GCATCGTCAACACCCTGTCTTGTC
Mm_HRas	NM_008284.2	F: GGCAGGGCGTGGAGGATG R: GCAGCCAGGACCACTCTCATCG
Mm_RRas	NM_009101.2	F: TGCCATTAACGACAGGCAG R: TGTTCCCAACCAACACAATG
Mm_RRas2	NM_025846.2	F: GGCAATAAAGCTGACCTGGA R: ATCCTGATCTTTGCCGATG
Mm_MRas	NM_008624.3	F: CCACCAGCTCATTCTGCGTGCAAGG R: CCTTGGTCCCTGGTGACTTTCCTTAGG
Mm_TNFalpha	NM_013693.2	F: ATCCGCGACGTGGAAGCTG

		R: CGAAGTTCAGTAGACAGAAGA
Mm_IL6	NM_031168.2	F: ACAACCACGGCCTTCCCTACTT R: CACGATTTCCCAGAGAACATGTG
Mm_Fnta	NM_008033.3	F: AGCATCGACAGTGGGTCATTC R: GACGAAGTGTCTTTGGTTCCAC
Mm_Fntb	NM_145927.2	F: GAGAAGATCCAGGAGGTCTTCAG R: CTCATAGGCATCTGTCAGTTGTC
Mm_Pggt1b	NM_172627.3	F: CCATCAAAGAATCCAGGAGCAG R: ATCCACACGGCCTAAGTCATCTC

Mm, *mus musculus*; F, forward primer; R, reverse primer

Table S2. Sequences of codon-optimized 3xHA-Ras, used for expression in HEK293 cells

3xHA_H-Ras	GGTACCACCATGTATCCTTACGATGTGCCTGACTATGCCTATCCTTACGATGTGC CAGATTACGCTTATCCCTACGATGTGCCAGATTACGCCAAGCTTGACACAGAGTA CAAACCTGGTGGTGGTGGGAGCTGGCGGAGTCGGGAAGAGCGCACTGACCATCCAG CTGATTACAGAACCACTTCGTGGACGAGTACGATCCCACAATCGAAGACTCCTATC GGAAACAGGTCGTGATCGATGGCGAGACATGTCTGCTGGACATCTGGATACCGC CGGACAGGAGGAATACAGTGTATGCGGGATCAGTATATGCGCACAGGGGAAGGC TTCCTGTGCGTGTTCGCCATTAACAATACTAAGAGTTTTGAGGACATCCATCAGT ACCGAGAACAGATTAAGAGGGTCAAAGATTCAGACGATGTGCCCATGGTCCCTGGT GGGAAACAAGTGCACCTGGCCGCTAGAACTGTGGAGAGCCGGCAGGCACAGGAT CTGGCACGCTCCTACGGGATCCCTTATATTGAAACCTCTGCAAAGACACGACAGG GCGTCGAGGACGCTTTCTATACCCTGGTGAGGGAAATCAGACAGCACAAAGCTGAG GAAACTGAACCCCTCCTGACGAATCTGGCCCTGGCTGTATGTCTGTAAGTGCGTG CTGTCTTGACTCGAG
3xHA_N-Ras	GGTACCACCATGTATCCTTACGATGTGCCTGACTATGCCTATCCTTACGATGTGC CAGATTACGCTTATCCCTACGATGTGCCAGATTACGCCAAGCTTGACACAGAGTA CAAACCTGGTGGTGGTGGGAGCTGGCGGAGTCGGGAAGAGCGCACTGACCATCCAG CTGATTACAGAACCACTTCGTGGACGAGTACGATCCCACAATCGAAGACTCCTATC GGAAACAGGTCGTGATCGATGGCGAGACATGTCTGCTGGACATCCTGGACACCGC CGGCCAGGAGGAGTACAGCGCCATGCGCGACCAGTACATGCGCACCGGCGAGGGC TTCCTGTGCGTGTTCGCCATCAACAACACAGCAAGAGCTTCGCCGACATCAACCTGT ACCGCGAGCAGATCAAGCGCGTGAAGGACAGCGACGACGCTGCCCATGGTGTCTGGT GGGCAACAAGTGCACCTGCCACCCGACCGTGGACACCAAGCAGGCCACAGG CTGGCCAAGAGCTACGGCATCCCCTTCATCGAGACCAGCGCCAAGACCCGCCAGG GCGTGGAGGACGCCTTCTACACCCTGGTGCGGAGATCCGCCAGTACCGCATGAA GAAGCTGAACAGCAGCGACGACGGCACCCAGGGCTGCATGGGCCTGCCCTGCGTG GTGATGTGACTCGAG
3xHA_K-Ras	GGTACCACCATGTATCCTTACGATGTGCCTGACTATGCCTATCCTTACGATGTGC CAGATTACGCTTATCCCTACGATGTGCCAGATTACGCCAAGCTTGACACAGAGTA CAAACCTGGTGGTGGTGGGAGCTGGCGGAGTCGGGAAGAGCGCACTGACCATCCAG CTGATTACAGAACCACTTCGTGGACGAGTACGATCCCACAATCGAAGACTCCTATC GGAAACAGGTCGTGATCGATGGCGAGACATGTCTGCTGGACATCCTGGACACCGC CGGCCAGGAGGAGTACAGCGCCATGCGCGACCAGTACATGCGCACCGGCGAGGGC TTCCTGTGCGTGTTCGCCATCAACAACACCAAGAGCTTCGAGGACATCCACCACT ACCGCGAGCAGATCAAGCGCGTGAAGGACAGCGAGGACGCTGCCCATGGTGTCTGGT GGGCAACAAGTGCACCTGCCAGCCGACCGTGGACACCAAGCAGGCCACAGGAC CTGGCCCCGAGCTACGGCATCCCCTTCATCGAGACCAGCGCCAAGACCCGCCAGG GCGTGGACGACGCCTTCTACACCCTGGTGCGGAGATCCGCAAGCACAAGGAGAA GATGAGCAAGGACGGCAAGAAGAAGAAGAAGAGCAAGACCAAGTGCGTGATC ATGTGACTCGAG

Table S3. ORF sequences of GFP-tagged Ras isoforms used for cellular localization assays (C-terminal 25 amino acids in blue)

Start	GFP	Ras (C-term 25 AA)	Restriction site
GFP-HRasCAAX Plasmid 1672	ATGGTGAGCAAGGGCGAGGAGCTGTTACCGGGGTGGTGCCCATCCTGGTCGAGC TGGACGGCGACGTAAACGGCCACAAGTTCAGCGTGTCCGGCGAGGGCGAGGGCGA TGCCACCTACGGCAAGCTGACCCTGAAAGTTCATCTGCACCACCGGCAAGCTGCCC GTGCCCTGGCCCACCCTCGTGACCACCCTGACCTACGGCGTGCAGTGCTTCAGCC GCTACCCCGACCACATGAAGCAGCAGACTTCTTCAAGTCCGCCATGCCCGAAGG CTACGTCCAGGAGCGCACCATCTTCTTCAAGGACGACGGCAACTACAAGACCCGC GCCGAGGTGAAGTTCGAGGGCGACACCCTGGTGAACCGCATCGAGCTGAAGGGCA TCGACTTCAAGGAGGACGGCAACATCCTGGGGCACAAGCTGGAGTACAACACTACAA CAGCCACAACGTCTATATCATGGCCGACAAGCAGAAGAACGGCATCAAGGTGAAC TTCAAGATCCGCCACAACATCGAGGACGGCAGCGTGCAGCTCGCCGACCACTACC AGCAGAACACCCCCATCGGGCGACGGCCCCGTGCTGCTGCCCGACAACCACTACCT GAGCACCCAGTCCGCCCTGAGCAAAGACCCCAACGAGAAGCGCGATCACATGGTC CTGCTGGAGTTCGTGACCGCCGCCGGGATCACTCTCGGCATGGACGAGCTGTACA AGTCCGGACTCAGATCT (<i>Bgl</i> II) CAGCACAAGCTGAGGAACTGAACCCCTCCTG ACGAATCTGGCCCTGGCTGTATGTCTGTAAAGTGGTGTCTTGA GAATTC (<i>E</i> coRI)		
GFP-NRasCAAX Plasmid 1673	ATGGTGAGCAAGGGCGAGGAGCTGTTACCGGGGTGGTGCCCATCCTGGTCGAGC TGGACGGCGACGTAAACGGCCACAAGTTCAGCGTGTCCGGCGAGGGCGAGGGCGA TGCCACCTACGGCAAGCTGACCCTGAAAGTTCATCTGCACCACCGGCAAGCTGCCC GTGCCCTGGCCCACCCTCGTGACCACCCTGACCTACGGCGTGCAGTGCTTCAGCC GCTACCCCGACCACATGAAGCAGCAGACTTCTTCAAGTCCGCCATGCCCGAAGG CTACGTCCAGGAGCGCACCATCTTCTTCAAGGACGACGGCAACTACAAGACCCGC GCCGAGGTGAAGTTCGAGGGCGACACCCTGGTGAACCGCATCGAGCTGAAGGGCA TCGACTTCAAGGAGGACGGCAACATCCTGGGGCACAAGCTGGAGTACAACACTACAA CAGCCACAACGTCTATATCATGGCCGACAAGCAGAAGAACGGCATCAAGGTGAAC TTCAAGATCCGCCACAACATCGAGGACGGCAGCGTGCAGCTCGCCGACCACTACC AGCAGAACACCCCCATCGGGCGACGGCCCCGTGCTGCTGCCCGACAACCACTACCT GAGCACCCAGTCCGCCCTGAGCAAAGACCCCAACGAGAAGCGCGATCACATGGTC CTGCTGGAGTTCGTGACCGCCGCCGGGATCACTCTCGGCATGGACGAGCTGTACA AGTCCGGACTCAGATCT (<i>Bgl</i> II) CAGTACCGCATGAAGAAGCTGAACAGCAGCG ACGACGGCACCCAGGGCTGCATGGGCCTGCCCTGCGTGGTGATGTGA GAATTC (<i>E</i> coRI)		
GFP-KRasCAAX Plasmid 1674	ATGGTGAGCAAGGGCGAGGAGCTGTTACCGGGGTGGTGCCCATCCTGGTCGAGC TGGACGGCGACGTAAACGGCCACAAGTTCAGCGTGTCCGGCGAGGGCGAGGGCGA TGCCACCTACGGCAAGCTGACCCTGAAAGTTCATCTGCACCACCGGCAAGCTGCCC GTGCCCTGGCCCACCCTCGTGACCACCCTGACCTACGGCGTGCAGTGCTTCAGCC GCTACCCCGACCACATGAAGCAGCAGACTTCTTCAAGTCCGCCATGCCCGAAGG CTACGTCCAGGAGCGCACCATCTTCTTCAAGGACGACGGCAACTACAAGACCCGC GCCGAGGTGAAGTTCGAGGGCGACACCCTGGTGAACCGCATCGAGCTGAAGGGCA TCGACTTCAAGGAGGACGGCAACATCCTGGGGCACAAGCTGGAGTACAACACTACAA CAGCCACAACGTCTATATCATGGCCGACAAGCAGAAGAACGGCATCAAGGTGAAC TTCAAGATCCGCCACAACATCGAGGACGGCAGCGTGCAGCTCGCCGACCACTACC AGCAGAACACCCCCATCGGGCGACGGCCCCGTGCTGCTGCCCGACAACCACTACCT GAGCACCCAGTCCGCCCTGAGCAAAGACCCCAACGAGAAGCGCGATCACATGGTC CTGCTGGAGTTCGTGACCGCCGCCGGGATCACTCTCGGCATGGACGAGCTGTACA AGTCCGGACTCAGATCT (<i>Bgl</i> II) CGCAAGCACAAGGAGAAGATGAGCAAGGACG GCAAGAAGAAGAAGAAGAAGAGCAAGACCAAGTGGTGTATCATGTGA GAATTC (<i>E</i> coRI)		

Table S4. Antibodies used for immunoblotting

Antibody		Company/Cat. Nr.
p110g (aa 97-335)	Clone H1 (<i>the russian</i>), mouse IgG2a	Alexis, 804-230-L001 (currently no commercial source)
p101 (aa 508)	clone D32A5, rabbit IgG	Cell Signaling, 5569S
p84 (aa 1-162)	Polyclonal, rabbit serum	Wymann Lab, rabbit 1, serum1
K-Ras (aa 54-189)	Clone F234, mouse IgG2a	Santa Cruz, Sc-30
N-Ras	Clone F155, mouse IgG1	Santa Cruz, sc31n
H-Ras	Clone Y132, rabbit IgG	Abcam, ab32417
R-Ras (aa 11-31)	Rabbit IgG	Abcam, ab47536
Lamin	Polyclonal, Goat IgG	Santa Cruz, sc-6215
Pre-Lamin	Polyclonal, goat IgG	Santa Cruz, sc-6214
Rap1A/B	Clone 26B4, rabbit IgG	Cell signaling, 2399
pS473 PKB	clone 193H12, Rabbit IgG	Cell Signaling, 4058
pT308 PKB	clone 244F9, Rabbit IgG	Cell Signaling, 4056
PKB	clone 40D4, Mouse IgG1	Cell Signaling, 2920
pMAPK (pERK-1&2)	mouse monoclonal anti-MAPK, activated, diphosphorylated ERK-1&2, clone MAPK-YT, ascites fluid IgG1	Sigma-Aldrich, M8159
MAPK (ErK-1, aa351-368)	polyclonal rabbit anti-ERK-1 (aa351-368)	Sigma-Aldrich, M7927
pS133 CREB	Clone 87G3, rabbit IgG	Sigma-Aldrich, 9198
GAPDH	clone GAPDH-71.1, mouse IgM	Sigma-Aldrich, G8795
Tubulin	clone DM1A, mouse IgG1	Sigma-Aldrich, T9026
Anti-Rabbit IgG-Peroxidase conjugate	Polyclonal, Goat	Sigma-Aldrich, A6154
Anti-Rabbit IgG Peroxidase conjugate	Polyclonal, Goat	Sigma-Aldrich, A4416

Anti-Goat IgG-HRP conjugate	Polyclonal, Donkey	Santa Cruz, sc-2020
-----------------------------	--------------------	---------------------

4.1. Project 2: PI3K γ Adaptor Subunit p84 Controls Adipose Lipolysis and Hepatic Steatosis

PI3K γ Adaptor Subunit p84 Controls Adipose Lipolysis and Hepatic Steatosis

Julie R. Jin, Ana R. Xavier, Jan Voelzmann, Thorsten Schäfer, Matthias P. Wymann

Department of Biomedicine, University of Basel, Basel, Switzerland

Abstract

Obesity due to alimentary nutrient excess is the leading cause of metabolic syndrome. Therefore weight reduction and modulation of immune cell activation ameliorates progression of type 2 diabetes and other obesity-related diseases. The previously recognized double role of Phosphoinositide 3-kinase γ (PI3K γ) in weight control and inflammation demands for further exploration how manipulation of this signaling pathway could be capitalized in the therapy of metabolic syndrome. We hypothesize that PI3K γ adaptor proteins p84 and p101 might direct physiologically distinct mechanisms. A high-fat diet (HFD) induced obesity model was used to provoke weight gain, hyperglycemia, hyperinsulinemia and hepatic steatosis in wild-types and mice devoid of PI3K γ enzyme complex components p110 γ , p84 and/or p101. p84 and p101- deficiency displayed distinct phenotypes from each other and from mice lacking functional p110 γ catalytical subunit. p84 as well as p101 knockout mice become obese when placed on a HFD for 12 weeks. In contrast, p110 γ and p84/p101 double knockouts maintain lean body weight. Despite adiposity p84^{-/-} animals are protected from hyperinsulinemia. Furthermore, in the white adipose tissue (WAT) of p84^{-/-} mice hormone sensitive lipase (HSL)-dependent lipolysis is left unrestrained, and uncoupling protein 1 (UCP-1) is upregulated, which is indicative for adipose browning and increased energy expenditure. Yet WAT mass is not significantly reduced in p84^{-/-} mice, proposing that free fatty acids (FFA) are nonetheless deposited in the WAT rather than taken up by other tissues. Indeed, p84 elimination protects

Project 2: PI3K γ Adaptor Subunit p84 Controls Adipose Lipolysis and Hepatic Steatosis

from lipid accumulation in the liver and steatosis, a process aggravated by hyperinsulinemia. Thus, we propose that normalization of insulin levels in p84^{-/-} mice allows HSL-dependent triglyceride hydrolysis, but since the liver requires strong insulin signaling to dispose FFA and use it for lipogenesis, p84^{-/-} mice do not develop hepatic steatosis. p101 adaptor protein on the other hand is prominently expressed in many leukocyte types where the p101/p110 γ complex is a major regulator of inflammation and resolution. In the HFD context, p101 elimination is associated with improved fasting glucose and glycated hemoglobin (HbA1c) levels, reflecting the involvement of p101 in chronic subclinical metabolic inflammation. PI3K γ adaptor proteins p84 and p101 thus affect systemic metabolism on different levels, with p84 regulating energy expenditure and p101 driving lymphocyte activation.

Introduction

Metabolic syndrome involves multiple related pathological conditions including excessive body mass index, insulin resistance and arterial hypertension, that are associated with ectopic triglyceride accumulation and lipotoxicity (1). All these disorders also harbor inflammatory components, and the recognition of obesity and metabolic syndrome as a systemic chronic inflammatory condition opens new therapeutic opportunities beyond traditional treatment options to type 2 diabetes. PI3K γ is actively pursued as a therapeutical target in immuno-oncology (2), and expansion to non-malignant diseases such as allergy, autoimmunity and chronic inflammation are of great medical interest.

PI3K γ is an intracellular signaling molecule highly expressed in leukocytes of the myeloid and lymphoid lineage. PI3K γ integrates inputs from transmembrane G-protein coupled receptors (GPCRs) by generating second messenger phosphatidylinositol (3,4,5)-trisphosphate (PtdIns(3,4,5)P₃) upon engagement with the G $\beta\gamma$ subunit. PtdIns(3,4,5)P₃-responsive downstream targets contain Pleckstring homology (PH) domains, which prompts the effector

Project 2: PI3K γ Adaptor Subunit p84 Controls Adipose Lipolysis and Hepatic Steatosis

protein's translocation to the submembranous space. Such effectors include protein kinase B (PKB, Akt) and protein-dependent kinase 1 (PDK1), and in leukocytes Brutons tyrosine kinase (BTK) and Tec family kinases such as and Interleukin 2-inducible T-cell kinase (ITK) (3).

Genetic and pharmacological inactivation of PI3K γ ameliorates adiposity and metabolic parameters in obese mice (4, 5). Three distinct mechanisms have been recognized as protective qualities of PI3K γ inhibition: First, the catalytic subunit of PI3K γ , p110 γ , scaffolds signaling molecules that mediate cAMP depletion to regulate energy expenditure, fat mass and body weight. This effect was not transferrable by bone marrow transplantation and is thus located in a non-hematopoietic tissue. A second, kinase-dependent pathway to regulate thermogenesis was revealed by utilization of kinase-inactive PI3K γ ^{KD/KD} mice (4). Third, PI3K γ activity in hematopoietic cells fuels chronic low-grade inflammation in WAT and contributes to insulin resistance and hyperglycemia (6–8).

Activation of PI3K γ is modulated by two adaptor or regulatory subunits termed p84 (also known as p87 or p84^{PKAP}) and p101. When dimerized with the kinase subunit p110 γ at the plasma membrane, p84/p110 γ and p101/p110 γ complexes both catalyze the transformation of PtdIns(3,4)P₂ to PtdIns(3,4,5)P₃. Still, the two PI3K γ pairings exert different functions in cells and on an organism level. p101/p110 γ impacts innate and adaptive immunity through its role in neutrophil migration (9, 10), macrophage activation (11) and thymocyte development (12–14). On the other hand, p84/p110 γ directs mast cell degranulation and migration (11, 15, 16), neutrophil reactive oxygen species (ROS) formation (9, 10), and is implicated in myocardial contractility (17, 18)

We anticipated that these non-redundant functions of p101 and p84 in different cell types could have manifold consequences on systemic metabolism in the context of adiposity

and type 2 diabetes. In the current study we present the first *in vivo* mouse study on the role of p101 and p84 regulatory proteins in obesity-mediated metabolic syndrome.

Materials and Methods

Transgenic mouse models and animal experimentation

All mice used were backcrossed on a BL6/J background. p110 γ null line has been described previously (19). p84^{-/-} and p101^{-/-} strains were generated by injection of homologous recombinated embryonal stem cells in blastocytes. The p84 targeting construct contained a conditional allele of PI3KR6 with exon 4 flanked by loxP sites. The p101 construct has two LoxP sites flanking exon 3 of PIK3R5. Recombination by crossing with mice expressing Cre under the control of the ubiquitous CMV promoter leads to deletion and translational frameshift in all tissues. To generate p84/p101 double knockouts (p84^{-/-}/p101^{-/-}), we started with oocytes from p101^{-/-} mice and targeted the p84 locus with CrisprCas9 by usage of single guide RNA (sgRNA) corresponding to a 20 nucleotide fraction of exon 4. Deletion of 16 nucleotides and subsequent frameshift mutation led to loss of p84 expression. More detailed information on genetic targeting and mouse line validation can be found in the supplementary information (Figure S1&2).

All wild-type (WT) and transgenic mice used in this study were bred and housed according to institutional guidelines. All animal experiments were approved by the Swiss Federal Veterinary Office (SFVO) and the Cantonal Veterinary Office of Basel-Stadt (license number 2338). F3282 Mouse High Fat Diet (HFD) was purchased from BioServ (Frenchtown, NJ) and Chow diet 3436 from Kliba/NAFAG (Kaiseraugust, AG). Male mice started HFD at 6 weeks of age until age 9 or 18 weeks as indicated in each experiment with weekly monitoring of weight and well-being. Glucose tolerance test (GTT) and Insulin tolerance test (ITT) were carried out with 18 week old HFD or Chow diet control animals. For GTT we injected 1g

Project 2: PI3K γ Adaptor Subunit p84 Controls Adipose Lipolysis and Hepatic Steatosis

glucose per kg body weight intraperitoneally (i.p.) into mice fasted for 6 hours. Glycemia was subsequently monitored for 2 hours every 30 minutes using Abbot FreeStyle glucometer and Freedom Lite strips. For ITT in HFD fed mice we utilized 1 IU insulin (Actrapid, Novo Nordisk, kind gift from Daniel Zeman) per kg body weight. In Chow animals the insulin dose was reduced to 0.75 IU/kg body weight respectively to avoid hypoglycemia. Subsequent glucose monitoring was identical to GTT.

HOMA-IR score

Homeostatic assessment of insulin resistance (HOMA-IR) score was calculated according to the method of Matthews et al. (20):

$$\text{Fasting plasma glucose [mmol/l]} \times \text{Fasting serum insulin [mU/l]} / 22.5$$

HbA1c

Glycated hemoglobin (HbA1c) was measured using mouse HbA1c assay kit from Cristal Chem (80310) according to manufacturer's instructions.

Histological methods

Epididymal WAT (eWAT) samples for histological analysis were fixed in 10 % paraformaldehyde (PFA, Sigma 158127) for 72 hours and then transferred to 70 % ethanol for 48 hours. Following paraffin embedding, tissue blocks were cut into 4 μ m sections and subjected to different staining methods. To visualize mast cells we utilized 0.5% Toluidine blue staining (Sigma 198164).

Liver tissue was fixed in 4 % PFA and embedded in paraffin for hematoxylin/eosin (H&E) staining. A separate liver lobe was fresh frozen in O.C.T. compound for cryosectioning and Oil Red O staining (Sigma O1391).

Cell culture

Bone marrow derived macrophages (BMDMs) were cultured from wild-type and transgenic mice by differentiating bone marrow in RPMI plus 10% HI-FCS, 2mM glutamine, 100 μ g/ml Penicillin/Streptomycin, 50mM 2-Mercaptoethanol and 20 % L292 conditioned medium for 7 days. Differentiated macrophages were checked for F4/80 and CD11b expression by flow cytometry and utilized for stimulation experiments. For chemokine stimulation BMDMs were starved for 4 hours and stimulated for 2 minutes with C5a, C3a, RANTES, MIP1a or MCP-1.

RT-qPCR

For mRNA extraction from WAT we utilized TRIzol reagent (Invitrogen) according to manufacturer's instructions. Reverse transcription was conducted with PrimeScript RT Reagent (Takeda RR036A) and cDNA was measured by quantitative polymerase chain reaction (qPCR) on StepOnePlus Real-Time PCR System (Applied Biosystems) with Takyon ROX SYBR 2x MasterMix dTTP (Eurogentec UF-RSMT-B0705). The list of primers is available in the supplementary section (Table S1). Relative mRNA expression was calculated from CT values of target gene and GAPDH normalized to a reference sample according to the ddCT method:

$$\text{relative mRNA} = 2^{-\text{ddCT}}$$

and

$$\text{ddCT} = \text{dCT}_{\text{sample}} - \text{dCT}_{\text{reference}}$$

Western blot

WAT lysis buffer (20mM Tris-HCl pH=8,5% glycerol, 138 glycerol, 2.7 mM KCl, 1% NP-40, 5mM EDTA) was supplemented with cComplete protease inhibitors (Roche 11697498001) and PhosSTOP phosphatase inhibitor cocktail (Roche 4906845001) and added to frozen pulverized tissue. After centrifugation of the lysate at 16'000 x g at 4°C for 10 minutes, clear tissue lysate containing proteins were separated from the fat cake. Clear lysate fraction was collected and protein concentrations were determined with Pierce BCA assay (Pierce Cat#23225). We added sample buffer (2.5 ml 1.25M Tris-HCl pH 6.8, 1g SDS, 2.5 ml 2-mercaptoethanol, 5.8ml 87% glycerol, 5mg Bromophenol blue) to the lysate and boiled samples at 96°C for 7 minutes to denature proteins. BMDMs were lysed directly in 2x sample buffer and boiled at 96°C for 7 minutes prior loading on SDS-PAGE. Lysates were resolved on 7.5 or 10% SDS-PAGE gels, transferred to PDVF membrane (Millipore IPVH00010) and subsequently incubated in primary antibody overnight (List of Western blot antibodies is provided in Table S2). After incubation with HRP-conjugated secondary antibody for 60 minutes membranes were revealed by addition of ECL substrate reagents (Millipore WBKLS0500). Chemiluminescence was detected in a Fusion FX imager (Vilber Lourmat) and we quantified band intensities in Image J software.

Statistical analysis

Data is represented as mean \pm SEM and number of replicates (N) is specified in the figure legend for each figure panel. We utilized non-parametric Mann-Whitney test (GraphPad prim, V9) for statistical comparison of non-paired results. In case of paired data non-parametric Wilcoxon-Test was chosen. Two-way ANOVA was applied on data sets comparing effects of two variables (time/genotype; dose/genotype) on a given parameter. The p-values are indicated as: not significant (ns): $p > 0.05$; *: $p \leq 0.05$, **: $p \leq 0.01$, ***: $p \leq 0.001$; ****: $p \leq 0.0001$).

If not stated otherwise in the figure legend, the comparison was made between WT group and transgenic group.

.....

Results

p84 and p101 targeted mice become obese on HFD

First we assessed to role of PI3K γ adaptor proteins p101 and p84 in weight gain. 6 week old male mice were placed on a HFD (60% fat calories) and their body weight was monitored weekly over a period of three month. To assess which adaptor protein is responsible for body weight control we tracked p101 and p84 null mice but those reached comparable final body weight as wild-type animals on HFD (Figure 1A). The growth curves of p84^{-/-} mice deviates slightly but significantly from wild-type mice (p=0.0091), however p101^{-/-} mice do not show impaired body mass gain (p=0.8661). Since elimination of a single adaptor protein did not have the prominent effect on body mass of p110 γ deletion (Figure 1B), we decided to generate p84^{-/-}/p101^{-/-} double knockout mice to assess whether simultaneous elimination of both adaptor proteins would protect from obesity. The p84^{-/-}/p101^{-/-} mouse line was derived from p101^{-/-} null oocytes in which we targeted the p101 allele with Cas9 nuclease (see supplementary Figure S2). Since this strain underwent additional genetical engineering, we accounted for possible strain effects by comparing p84^{-/-}/p101^{-/-} double knockout mice with their respective heterozygous littermate controls (p84^{-/-}/p101^{+/-}): Homozygous p84^{-/-}/p101^{-/-} mice stayed significantly leaner than heterozygous brothers (p= 0.007, Figure 1C). Area under the curve (AUC) of growth curves confirm the strongest effect on body weight gain from combined p84/p101 targeting and p110 γ , while p84 had marginal and p101 deletion had no effect. Overall, wild-type animals gain on average 25.6g (\pm 1.4) over the course of 12 weeks, while p110 γ deficient mice and gain on average only 20.2g (\pm 1.1) (Figure 1E). Although p84 and

p101 alone seem to be dispensable to maintain leanness, p84^{-/-}/p101^{-/-} double knockout mice reached the lowest body weight on HFD (Figure 1F) because after correction for starting weight they on average only gained 16.9g (± 2.1) (Figure 1E).

Figure 1. Neither p84 nor p101 ablation is protective against HFD-induced obesity

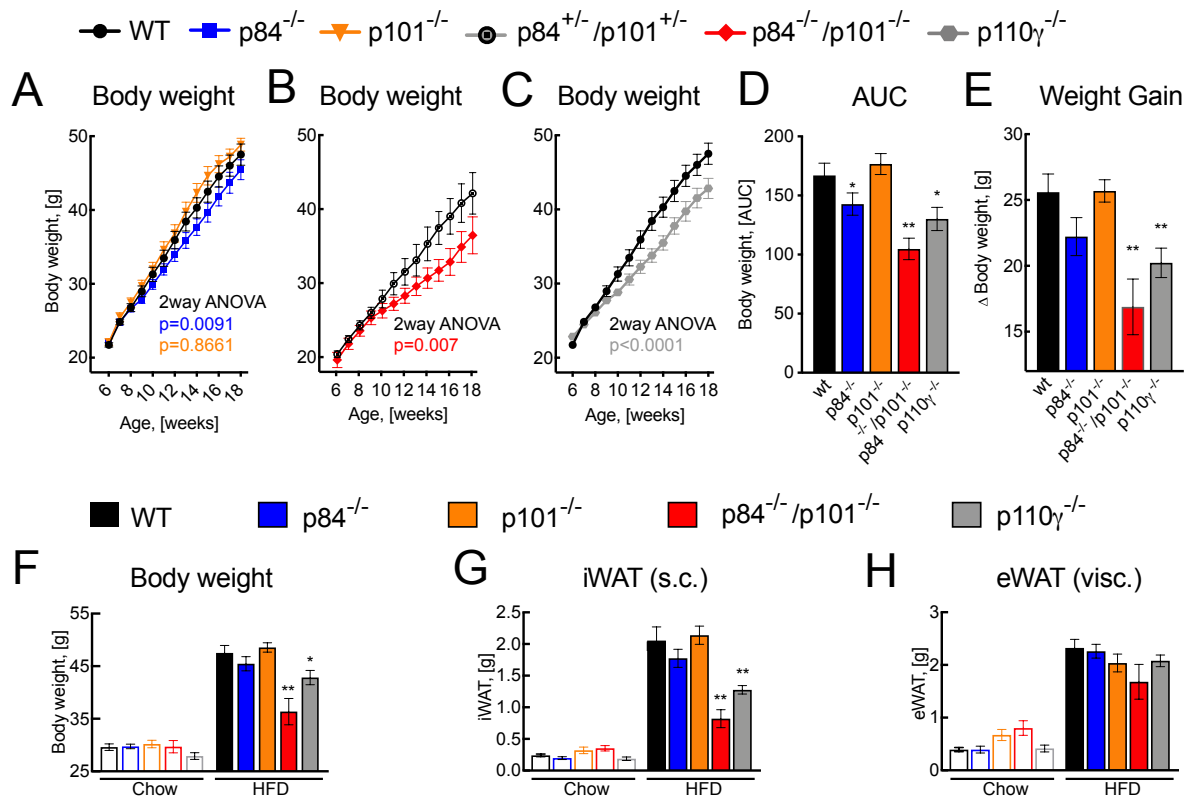


Figure 1. p84^{-/-} and p101^{-/-} mice become obese on HFD. (A,B&C) Male mice of indicated genotypes were placed on HFD starting at 6 weeks of age and body weight was recorded weekly. Two-way ANOVA was used for statistical evaluation and p-values of WT versus knockout comparison are indicated in the panel. (D) AUC values for the growth curves in (A-C). (E) Weight gain over 12 weeks of HFD was reduced in p110 γ and p101^{-/-}/p84^{-/-} double knockout strains but not in p101^{-/-} and p84^{-/-} mice. (F) shows the body weight at 18 weeks of age in Chow control group (empty boxes) and HFD-fed animals (filled boxes). (G&H) Inguinal and epididymal WAT depots (iWAT & eWAT) were collected from Chow and HFD mice. All data is presented as mean \pm SEM. Two-way ANOVA test is indicated for (A-C). Statistical analysis in (D-H) was performed with non-parametric Mann-Whitney Test in comparison to WT HFD group. p-values are *: p<0.05, **: p<0.01, ***: p<0.001, ****: p<0.0001. Number of HFD mice in all panels are n=17 for wt, n=18 for p84^{-/-}, n=14 for p101^{-/-}, n=7 heterozygous and n=6 homozygous p84^{-/-}/p101^{-/-} double knockouts, and n=13 for p110 γ ^{-/-}. Chow control group contains n=6 mice per genotype.

Obese phenotype parallels subcutaneous body fat accumulation

Elimination of p110 γ as well as double deletion of p84/p101 reduced subcutaneous inguinal white adipose tissue (iWAT) (Figure 1G). To our surprise, visceral epididymal fat pads (eWAT) did not change (Figure 1H). There while, neither p84 nor p101 alone significantly impacted iWAT or eWAT mass. Together with the growth curves and weight gain results, it appears that the lean body weight of p110 γ and p84/p101 double knockouts results from a reduction in subcutaneous rather than visceral adiposity.

p101 ablation reduces hyperglycemia in obese mice

Next, we performed glucose tolerance test (GTT) on the different mouse strains to assess their ability to metabolize i.p. injected glucose. Fasted mice were injected with 1g/kg body weight of glucose, and glycemia was monitored from the tail vein every 30 minutes for 2 hours (Figures 2A&B). The results from the GTT experiments are also represented as Area under the curve (AUC) values in Figure 2C. In HFD-fed mice, glucose elimination from the circulation was more effective in mice lacking p110 γ , p101 or both adaptor proteins. p84 on the other hand seems to alter the dynamics of glucose metabolism by shifting the glycemia peak towards 60 minutes post-injection instead of the normal peak at 30 minutes. However, the AUC and therefore overall systemic glucose exposure was not significantly reduced in p84^{-/-} mice.

We also assessed fasting glucose in the different genotypes (Figure 2D). Wild-type animals on HFD showed elevated blood glucose of 12.3 \pm 0.37mM after 6 hours of food withdrawal compared to age-matched animals on regular Chow diet (8.5 \pm 0.41mM), and comparable results were obtained from p84^{-/-} mice. However, in p101^{-/-} genotype hyperglycemia is significantly reduced (11.1 \pm 0.38mM), but to a lesser extent as in p110 γ ^{-/-} (9.7 \pm 0.23mM) and p84^{-/-}/p101^{-/-} double negative strain (9.4 \pm 0.32mM). This is remarkable because euglycemia

Project 2: PI3K γ Adaptor Subunit p84 Controls Adipose Lipolysis and Hepatic Steatosis

in p101 knockouts was maintained despite their obese body weight. Furthermore, fasting glucose was also ameliorated in p84/p101 double deficient mice in comparison to heterozygous littermates (Figure S4C).

Figure 2. p101 ablation improves glycemia while p84 targeting reduces fasting insulin

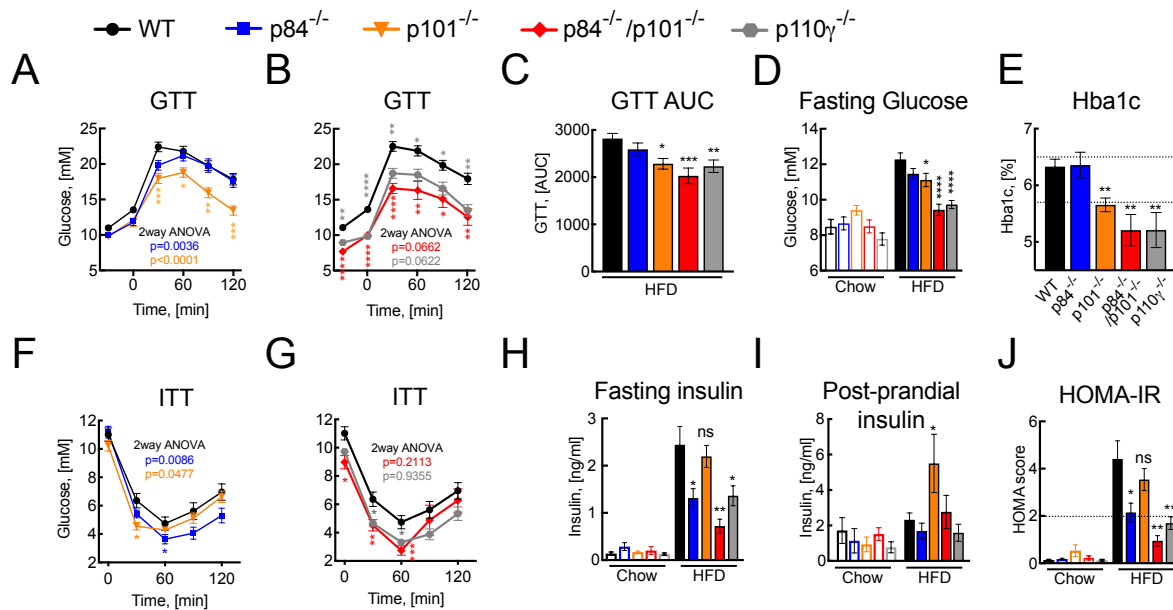


Figure 2. p84 and p101 exert non-redundant effects on glycemia and insulinemia. (A&B) Glucose tolerance test (GTT) in 18 week old HFD-fed mice was performed on starved animals with i.p. injection of 1g glucose per kg body weight. Glucose levels in venous blood was followed over 2 hours. (C) AUC representation of GTT results from HFD-fed mice in (A&B). (D) Fasting glucose was measured 6 hours post food withdrawal. (E) Glycated Hemoglobin (HbA1c) was detected in blood of 18 week old HFD fed mice (F&G) Insulin tolerance test (ITT) was performed on fasted HFD mice. (H) Fasting insulin was measured from plasma after 6 hours starvation. (I) Insulin concentration of fed mice receiving Chow or HFD ad libidum. (J) We calculated HOMA-IR score from fasting glucose and fasting insulin values of each mouse. All data is presented as mean \pm SEM. Chow controls contain n=6 mice per genotype and HFD group contains data from n=6-18 animals. Statistical analysis was performed with non-parametric Mann-Whitney Test. Results of Two-way ANOVA are indicated for GTT and ITT curves. p-values are *: p<0.05, **: p<0.01, ***: p<0.001, ****: p<0.0001.

Percentage of glycated hemoglobin (HbA1c) is routinely used as clinical parameter of chronic hyperglycemia as it correlates with glucose exposure of erythrocytes over 8-12 weeks. Healthy humans have less than 5.7% HbA1c and glycation above 6.5% confirms manifest type II diabetes (21). No clear cutoff references are available for mouse data since variation between strains exist . In our animals, HbA1c in healthy Chow animals ranged below 6% (WT

Project 2: PI3K γ Adaptor Subunit p84 Controls Adipose Lipolysis and Hepatic Steatosis

5.35 \pm 0.29%, Figure S3B) and rised to 6.33 \pm 0.13% in WT mice after the 12 week exposure to HFD. Further assessment of HFD-fed transgenic lines discovered significant improvement of long-term glyceic state in p110 γ ^{-/-} (5.2 \pm 0.31%), p101^{-/-} (5.65 \pm 0.12%) and p84^{-/-}/p101^{-/-} (5.21 \pm 0.28%) genotypes while p84^{-/-} mice (6.36 \pm 0.23%) were not protected from HbA1c elevation (Figure 2E).

p84^{-/-} mice are protected from hyperinsulinemia

Next, we performed insulin tolerance test (ITT) by injecting 1 IU/kg body weight insulin (Actrapid) i.p. and tracking glucose removal over 120 minutes. Remarkably, p84^{-/-} mice had significantly improved insulin response despite starting with equal fasting glucose levels at t=0 as the wild-type controls (Figure 2F). p101^{-/-} animals were also more insulin sensitive although this effect resulted from lower fasting glucose levels at the beginning of the experiment rather than increased glucose uptake. The ITT curves of p110 γ ^{-/-} and p84^{-/-}/p101^{-/-} mice reveal similar dynamics of glucose removal but since they also start with reduced fasting glucose levels they experience lower glycemia over the whole ITT experiment (Figure 2G).

HFD-induced hyperinsulinemia was significantly reduced in fasted p84^{-/-} and p110 γ ^{-/-} mice, and as to be expected also in p84^{-/-}/p101^{-/-} double knockouts (Figure 2H). Only p101 alone has no effect on fasting insulin. Of note, post-prandial insulin in mice offered food ad libidum was even elevated in p101^{-/-}, which crudely reflects pancreatic capability to secrete insulin on demand (Figure 2I). Homeostatic assessment of insulin resistance (HOMA-IR) was calculated from fasted serum glucose and fasted insulin to estimate insulin resistance (20). A score under 2 is regarded normal in humans. In our mice on BL6/J background HOMA-IR scores were below 0.5 for animals on Chow diet and increased to 4.4 \pm 0.77 in wild-type animals on HFD (Figure 2J). p84, p110 γ and p84/p101 targeting led to significant improvement of insulin sensitivity on HFD based on HOMA-IR score while p101^{-/-} genotype appears insignificant.

p101/p110 γ mediates chemokine signaling in bone-marrow derived macrophages

PI3K γ is known to transmit GPCR-mediated signaling for chemotaxis of various immune cells. Since PI3K γ has previously been reported to change immune cell infiltration in WAT, we checked macrophage marker F4/80 in visceral fat lobes, which was reduced in absence of p101 (Figure 3A). Macrophages express p101 and p84 but functional requirement for one or the other PI3K γ regulatory protein is not well established. To test whether macrophage infiltration into eWAT could be p101 dependent due to macrophage intrinsic necessity of p101/p110 γ complex for chemotaxis, we cultured bone-marrow derived macrophages (BMDM) from p101, p84 and p110 γ knockout mice, and stimulated them with various chemokines. Complement fragment C5a and C3a as well as RANTES, MCP-1 and MIP1a induce phosphorylation of protein kinase B (PKB, Akt) as surrogate marker for GPCR activation in BMDM. p101 and p110 γ null BMDMs are unable to convey signal transduction from chemokine receptor to PKB (Figure 3E). However, phosphorylation of mitogen-activated protein kinase (MAPK, ERK) is not affected by p101/p110 γ inactivation (Figure 5E), representing a PI3K γ independent signal pathway downstream of GPCRs. Importantly, genetic targeting of one adaptor protein did not provoke compensatory effects on mRNA (Figure 3B) or protein level (Figure 3C&D). In line with adaptor subunits role in complex stabilization p110 γ catalytic subunit was slightly but significantly reduced in p101^{-/-} genotype (Figure 3C). Together, our results demonstrate the requirement of p101 but not p84 for macrophage chemokine signaling.

Figure 3. p101 mediates macrophage chemokine signaling to PKB

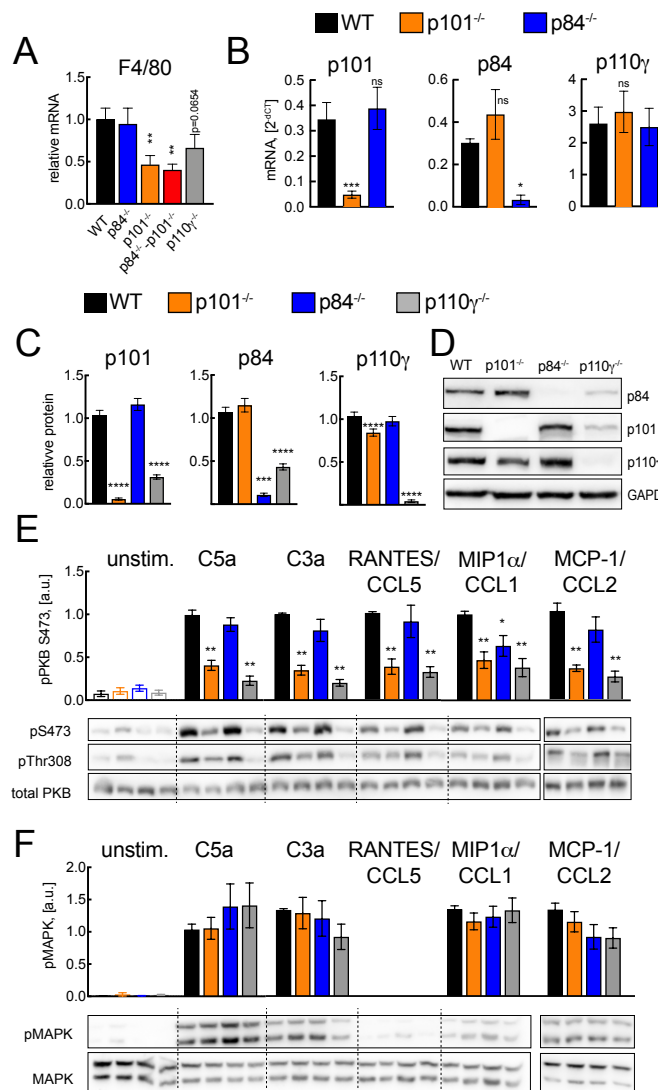


Figure 3. Role of p101 and p84 in macrophage chemotaxis and signaling.

(A) F4/80 expression in eWAT of HFD fed mice at age 18 weeks was determined using RT-qPCR. (B) BMDM differentiated from wild-type and knockout mouse bone marrow were lysed for mRNA extraction and quantification by RT-qPCR. Relative amount of p101, p84 and p110 γ mRNA has been normalized to GAPDH with the dCT method. N=4-12 from 4 independent BMDM cultures. (C) Protein levels of p101, p84 and p110 γ were detected in BMDM cell lysates by Western blot. N=11 independent BMDM cultures were quantified and protein abundance was normalized to GAPDH and wild-type cells (=1). (D) Representative Western blot image of PI3K γ expression in BMDM. (E&F) BMDM were stimulated with various chemokines. Concentration of C5a and C3a was 10nM, and RANTES, MIP1a and MCP-1 were used at 20nM. After 2 minutes of stimulation cells were lysed and subjected to Western blot analysis. Phosphorylation of PKB and MAPK were detected by Western blot and quantifications of n=3-6 independent experiments are represented as mean \pm SEM in the graphs. Representative Western blot images were selected to demonstrate phosphorylation of PKB at Ser473 and Thr308 as well as pMAPK levels. Statistical evaluation was performed with non-parametric Mann-Whitney correlation and p-values are *: p<0.05, **: p<0.01, ***: p<0.001, ****: p<0.0001. All data shown is presented as mean \pm SEM.

p84/p110 γ promotes HFD-induced liver steatosis

Non-alcoholic fatty liver disease (NAFLD) is one detrimental consequence of HFD feeding. p110 γ ^{-/-}, p84^{-/-} and p84^{-/-}/p101^{-/-} animals are protected from fatty liver as they maintain normal liver size (Figure 4A) as well as tissue architecture (Figure 4F). p101 deficiency on the other hand does not contribute to liver protective effects, since hepatomegaly and steatosis still

Project 2: PI3K γ Adaptor Subunit p84 Controls Adipose Lipolysis and Hepatic Steatosis

developed in those mice. Loss of p110 γ , p84 or both adaptor proteins had a significant impact on lipid vacuole number and steatotic area (Figure 4B&D). Since analysis of empty vacuoles in formalin fixed paraffin embedded tissue only gives a rough impression of steatosis we additionally stained fresh-frozen cryosections with Oil Red O (ORO). ORO stains neutral lipids and is a more direct readout of fat content in the organ. Quantification of ORO positive area confirms reduced fatty liver in p110 γ ^{-/-}, p84^{-/-} and p84^{-/-}/p101^{-/-} mice, while wild-type and p101^{-/-} animals develop substantial diet-induced steatosis (Figure 4E&G).

Figure 4. p84 null livers are protected from diet-induced steatosis

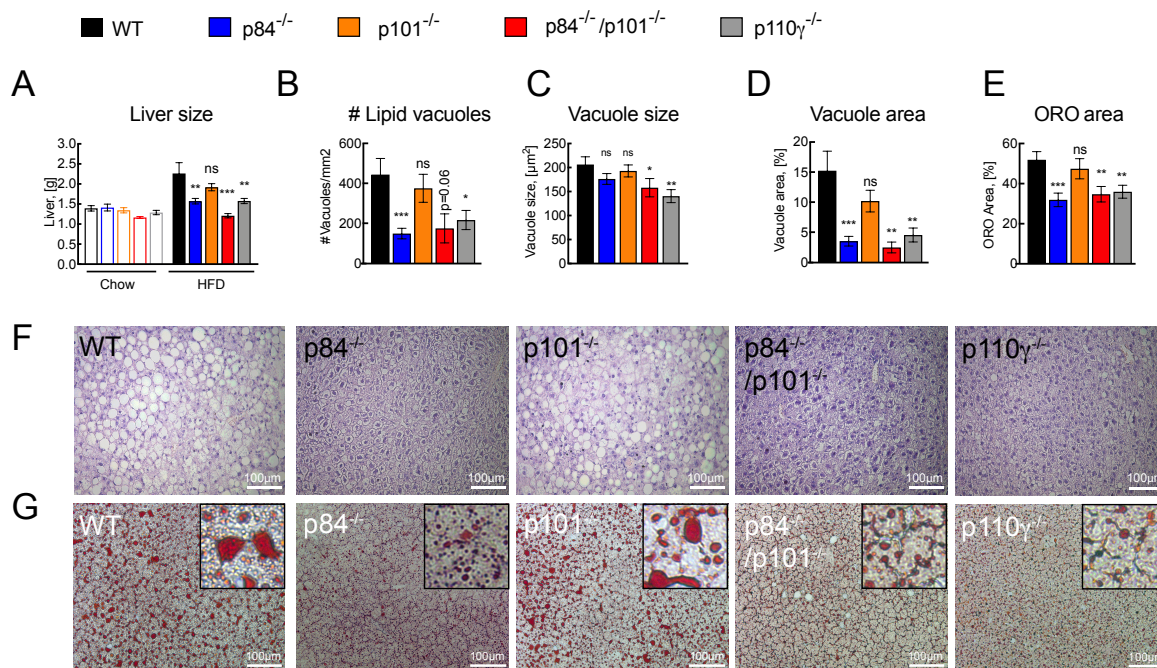


Figure 4. p84/p110 γ promotes liver steatosis. (A) Liver size of Chow and HFD-fed 18-week old male mice. WT and p101^{-/-} mice on HFD develop hepatic hypertrophy while p110 γ ^{-/-}, p84^{-/-}/p101^{-/-} and p84^{-/-} transgenic mice maintain normally sized liver. Chow group contains n=6 animals per genotype, HFD animals are n=6-18 (B, C, D) We quantified number, size and area of lipid vacuoles on H&E stained liver sections. Microscope images of liver sections for quantification were acquired using an 10x objective. (E) Oil Red O (ORO) staining of liver sections was used as alternative method to visualize steatosis by staining neutral lipids. For each genotype 4 animals were tested and we quantified 3 sections from different depth of the organ per animal. (F) Representative microscopy images of 20x magnified H&E stained liver sections. (G) ORO stained sections acquired with 20x objective. Scale and side of magnified squares are 100 μ m. All data is shown as mean \pm SEM. All statistical analysis was performed with Mann-Whitney non-parametric test. p-values are *: p<0.05, **: p<0.01, ***: p<0.001.

p84/p110 γ restrains HSL activity in eWAT

Lipolysis in WAT is a tightly regulated process ensuring that fatty acids are either stored or released depending on the nutritional situation. In times of caloric abundance fat is stored in form of triglycerides inside adipocytes under the influence of insulin. Reversely, cold or stress increase adrenalin release from sympathetic nerve endings in the WAT which increases intracellular cAMP concentration and activates cAMP-dependent protein kinase A (PKA). The subsequent phosphorylation of hormone sensitive lipase (HSL) allows hydrolysis of triglycerides to FFA and glycerol, which then enter the blood stream and are made available to peripheral organs. p110 γ has previously been identified to suppress HSL activation by facilitating phosphodiesterase (PDE)-mediated cAMP depletion (4). We have found now that p84 is also a suppressor of HSL phosphorylation. The two PKA-targeted serines S660 and S563 are hyper-phosphorylated while the AMPK-targeted S565 site remains unaffected in p84 knockouts (Figure 5C-F). HSL activation is apparent already at 3 weeks of HFD and in animals of comparable body mass and weight increase (Figure 5A&B). p101 does not have the same impact as p84 on HSL phosphorylation state in eWAT. Additionally, after 12 weeks of HFD the brown adipose marker uncoupling protein 1 (UCP-1) becomes upregulated in eWAT of p84^{-/-} mice, whereas p101 on the other hand had a minute effect on UCP-1 expression. The ubiquitous UCP-2 transcript was not affected in eWAT of transgenic mice (Figure 5G).

Figure 5. p84 elimination alleviates restraint on HSL activity and adipose browning

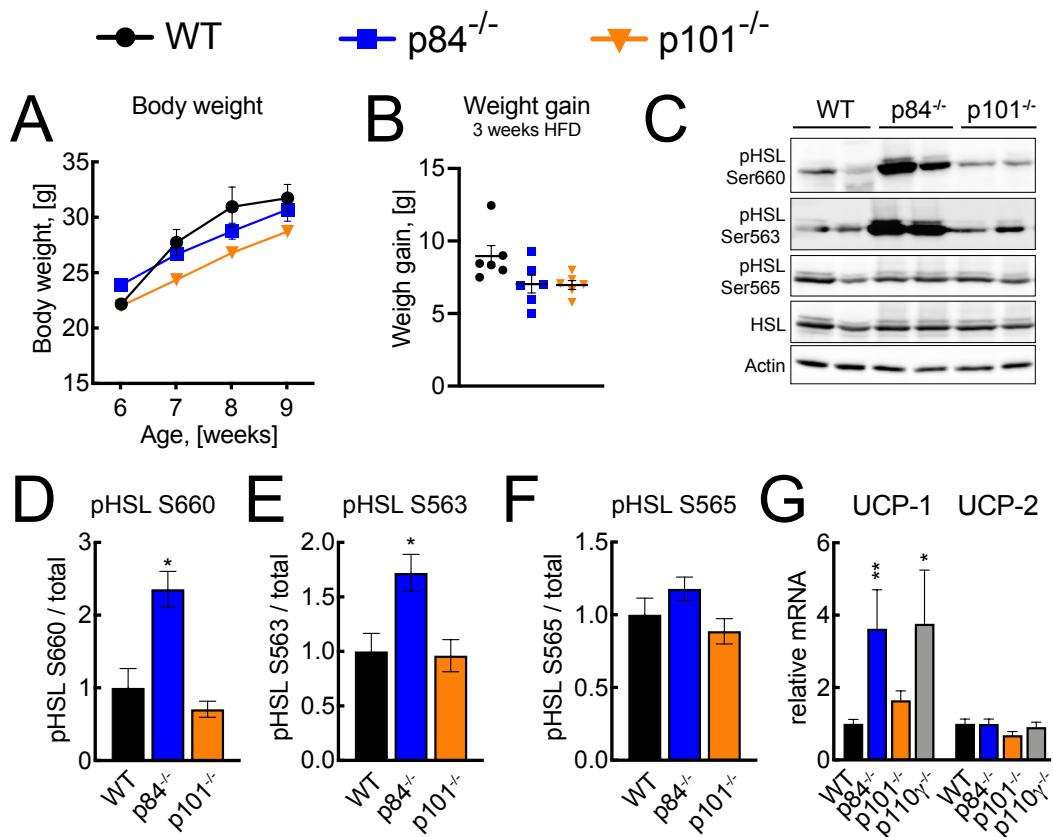


Figure 5. HSL activation and UCP-1 upregulation in p84 deficient mice. (A) Weekly body weight measurement from 6 to 9 weeks old while placed HFD. (B) Total weight gain over 3 weeks of HFD feeding. (C) eWAT from 9 week old male mice fed a HFD for 3 weeks were subjected to Western blot analysis and probed for phospho-HSL (pHSL). Representative Western blot image is shown. (D-F) Quantification of pHSL from N=6 animals per genotype. (G) Expression of UCP-1 and UCP-2 in eWAT of 18 week old mice fed HFD for 12 weeks. Relative mRNA was normalized to GAPDH and WT reference using the ddCT calculation. Results are mean \pm SEM. Statistical evaluation was performed with non-parametric Mann-Whitney correlation while $p < 0.05$ is indicated with * and $p < 0.01$ with **.

p84/p110 γ sensitizes adipocytes to β 3-adrenergic stimulation

We next assessed adrenergic stress responses in adipocytes from p84 and p101-deficient mice. We isolated adipocytes from visceral WAT of lean Chow-fed 8-12 week old animals, applied collagenase digest and separated adipocytes and stromal vascular fraction (SVF) by centrifugation. We collected the floating adipocyte layer and stimulated the β adrenalin receptor (β AR) with β 2AR-selective agonist Salbutamol or β 3AR-selective agonist

Project 2: PI3K γ Adaptor Subunit p84 Controls Adipose Lipolysis and Hepatic Steatosis

Mirabegron. Forskolin is a direct activator of adenylyl cyclase (AC) served as a control for integrity and functionality of the cAMP generating machinery. Mirabegron and Forskolin induce phosphorylation of HSL at PKA-activated S660 and S563. The AMPK-phosphorylation site S565 was only activated by Forskolin but not Mirabegron (Figure 6A&C). β 2AR agonist Salbutamol however did not induce phosphorylation of HSL (Figure 6B,G,H&I, S6B). Dose dependent phosphorylation of HSL upon Mirabegron stimulation and insensitivity towards Salbutamol implies that β 3AR rather than β 2AR is the relevant isoform relying catecholamine signals in white adipocytes. Furthermore, we could not observe changes in the activation state of PKB nor MAPK that would have indicated PI3K-derived PtdIns(3,4,5)P3 synthesis.

Unexpectedly, adipocytes from p84^{-/-} or p110 γ ^{-/-} mice showed reduced responsiveness to Mirabegron, as they failed to generate a concentration dependent increase of pHSL at S660 and S563 (Figure 6A,D,E&F). These results show an inversed picture of the hyperactivated HSL status in p84^{-/-} eWAT from HFD mice, and disclose that p84 differentially regulates stress and diet related engagement of lipolytic pathways.

Figure 6. p84^{-/-} and p110 γ ^{-/-} adipocytes become insensitive to β 3AR stimulation

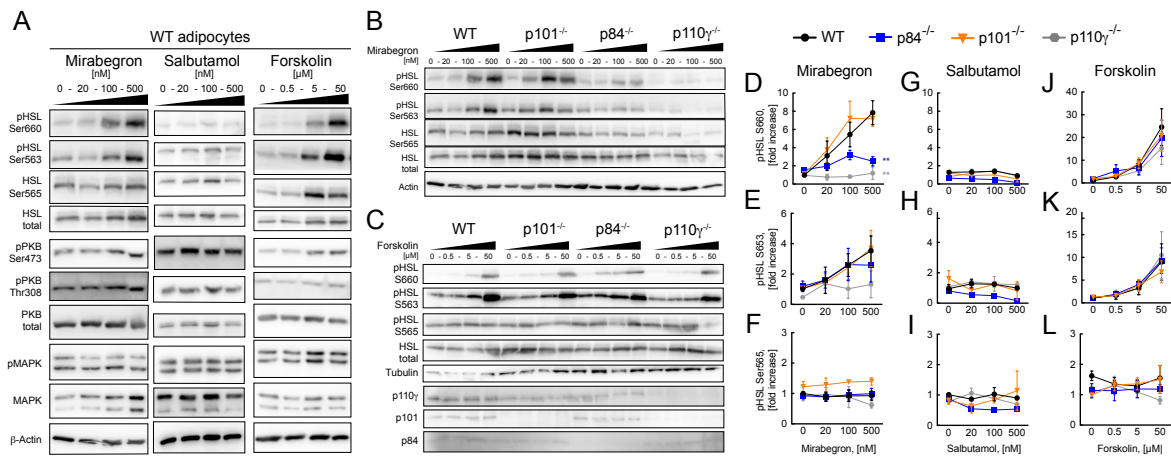


Figure 6. β 3 adrenergic signaling in adipocytes requires p84/p110 γ (A). Adipocytes isolated from WT mouse visceral adipose tissue were stimulated with increasing concentrations of indicated agonists for 20 minutes. Western blot analysis demonstrates concentration dependent phosphorylation of HSL on S660 and S563 for Forskolin and Mirabegron. PKB or MAPK phosphorylation were not affected under the used conditions. **(B)** Mirabegron stimulated adipocytes of indicated genotypes were analyzed for pHSL. **(C)** Adipocytes stimulated with increasing concentrations of Forskolin were subjected to immunoblotting for pHSL and PI3K γ . **(D-L)** Quantification of phosphorylation on S660, S563 and S565 normalized to total HSL levels in stimulated adipocyte lysates. All data are shown as mean \pm SEM. Forskolin experiments contain N=5 independent experiments. Mirabegron stimulation was repeated N=3 times. Salbutamol data combines data from N=2 experiments. Statistical analysis was done with paired t-test.

Discussion

The canonical sequence of events in HFD-induced obesity and metabolic derailment starts with excess caloric and triglyceride intake leading to saturation of white subcutaneous fat pads. Ectopic fat accumulates in visceral adipose depots, in skeletal muscle and in the liver. The resulting systemic and hepatic insulin resistance generally manifests in pathological GTT and ITT responses and post-prandial hyperglycemia with damaging consequences on vasculature and organs (22–24).

In p110 γ null mice, increase of lipolysis and thermogenesis has been previously observed to diminish obesity, insulin resistance and hepatic steatosis (4–6). In the current study, we decided to investigate the two PI3K γ complexes p84/p110 γ and p101/p110 γ in order to dissociate p84 and p101 action. Isolated examination of either p84 or p101 adaptor protein showed that PI3K γ acts on several levels of metabolic control and that the two complex variants are involved in separate processes. p84 null mice are protected from hyperinsulinemia and hepatic steatosis (Figures 2I&4). In non-alcoholic fatty liver disease (NAFLD) triacylglycerol (TAG) stems from three sources: dietary fatty acids, de-novo lipogenesis and increased lipolytic activity in WAT (25). Because p84^{-/-} animals, despite their gross body type, have astonishingly reduced lipid contents in the liver, the possibility of p84 acting on hepatocyte fatty acid uptake should be considered. This may include alimentary fat (in form of gut-derived FFA and chylomicrons) and lipolytic products exiting from saturated WAT stores. The scavenger receptor CD36 (also known as fatty acid translocase, FAT) acts as a fatty acid, lipoprotein and phospholipid shuttle in several cell types including hepatocytes and immune cells. Transgenic mice with liver-specific CD36 disruption are indeed protected from NAFLD and show improved insulin sensitivity in the ITT but no changes in the GTT (31). In fact, lipid uptake into macrophages during foam cells formation has hitherto been demonstrated to depend on PI3K γ . However, the incorporation of oxidized low density lipoproteins (oxLDL) in this

Project 2: PI3K γ Adaptor Subunit p84 Controls Adipose Lipolysis and Hepatic Steatosis

case could not be attributed to CD36 mediated transport but rather to engulfment of lipid particles by fluid phase micropinocytosis (32). Pinocytosis is currently not known as a major lipid transport mechanism in hepatocytes and a corresponding role for PI3K γ in hepatic lipid uptake remains to be defined.

It is worth discussing whether p84 could promote fatty liver disease through insulin-dependent de-novo lipogenesis. In the beginning stages of metabolic syndrome, ectopic lipid accumulation in skeletal muscle renders myocytes insulin insensitive. Excess nutrients are subsequently redirected to the liver. According to the “theory of selective insulin resistance” (26), hyperglycemia and chronically elevated insulin favor de-novo synthesis of triglycerides but desensitizes the liver for insulin’s inhibitory effect on gluconeogenesis, which results in raised fasting glucose. Therefore, chronic caloric surplus with fat and carbohydrates predisposes for NAFLD and its more aggressive form non-alcoholic steatohepatitis (NASH), and simultaneously worsens hyperglycemia and insulin resistance in type II diabetes (22, 27). However, PI3K γ is dispensable for insulin signaling to Akt/PKB in hepatocytes, a process largely relying on PI3K α and β isoforms. The dominance of PI3K isoforms other than PI3K γ in insulin signaling speak against a major role regarding hepatic insulin sensitivity (28). Nevertheless, attenuation of steatosis in p84 null mice itself could be the cause of repelled hepatic insulin resistance, without necessarily altering systemic/skeletal muscle insulin sensitivity. Likewise, it is possible that alterations in FFA and diacylglycerol release from p84^{-/-} adipose tissues secondarily impact liver lipid content.

Several observations indicate the participation of p84 in lipolytic pathways. Firstly, p84^{-/-} mice present delayed body mass gain on HFD (Figure 1A), even though the effect was far less pronounced than in p110 γ ^{-/-} mice, and the animals final body weight after 12 weeks of HFD were not statistically different to wild-type controls. Still, this could be a subtle cue that p84 impacts flux of alimentary lipids or metabolic rate. Strong evidence for lipolytic activity in p84

Project 2: PI3K γ Adaptor Subunit p84 Controls Adipose Lipolysis and Hepatic Steatosis

β -WAT comes from the overactivation of HSL, the main enzyme hydrolyzing stored TAG (Figure 5). The inhibitory impact on HSL-dependent lipolysis positions p84 in a scaffolding structure containing p110 γ that facilitates PDE and PKA interaction. Such a kinase independent role of the p84/p110 γ complex has previously been established in cardiomyocytes (17). p84 has been detected in healthy cardiomyocytes and was proposed to interact with PDE3B in conjunction to regulate cAMP levels (18). A later report described a direct negative feedback by PKA phosphorylating p110 γ and blunting PI3K γ derived PtdIns(3,4,5)P3 (29). The authors concluded that under physiological conditions PI3K γ has a minute signaling role, but primarily serves as docking platform for PDE3B and PKA-anchoring proteins. Intriguingly, the same study discovered that cardiac p101/p110 γ is upregulated during heart failure and that high expression of p101/p110 γ leads to internalization of β 2AR in chronically pressured myocardium and decreased contractility. In healthy adipose tissue high sympathetic tonus in the catabolic state activates cAMP-dependent pathways that lead to hydrolyzation of stored TAG. Free FFA and glycerol are then released and reach the liver through the portal vein to supply hepatic triacylglycerol synthesis (24). Since only p84 $^{-/-}$ but not p101 $^{-/-}$ adipocytes isolated from lean mice become insensitive to β 3AR stimulation (Figure 6), p84 appears to regulate adrenergic signaling during cAMP-dependent lipolysis. The first perception that p84/p110 γ could directly convey β 3AR signal transduction by engaging with its G γ β subunit is tempting but represents a premature conclusion. β ARs are G α s-coupled receptors that exert their function through activation of adenylyl cyclase (AC) and cAMP production. PI3K γ on the other hand is activated by pertussis-toxin sensitive G α i type GPCRs and inhibits AC. The cAMP-dependent phosphorylation of HSL and the lack of PKB phosphorylation as PtdIns(3,4,5)P3-dependent readout both speak against an involvement of PI3K γ as lipid kinase in this context. As an alternative explanation, β 3AR density on the cell surface or other desensitization

Project 2: PI3K γ Adaptor Subunit p84 Controls Adipose Lipolysis and Hepatic Steatosis

mechanisms should be considered. Unlike β 1AR and β 2AR that are internalized via β -arrestin-dependent sequestration, β 3AR in WAT is regulated on the transcriptional level by a Foxp1-dependent negative feedback loop following β 3AR activation itself (30). In this light, we could speculate that healthy adipocytes utilize p84/p110 γ to regulate β 3AR expression for adaptation of basal-metabolic rate and maintenance of set-point body weight. In turn, anabolic conditions under HFD-feeding are marked by high insulin input where p84/p110 γ restrains FFA mobilization in adipose depots. The lean body weight of p110 γ ^{-/-} genotype and upregulation of UCP-1 in eWAT are in line with increased energy expenditure through thermogenesis.

Besides catecholamine, we considered that immune derived signals might elicit WAT browning. Curiously, we detected ablation of mast cell populations in eWAT of p84 null mice (Figure S5). Mast cell migration has also been clearly linked to p84 in previous publications in the context of allergic diseases {11, 15, 35}. However the relevance of eWAT mast cells regarding obesity and insulin resistance remain debated since controversial results have come from mast cell deficient mouse lines depending on their stem cell receptor (SCF, kit-) status. Although in our study low eWAT mast cell density correlated with normalization of fasting insulin and diminished hepatic steatosis, Cpa3^{Cre/+} mast cell-deficient mice were not spared from HFD-induced hyperinsulinemia nor hepatic hypertrophy (36, 37).

Although in p84^{-/-} mice the net effect of thermogenesis appears to be insufficient to significantly reduce total body mass, enough calories seem to be eliminated to spare the liver from ectopic lipid accumulation in p84 null genotype. Liver and adipose tissues form a metabolic unit when it comes to lipid storage and handling. Since WAT lipolysis and hepatic lipogenesis are both heavily regulated by insulin, the question naturally arises whether endocrine pancreatic functions are altered in p84 and p101 knockouts. It has been previously reported that PI3K γ deletion in leptin-deficient ob/ob mice (which are prone to β -cell failure)

Project 2: PI3K γ Adaptor Subunit p84 Controls Adipose Lipolysis and Hepatic Steatosis

protects against apoptosis of pancreatic β -cells inside islets of Langerhans (33). Moreover, p110 γ is present in rodent and human pancreatic islets and has also been proposed to direct insulin secretory granule release through incretin hormone glucose-dependent insulintropic peptide (GIP) binding to G α s-coupled receptors. Upon GIP stimulation pancreatic p110 γ -Rac1 interactions stimulate actin remodeling that target secretory granules to the plasma membrane (34). Since fasting insulin in p84^{-/-} mice did not increase despite adiposity and pathological glucose handling in the GTT (Figure 2A&D), this could hint towards β -cell failure and/or inadequate insulin secretion. Complementary, p101 null mice have elevated fasting and fed insulin levels while fasting glucose and Hb1ac are compensated (Figure 2D,E&S2E). Although this constellation corresponds to pre-diabetic disease stage, this could likewise imply that endocrine pancreatic function is sustained in p101^{-/-} genotype, possibly according to anti-apoptotic effects as in the ob/ob p110 γ ^{-/-} strain. Furthermore, the improved GTT and ITT responses are in line with the role of p101 in leukocyte chemotaxis and inflammation that advances metabolic derailment. Therefore, it remains to be clarified whether inhibition of systemic inflammation or β -cell-autonomous effects could be the underlying reason for rescued insulin secretion in p101^{-/-} mice.

Our results do argue for p101/p110 γ complex promoting hyperglycemia by stimulating macrophage functions. We found decreased F4/80 expression in visceral WAT of p101^{-/-}, p101^{-/-}/p84^{-/-} and p110 γ ^{-/-} deficient mice, indicating a need for p101/p110 γ complex for chemotaxis of macrophages (Figure 3A). These findings were in line with experiments using BMDM that revealed chemokine signaling with C5a, C3a, RANTES, MIP-1a and MCP-1 are transduced through p101/p110 γ but not through p84/p110 γ (Figure 3E). Breasson et al. have previously demonstrated that PI3K γ has only modest effects on macrophage autonomous preference for M1 polarization in adipose tissues, but alters the immune cell composition and pro-

Project 2: PI3K γ Adaptor Subunit p84 Controls Adipose Lipolysis and Hepatic Steatosis

inflammatory environment. Therefore the importance of p101 over p84 for macrophage activation only partially explains improved glucose metabolism in p101^{-/-} mice. Other immune subsets, such as granulocytes and lymphocytes are likely to contribute to metabolic inflammation, and should be considered in follow-up investigations.

In summary, we provide here the first description of non-redundant functions of p84 and p101 in metabolic syndrome and refined the understanding of PI3K γ interfering with energy balance, lipid metabolism and insulin resistance. We could attribute p84/p110 γ to development of hepatic steatosis, constraint on lipolysis in WAT and adipose browning, while p101/p110 γ has a clear role in macrophage activation. Both signaling routes impair glucose homeostasis and contribute to progression of metabolic syndrome. Our approach using transgenic mouse lines has revealed that PI3K γ inhibition restricts progression of metabolic syndrome beyond control of gross body weight. Future investigation of tissue specific p84 and p101 targeted mice will help to deconvolute the role of PI3K γ and adaptor proteins in different cell compartments, namely adipose, liver, pancreas and hematopoietic lineages. Because metabolic syndrome is a multifactorial disease with several dysregulated pathways, it is beneficial to define multiple therapeutic entry points to break the vicious cycle of obesity, insulin resistance, ectopic lipogenesis and hyperglycemia. We propose that p84 attenuation might be valuable in patient subsets with NAFLD and predisposition to hepatic insulin resistance, while p101 inhibition is directed against leukocyte activation that aggravates hyperglycemia in type II diabetes.

Acknowledgements

We thank Angelika Offinger, Emilia Stanislawka Terszowska and Vanessa Schull for taking care of mice and weight tracking, Eleni Panoussis and Isabel Galm for help with histological techniques, Pascal Lorenz and Loic Sauter for microscope support and image analysis, Dominic Schmid for technical support, Daniel Zemmann for expert advice on GTT and ITT practice and interpretation, and providing Actrapid Insulin, and Pawel Pelczar and the center of transgenic models (CTM) Basel for the generation p84^{-/-}/p101^{-/-} double knock-out mice.

References

1. Unger, R. H., G. O. Clark, P. E. Scherer, and L. Orci. 2010. Lipid homeostasis, lipotoxicity and the metabolic syndrome. *Biochim Biophys Acta* 1801: 209-214.
2. Vanhaesebroeck, B., M. W. D. Perry, J. R. Brown, F. André, and K. Okkenhaug. 2021. PI3K inhibitors are finally coming of age. *Nat Rev Drug Discov*
3. Wymann, M. P., and C. Schultz. 2012. The chemical biology of phosphoinositide 3-kinases. *Chembiochem* 13: 2022-2035.
4. Becattini, B., R. Marone, F. Zani, D. Arsenijevic, J. Seydoux, J. P. Montani, A. G. Dulloo, B. Thorens, F. Preitner, M. P. Wymann, and G. Solinas. 2011. PI3K γ within a nonhematopoietic cell type negatively regulates diet-induced thermogenesis and promotes obesity and insulin resistance. *Proc Natl Acad Sci U S A* 108: E854-63.
5. Kobayashi, N., K. Ueki, Y. Okazaki, A. Iwane, N. Kubota, M. Ohsugi, M. Awazawa, M. Kobayashi, T. Sasako, K. Kaneko, M. Suzuki, Y. Nishikawa, K. Hara, K. Yoshimura, I. Koshima, S. Goyama, K. Murakami, J. Sasaki, R. Nagai, M. Kurokawa, T. Sasaki, and T. Kadowaki. 2011. Blockade of class IB phosphoinositide-3 kinase ameliorates obesity-induced inflammation and insulin resistance. *Proc Natl Acad Sci U S A* 108: 5753-5758.
6. Breasson, L., B. Becattini, C. Sardi, A. Molinaro, F. Zani, R. Marone, F. Botindari, M. Bousquenaud, C. Ruegg, M. P. Wymann, and G. Solinas. 2017. PI3K γ activity in leukocytes promotes adipose tissue inflammation and early-onset insulin resistance during obesity. *Sci Signal* 10:
7. Wymann, M. P., and G. Solinas. 2013. Inhibition of phosphoinositide 3-kinase γ attenuates inflammation, obesity, and cardiovascular risk factors. *Ann N Y Acad Sci* 1280: 44-47.
8. Solinas, G., and B. Becattini. 2017. The role of PI3K γ in metabolism and macrophage activation. *Oncotarget* 8: 106145-106146.
9. Deladeriere, A., L. Gambardella, D. Pan, K. E. Anderson, P. T. Hawkins, and L. R. Stephens. 2015. The regulatory subunits of PI3K γ control distinct neutrophil responses. *Sci. Signal.* 8:
10. Rynkiewicz, N. K., K. E. Anderson, S. Suire, D. M. Collins, E. Karanasios, O. Vadas, R. Williams, D. Oxley, J. Clark, L. R. Stephens, and P. T. Hawkins. 2020. G $\beta\gamma$ is a direct regulator of endogenous p101/p110 γ and p84/p110 γ PI3K γ complexes in mouse neutrophils. *Sci Signal* 13:
11. Jin, J. R., E. Gogvadze, A. R. Xavier, T. Bohnacker, J. Voelzmann, and M. P. Wymann. 2020. PI3K γ Regulatory Protein p84 Determines Mast Cell Sensitivity to Ras Inhibition—Moving Towards Cell Specific PI3K Targeting? *Front Immunol* 11: 585070.
12. Sasaki, T., J. Irie-Sasaki, R. G. Jones, A. J. Oliveira-dos-Santos, W. L. Stanford, B. Bolon, A. Wakeham, A. Itie, D. Bouchard, I. Koziaradzki, N. Joza, T. W. Mak, P. S. Ohashi, A. Suzuki, and J. M. Penninger. 2000. Function of PI3K γ in thymocyte development, T cell activation, and neutrophil migration. *Science* 287: 1040-1046.
13. Ji, H., F. Rintelen, C. Waltzinger, D. Bertschy Meier, A. Bilancio, W. Pearce, E. Hirsch, M. P. Wymann, T. Rückle, M. Camps, B. Vanhaesebroeck, K. Okkenhaug, and C. Rommel. 2007. Inactivation of PI3K γ and PI3K δ distorts T-cell development and causes multiple organ inflammation. *Blood* 110: 2940-2947.
14. Janas, M. L., G. Varano, K. Gudmundsson, M. Noda, T. Nagasawa, and M. Turner. 2010. Thymic development beyond beta-selection requires phosphatidylinositol 3-kinase activation by CXCR4. *J Exp Med* 207: 247-261.

15. Bohnacker, T., R. Marone, E. Collmann, R. Calvez, E. Hirsch, and M. P. Wymann. 2009. PI3K γ adaptor subunits define coupling to degranulation and cell motility by distinct PtdIns(3,4,5)P₃ pools in mast cells. *Sci Signal* 2: ra27.
16. Walser, R., J. E. Burke, E. Gogvadze, T. Bohnacker, X. Zhang, D. Hess, P. Küenzi, M. Leitges, E. Hirsch, R. L. Williams, M. Laffargue, and M. P. Wymann. 2013. PKC β phosphorylates PI3K γ to activate it and release it from GPCR control. *PLoS Biol* 11: e1001587.
17. Patrucco, E., A. Notte, L. Barberis, G. Selvetella, A. Maffei, M. Brancaccio, S. Marengo, G. Russo, O. Azzolino, S. D. Rybalkin, L. Silengo, F. Altruda, R. Wetzker, M. P. Wymann, G. Lembo, and E. Hirsch. 2004. PI3K γ modulates the cardiac response to chronic pressure overload by distinct kinase-dependent and -independent effects. *Cell* 118: 375-387.
18. Voigt, P., M. B. Dorner, and M. Schaefer. 2006. Characterization of p87PIKAP, a novel regulatory subunit of phosphoinositide 3-kinase γ that is highly expressed in heart and interacts with PDE3B. *J Biol Chem* 281: 9977-9986.
19. Hirsch, E., V. L. Katanaev, C. Garlanda, O. Azzolino, L. Pirola, L. Silengo, S. Sozzani, A. Mantovani, F. Altruda, and M. P. Wymann. 2000. Central role for G protein-coupled phosphoinositide 3-kinase γ in inflammation. *Science* 287: 1049-1053.
20. Matthews, D. R., J. P. Hosker, A. S. Rudenski, B. A. Naylor, D. F. Treacher, and R. C. Turner. 1985. Homeostasis model assessment: insulin resistance and beta-cell function from fasting plasma glucose and insulin concentrations in man. *Diabetologia* 28: 412-419.
21. Kilpatrick, E. S., Z. T. Bloomgarden, and P. Z. Zimmet. 2009. International Expert Committee report on the role of the A1C assay in the diagnosis of diabetes: response to the International Expert Committee. *Diabetes Care* 32: e159; author reply e160.
22. Samuel, V. T., and G. I. Shulman. 2016. The pathogenesis of insulin resistance: integrating signaling pathways and substrate flux. *J Clin Invest* 126: 12-22.
23. Czech, M. P. 2017. Insulin action and resistance in obesity and type 2 diabetes. *Nat Med* 23: 804-814.
24. Scheja, L., and J. Heeren. 2016. Metabolic interplay between white, beige, brown adipocytes and the liver. *J Hepatol* 64: 1176-1186.
25. Donnelly, K. L., C. I. Smith, S. J. Schwarzenberg, J. Jessurun, M. D. Boldt, and E. J. Parks. 2005. Sources of fatty acids stored in liver and secreted via lipoproteins in patients with nonalcoholic fatty liver disease. *J Clin Invest* 115: 1343-1351.
26. Brown, M. S., and J. L. Goldstein. 2008. Selective versus total insulin resistance: a pathogenic paradox. *Cell Metab* 7: 95-96.
27. Sanders, F. W., and J. L. Griffin. 2016. De novo lipogenesis in the liver in health and disease: more than just a shunting yard for glucose. *Biol Rev Camb Philos Soc* 91: 452-468.
28. Molinaro, A., B. Becattini, A. Mazzoli, A. Bleve, L. Radici, I. Maxvall, V. R. Sopsakis, A. Molinaro, F. Bäckhed, and G. Solinas. 2019. Insulin-Driven PI3K-AKT Signaling in the Hepatocyte Is Mediated by Redundant PI3K α and PI3K β Activities and Is Promoted by RAS. *Cell Metab*
29. Perino, A., A. Ghigo, E. Ferrero, F. Morello, G. Santulli, G. S. Baillie, F. Damilano, A. J. Dunlop, C. Pawson, R. Walser, R. Levi, F. Altruda, L. Silengo, L. K. Langeberg, G. Neubauer, S. Heymans, G. Lembo, M. P. Wymann, R. Wetzker, M. D. Houslay, G. Iaccarino, J. D. Scott, and E. Hirsch. 2011. Integrating cardiac PIP₃ and cAMP signaling through a PKA anchoring function of p110 γ . *Mol Cell* 42: 84-95.
30. Liu, P., S. Huang, S. Ling, S. Xu, F. Wang, W. Zhang, R. Zhou, L. He, X. Xia, Z. Yao, Y. Fan, N. Wang, C. Hu, X. Zhao, H. O. Tucker, J. Wang, and X. Guo. 2019. Foxp1

- controls brown/beige adipocyte differentiation and thermogenesis through regulating β 3-AR desensitization. *Nat Commun* 10: 5070.
31. Wilson, C. G., J. L. Tran, D. M. Erion, N. B. Vera, M. Febbraio, and E. J. Weiss. 2016. Hepatocyte-Specific Disruption of CD36 Attenuates Fatty Liver and Improves Insulin Sensitivity in HFD-Fed Mice. *Endocrinology* 157: 570-585.
 32. Anzinger, J. J., J. Chang, Q. Xu, M. K. Barthwal, T. Bohnacker, M. P. Wymann, and H. S. Kruth. 2012. Murine bone marrow-derived macrophages differentiated with GM-CSF become foam cells by PI3K γ -dependent fluid-phase pinocytosis of native LDL. *J Lipid Res* 53: 34-42.
 33. Breasson, L., C. Sardi, B. Becattini, F. Zani, and G. Solinas. 2018. PI3K γ ablation does not promote diabetes in. *FASEB J* 32: 319-329.
 34. Kolic, J., A. F. Spigelman, A. M. Smith, J. E. Manning Fox, and P. E. MacDonald. 2014. Insulin secretion induced by glucose-dependent insulinotropic polypeptide requires phosphatidylinositol 3-kinase γ in rodent and human β -cells. *J Biol Chem* 289: 32109-32120.
 35. Collmann, E., T. Bohnacker, R. Marone, J. Dawson, M. Rehberg, R. Stringer, F. Krombach, C. Burkhart, E. Hirsch, G. J. Hollingworth, M. Thomas, and M. P. Wymann. 2013. Transient targeting of phosphoinositide 3-kinase acts as a roadblock in mast cells' route to allergy. *J Allergy Clin Immunol* 132: 959-968.
 36. Feyerabend, T. B., D. A. Gutierrez, and H. R. Rodewald. 2016. Of Mouse Models of Mast Cell Deficiency and Metabolic Syndrome. *Cell Metab* 24: 1-2.
 37. Gutierrez, D. A., S. Muralidhar, T. B. Feyerabend, S. Herzig, and H. R. Rodewald. 2015. Hematopoietic Kit Deficiency, rather than Lack of Mast Cells, Protects Mice from Obesity and Insulin Resistance. *Cell Metab* 21: 678-691.

Supplementary Information

Figure S1. Characterization of p84 and p101 transgenic mice

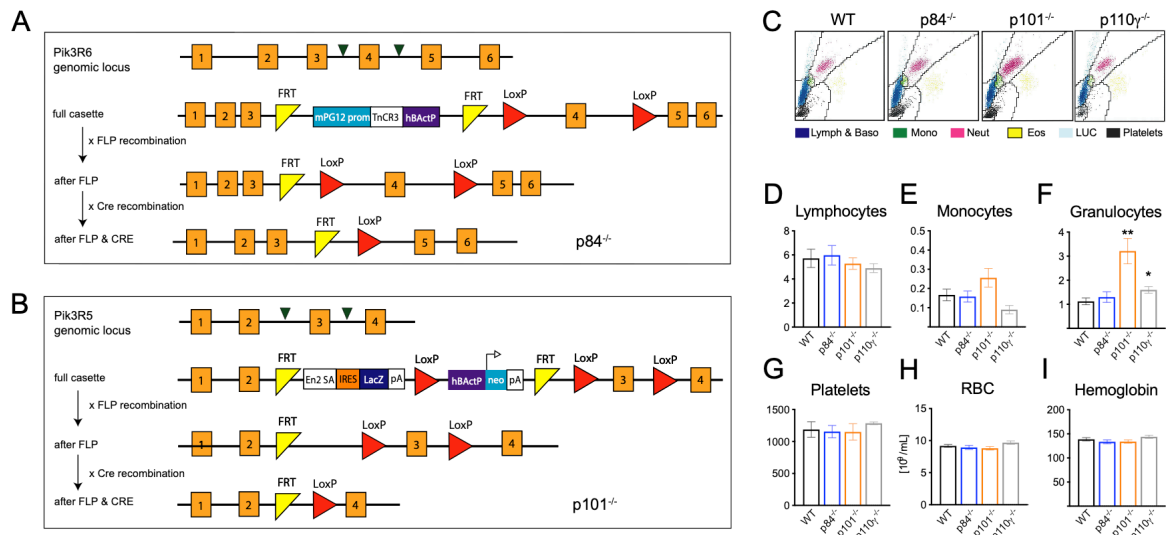


Figure S1. Generation and characterization of p84 and p101 null mice. (A) Targeting strategy of PIK3R6/p84 genomic locus and crossing scheme with FLP and Cre deleter mice to generate p84^{-/-} strain. (B) Targeting strategy of PIK3R5/p101 genomic locus and subsequent crossing scheme to generate p101^{-/-} mice. (C) Representative hematograms of 8-12 week old WT and transgenic mice measured on a Advia hemocytometer. (D-I) Lymphocyte, monocyte, granulocyte, platelet and red blood cell count in peripheral blood of n=6-9 healthy mice on regular Chow diet. Data is shown as mean \pm SEM. Statistical significance is indicated as ns: p>0.05, *: p<0.05, **: p<0.01 using Mann-Whitney non-parametric test.

Figure S2. Generation of p84/p101 double knockout

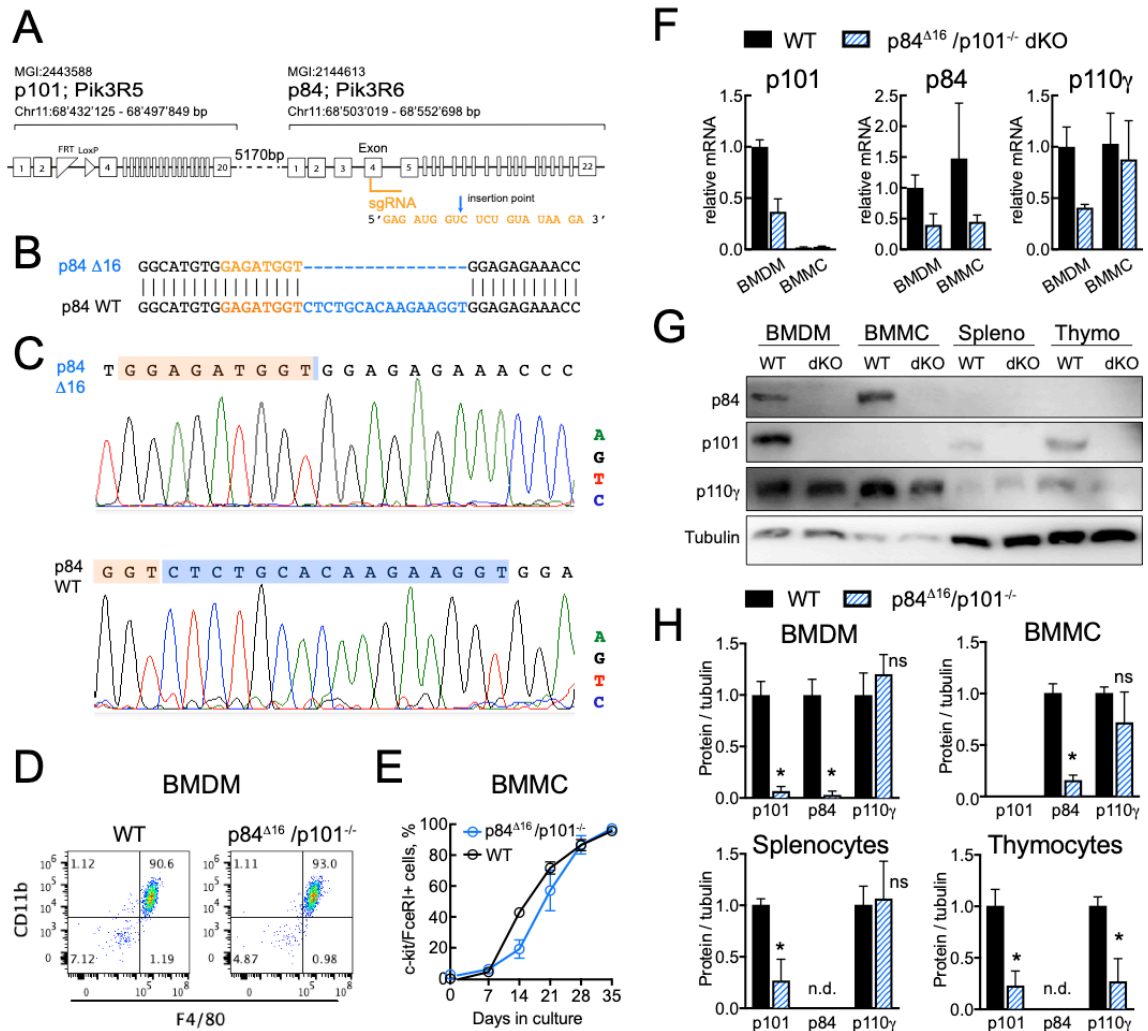


Figure S2. Generation of p84/p101 double deficient line. (A) Genetic locus of mouse PIK3R5 and PIK3R6 on chromosome 11. First, exon 3 of PIK3R5 was eliminated by insertion of 2 LoxP sites and crossing with systemic Cre delete. In a second step exon 4 of PIK3R6 was targeted with corresponding sgRNA sequence and Cas9. (B&C) A 16 nucleotide deletion was produced by Cas9 nuclease that results in a frameshift mutation. (D&E) Bone marrow derived macrophages (BMDM) and mast cells (BMCC) differentiate normally from p84/p101 null mouse bone marrow. (F) mRNA expression of both adaptor proteins is abrogated in transgenic cells. (G&H) Western blot analysis confirms deletion of p84 and p101 protein expression.

Figure S3. Chow control animals

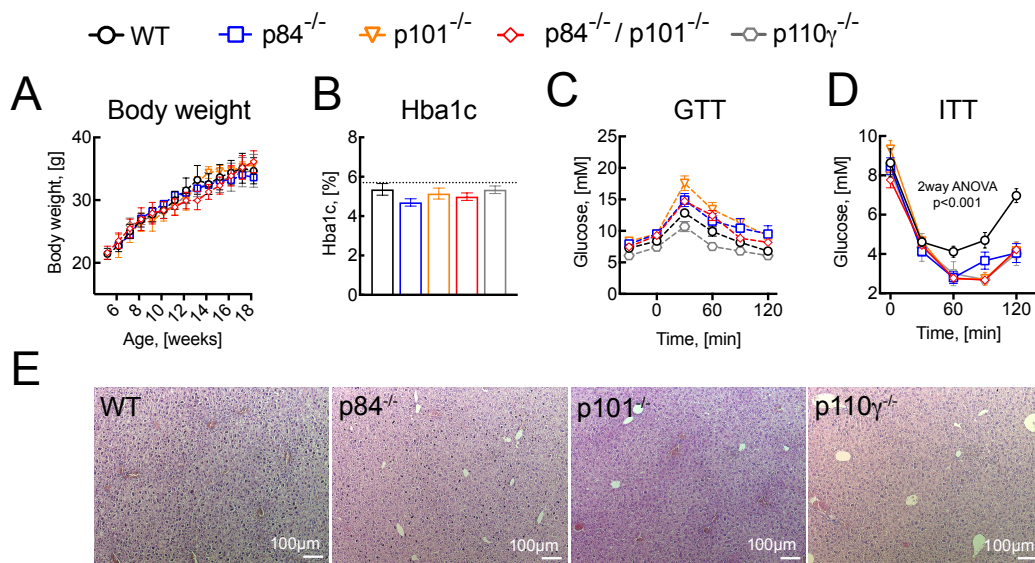


Figure S3. Chow control group. (A) Body weight of knockout animals on Chow diet over 18 weeks does not differ between transgenic and WT mice. (B) HbA1c indicates no difference in long-term serum glucose levels until age 18 weeks. (C) GTT of Chow diet animals using 1g per kg body weight of glucose. (D) ITT with 0.75 IU Insulin per kg body weight. (E) Representative H&E histology slides of liver. N=6 male mice per group were tested. Data is shown as mean \pm SEM and statistics were done with non-parametric Mann-Whitney correlation. p-values are *: p<0.05, ns: p>0.05.

Figure S4. p84/p101 heterozygous littermate controls

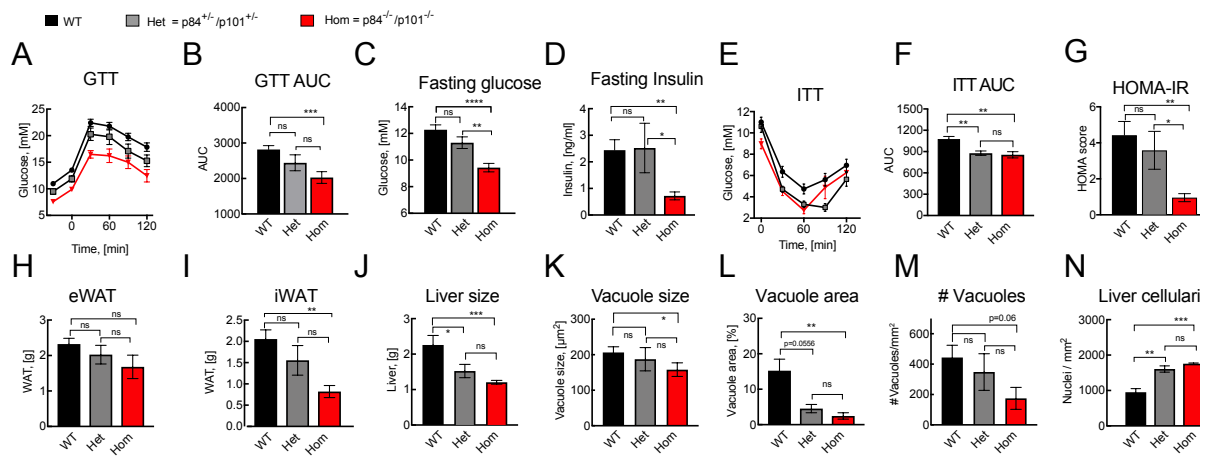


Figure S4. p84/p101 knockout mice compared to heterozygous littermate controls.

(A&B) Glucose tolerance test time course and AUC show intermediate non-significant phenotype of the heterozygous littermates. (C)Fasting glucose, (D)fasting insulin and (G)HOMA-IR score were significantly reduced in homozygous compared to heterozygous mice as well as WT controls. (E&F) ITT serum glucose curve and AUC after i.p. injection of insulin 1 IU per kg body weight. (H) Epididymal WAT mass was indifferent in the three groups. (I) Inguinal fat pad however, was smaller in p101/p84 double knockouts. (J-N) Liver size, steatosis and nucleus counts quantified from H&E stained liver sections indicate reduced hepatic lipid accumulation in p84/p101 double knockout mice on HFD. N=6 homozygous and n=6 heterozygous p101/p84 mice from 3 litters were analyzed. Wild-type controls contain data from n=17 male mice. Mean values \pm SEM are shown and statistics were done with non-parametric Mann-Whitney correlation. p values indicate ns: p>0.05, *: p<0.05, **: p<0.01, ***: p<0.001, ****: p<0.0001.

Figure S5. p84 targeting diminishes mast cell population in eWAT

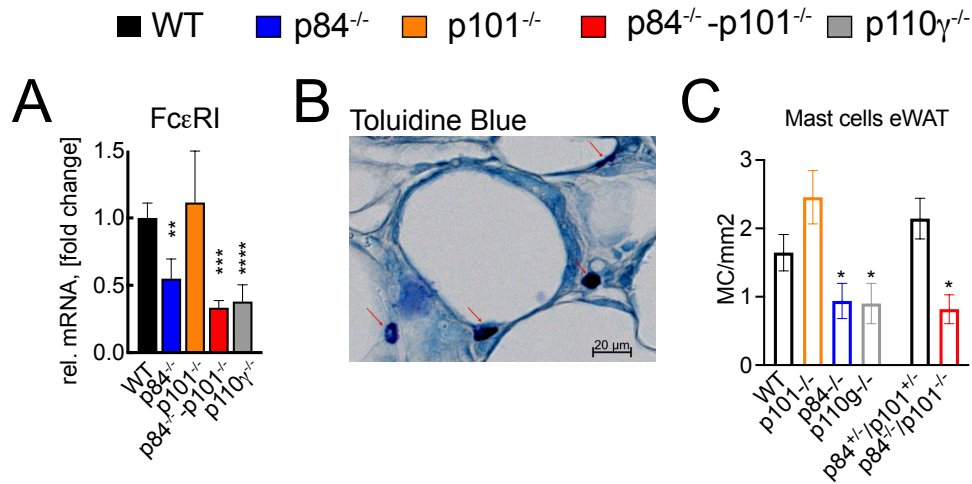


Figure S5. p84 targeting diminishes mast cell population in eWAT. (A) Visceral fat pad (eWAT) was excised from 18 week old male mice that have been fed with HFD for 12 weeks. Relative Fc ϵ RI mRNA was normalized to GAPDH and WT control animals using the ddCT method. (B) eWAT sections were stained with Toluidine blue to identify mast cells. (C) Number of mast cells per mm² from 10 eWAT sections obtained from 5 animals per genotype. Data is shown as mean \pm SEM and statistics were done with non-parametric Mann-Whitney correlation. p-values are *: p<0.05, **: p<0.01, ***: p<0.001.

Figure S6. PI3K γ expression in WAT and β 2-adrenergic stimulation of isolated adipocytes

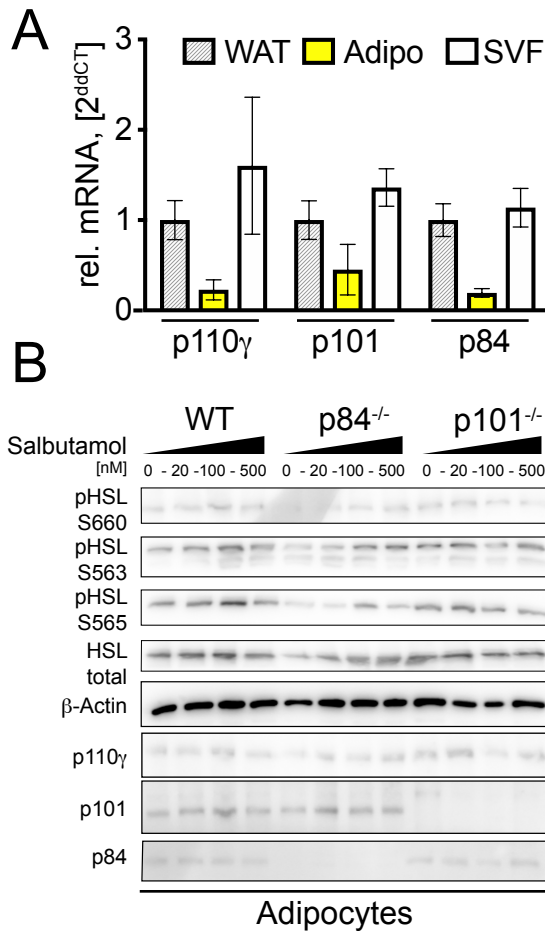


Figure S6A. PI3K γ expression in adipocytes and WAT stroma. PI3K γ mRNA was quantified in crude WAT as well as adipocytes and stromal vascular fraction (SVF) isolated from collagenase-digested WAT. N=5 qPCR measurements from 3 independent isolations.

Figure S6B. β 2-adrenergic agonist Salbutamol does not activate HSL in adipocytes. Representative Western blot of Salbutamol stimulated adipocytes isolated from WT and transgenic WAT from Chow-fed lean mice. WAT was subjected to collagenase digestion to separate adipocyte fraction from SVF. Adipocytes were then incubated with Salbutamol at indicated concentrations for 20 minutes before lysis and separation on SDS-PAGE for immunoblotting.

Project 2: PI3K γ Adaptor p84 Controls Adipose Lipolysis and Hepatic Steatosis

Table S1. RT-PCR primer list		
Target gene	Forward primer	Reverse primer
GAPDH	CTG CAC CAC CAA CTG CTT AG	CCA TCC ACA GTC TTC TGG GTG
18S	CCT GGA TAC CGC AGC TAG GA	GCG GCG CAA TAC GAA TGC CCC
Fc ϵ RI	TAG CAC TGC TGT TCA TGT CTC	GAG TTC ATT TGA AGG TGA TTG TT
F4/80	CTT TGG CTA TGG GCT TCC AGT C	GCA AGG AGG ACA GAG TTT ATC GTG
UPC-1	CCT GCC TCT CTC GGA AAC AA	TCT GGG CTT GCA TTC TGA CC
UPC-2	GGA AAA TCG AGG GGA TCG GG	GGA GTT CTG GAG GCT GCT TT
p101 (PIK3R5)	GCT GTG TCT GAA CTG CTG GA	CAG GAG GAT GAG GAA GTG GC
p84 (PIK3R6)	AGA GCT CAA CAC CCC AAA CC	TCC TGG GTT TCT CTC CAC CT
p110 γ (PIKCG)	CCC TGG TGA TCG AGA AAT GC	GTC TTG GCG CAG ATC ATC AC

Table S2. Antibodies for Western blot	
Antibody	Source
Mouse Anti-total-Akt	Cell Signaling, Cat# 2920S, clone 40D4
Rabbit Anti-Phospho-Akt Ser 473	Cell signaling, Cat# 4058, clone 193H12
Rabbit Anti-Phospho-Akt Thr308	Cell signaling, Cat# 4056, clone 244F9
Rabbit Anti-total MAPK	Sigma Aldrich, Cat# M7927, polyclonal
Mouse Anti-Phospho-MAPK p44p42	Sigma Aldrich, Cat# M8159, clone MAPK-YT
Rabbit Anti-HSL (total)	Cell Signaling, Cat# 4107, polyclonal
Rabbit Anti-HSL pSer660	Cell Signaling, Cat# 4126, polyclonal
Rabbit Anti-HSL pSer565	Cell Signaling, Cat# 4137, polyclonal
Rabbit Anti-HSL pSer563	Cell Signaling, Cat# 4139, polyclonal
Rabbit Anti-Perilipin 1	Cell Signaling, Cat# 9349, polyclonal
Mouse Anti-PI3K γ (Russian)	Alexis, clone H1
Rabbit Anti-p84 (Anti-p87)	Rabbit serum, epitope N-terminus of p84 (aa 1-162)

Project 2: PI3K γ Adaptor p84 Controls Adipose Lipolysis and Hepatic Steatosis

Rabbit Anti-p101	Cell Signaling Cat# 5569, clone D32A5
Mouse Anti-GAPDH	Sigma-Aldrich Cat# G8795, clone GAPDH-71.1
Mouse Anti-alpha Tubulin	Sigma-Aldrich Cat# T9026, clone DM1A
Mouse Anti-beta Actin	Sigma Aldrich, Cat# A5441, clone AC-15
Goat Anti-Rabbit IgG-Peroxidase	Sigma Aldrich, Cat# A6154, polyclonal
Goat Anti-Mouse IgG-Peroxidase	Sigma Aldrich, Cat# A4416, polyclonal

4.3. Project 3: Targeting of PI3K γ Adaptor p101 Deteriorates Th2 Inflammation in Autoimmunity-Prone PI3K δ ^{pp101 Δ} Mice

Manuscript in preparation

Targeting of PI3K γ Adaptor p101 Deteriorates Th2 Inflammation in Autoimmunity-Prone PI3K δ^{D910A} Mice

Julie R. Jin, Ana R. Xavier, Jan Voelzmann, Saulius Zuklys, Matthias P. Wymann
Department of Biomedicine, University of Basel, Basel, Switzerland

Abstract

Phosphoinositide-3-kinases (PI3Ks) in leukocytes have multiple roles in lymphocyte and myeloid development, activation and immune regulation. Receptor tyrosine, Src-related and Zap-70/Syk family kinases engage class IA PI3Ks, including PI3K δ isoform to promote growth as well as T and B cell receptor derived signals. The class IB PI3K, namely PI3K γ , however integrates G-protein coupled receptor signaling which mediates chemokine sensing and migration.

Here, we investigated the roles of PI3K γ and PI3K δ in regulation of inflammatory and tolerance signals. Transgenic mice lacking functional p110 δ kinase (p110 δ^{D910A}) were crossed with mice lacking either PI3K γ regulatory protein p84 or p101. The resulting p101 $^{-/-}$ /p110 $\delta^{D910A/D910A}$ off-springs develop severe colon inflammation with lymphocytic and eosinophilic infiltrates, loss of normal spleen architecture and hypomorph thymus, blood eosinophilia and lymphopenia. p84 $^{-/-}$ /p110 $\delta^{D910A/D910A}$ mice on the other hand show regular histology of lymphatic organs, no histological or serological signs of inflammation and exhibit normal circulating blood cells in the hematogram. More indebt investigations revealed that combinatory loss of p110 δ and either p101 or p84 results in elevated Immunoglobulin (Ig)E serum titers, reduction of IgG, IgA and IgM isotypes as well as reduction of B lymphocytes in the spleen, but p101 had a more pronounced effect than p84. These findings are in line with previous studies proposing that by hindering p110 δ and p101/p110 γ signaling, lymphopenia and limited T regulatory cell repertoire permit homeostatic expansion of auto-reactive cells to instigate Th2 bias and autoimmunity. Importantly, lymphocyte PI3K γ function depends on p101 while p84 is enriched in the myeloid lineage. Therefore, splenic lymphocyte deficit in p84 $^{-/-}$ /p110 $\delta^{D910A/D910A}$ mice implies non-lymphocyte-autonomous contribution of p84 to humoral immunity.

Introduction

Class I phosphoinositide 3-kinases (PI3Ks) provide lipid messenger phosphoinositide(3,4,5)trisphosphate (PtdIns(3,4,5)P3) signals that sustain cell survival, growth, proliferation, motility and more. The PI3K γ and PI3K δ isoforms are highly enriched in hematopoietic cells where they mediate critical signaling cascades in innate and adaptive immunity (1–4). PI3K δ is a dimeric complex assembled from the p110 δ catalytic and a p85-type regulatory subunit that is recruited by receptor and non-receptor tyrosine kinases. PI3K δ signaling has important roles downstream of growth receptors such as stem cell factor (SCF) receptor c-kit (5), in B cell signalosome formation as well as T cell receptor (TCR) dependent immune responses (6–8). The PI3K γ isoform in turn responds to G-protein coupled receptors (GPCRs) to integrate chemokine stimulation, cell motility and respiratory burst (9, 10).

Overt PtdIns(3,4,5)P3 production is present in many inflammatory conditions. Conversely, attenuation of Class I PI3K activity by genetical methods can resolve overshooting leukocyte activity in animal models of autoimmunity, allergy and chronic inflammation (11). In human disease heterozygous gain-of-function (GOF) mutations in the p110 δ or p85 encoding gene loci as well as homozygous loss-of-function (LOF) mutations are associated with primary immunodeficiency (12). Moreover, pharmacological inhibition of PI3K δ with the isoform-selective compound Idelalisib in patients with B cell malignancies suffers from autoimmune side-effects in the form of inflammatory bowel syndrome (13, 14). These seemingly contradictory results demonstrate the importance of fine-tuned and well dosed PI3K δ signaling for balanced immune responses.

Diminished PI3K δ signaling by transgenic introduction of a kinase-inactive p110 δ^{D910A} protein attenuates CD4⁺CD25⁺FoxP3⁺ T regulatory cell (Treg) suppressor function in the periphery (15). This phenotype is aggravated in PI3K $\gamma^{\text{-/-}}$ PI3K $\delta^{\text{D910A/D910A}}$ mice with spontaneous onset of multi-organ inflammation, predominantly in the gastrointestinal tract (7). In PI3K $\gamma^{\text{-/-}}$ PI3K $\delta^{\text{-/-}}$ as well as the PI3K $\gamma^{\text{-/-}}$ PI3K $\delta^{\text{D910A/D910A}}$ genotype thymus development is halted in the CD4-CD8-CD25⁺CD44⁻ DN3 stage marking massive apoptosis of immature thymocytes and unsuccessful TCR β gene arrangement (16, 17). Lymphopenia and limited TCR repertoire can indeed lead to homeostatic expansion of autoreactive T cells due to lack of adequate Treg control (18). The questions however arises whether and how non-T cells further contribute to autoimmunity in systemic absence of PI3K γ and PI3K δ signaling. Impaired B cell development

Project 3. Targeting of PI3K γ Adaptor p101 Deteriorates Th2 Inflammation

and deficit of splenic B cell survival factors are also associated with PI3K $\gamma\delta$ double deficiency, which explains abnormal spleen architecture and low basal antibody production (19). Myeloid derived signals in the spleen are likely to provide non-lymphocyte autonomous survival signals, and are hypothetically involved in Th1/Th2 balance and immunoglobulin class switching. Furthermore, functionality of effector cells that ultimately cause end organ damage are also altered by systemic PI3K $\gamma\delta$ inactivation. For example IgE-mediated asthma is attenuated in PI3K $\gamma^{-/-}$ PI3K $\delta^{D910A\Delta910A}$ genotype despite the Th2 biased cytokine and immunoglobulin profile (20), and neutrophil homeostasis is affected by aberrant IL-17 secretion (21).

PI3K γ exists in two complex variants, p110 γ /p101 and p110 γ /p84, that are unequally distributed throughout the hematopoietic lineages. While p101 is expressed in both the myeloid and lymphoid lineage, p84 is predominantly found in myeloid cells (22–24). Since p101/p110 γ and p84/p110 γ fulfil non-redundant functions in granulocytes (25, 26), mast cells (23, 27), and monocytes/macrophages (28), we investigated how the two PI3K γ variants affect cytokine secretion and systemic inflammation. We hypothesized that some myeloid branches of the innate immune system might aggravate and others resolve inflammation in mice prone to autoimmunity due to defective PI3K δ signaling in lymphocytes.

Materials and Methods

Mice

p110 δ^{D910A} , p110 $\gamma^{-/-}$, p101 $^{-/-}$ and p84 $^{-/-}$ mice were previously described (29, 9, Jin & Da Costa Xavier, *manuscripts in preparation*). Crossing scheme to generate double mutants is shown in Figure 1. Of note, p84 $^{-/-}$ /p110 $\delta^{-/-}$ mice do breed homozygously with normal litter sizes. Conversely, p101/p110 δ as well as p110 γ /p110 δ mutants had to be bred with heterozygous parents (p101 $^{-/-}$ /p110 $\delta^{D910A/WT}$ and p110 $\gamma^{-/-}$ /p110 $\delta^{D910A/WT}$ respectively) since homozygous animals would not generate offspring and periodically experience diarrhea and weight loss when reaching mating age. Homozygous double mutants from all mouse lines were sacrificed between 8-12 weeks of age for histological or serum analysis. Thymus and spleen samples were taken from 3-4 week old animals. All mice were on BL6/J background and all animal experiments were approved by the Swiss Federal Veterinary Office (SFVO) and the Cantonal Veterinary Office of Basel-Stadt (license number 29615).

Hematograms and serum analysis

Animals were sacrificed with CO₂ and full blood samples were drawn from heart puncture into EDTA coated tubes for blood cell count. ADVIA hemocytometer (Siemens) was used for automated profiling of blood cells. For serum analysis a second aliquot of untreated full blood was allowed to clot and subsequently centrifuged at 900 x g for 10 minutes at 4°C to separate serum from cells. Cytokines were measured on Mesoscale 7-Plex pro-inflammatory kit (MSD K15012B) and immunoglobulins (except IgE) were detected using Mesoscale Mouse Isotyping Panel 1 kit (MSD K15183B). Serum IgE was measured by ELISA with a commercial kit from Sigma (RA-B0799).

Histology

Histopathological assessment was conducted by mouse pathologists of Frimorfo (Fribourg, Switzerland). Mice were perfused with a peristaltic pump through the left ventricle first with 0.9% saline, followed by 10 ml of 4% paraformaldehyde in 0.1M phosphate buffer, pH 7.3. The organs were left *in situ* overnight and dissected the following day. Colon, thymus, spleen, lymph nodes and glands were then embedded in paraffin. Bones were immersed in decalcifying medium (Surgipath, Leica) for 3 weeks. Paraffin blocks were cut at various levels in 3 μ m sections with a Leica RM2135 microtome and mounted on Superfrost slides. Sections were stained with Hematoxylin-Eosin (H&E), May-Gruenwald-Giemsa and Periodic acid-Schiff (PAS). Images were acquired using a Leica DM6000 epifluorescence microscope equipped with a Hamamatsu C4742-95 camera and a Nanozoomer digital slide scanner.

Flow cytometry

Mouse spleens were manually disintegrated and filtered through a 70 μ m cell strainer to create single cell suspension. Red blood cells were lysed (eBioscience 00-4333-57) and splenocytes were treated with Fc receptor inhibitor (CD16/CD32; BD Biosciences 553142). The applied FACS antibody panel is provided in Table 1. Results were acquired on a Cytoflex LX 2-005 (Beckman Coulter) and analyzed with FloJo version 10.7.1 (Becton Dickinson & Company).

Project 3. Targeting of PI3K γ Adaptor p101 Deteriorates Th2 Inflammation

Table 1. FACS antibody mix for mouse peritoneal cells and splenocytes					
	mAb	Fluorochrome	Cytoflex laser	Concentration/Dilution	Volume in 100uL
Lymphoid cells	CD3	FITC	B525 FITC	0.25 μ g (1:200)	0.5
	CD8	APC-Cy7	R763 APCA750	0.06 μ g (1:320)	0.32
	CD4	BV785	V763	0.12 μ g (1:160)	0.63
	Nk1.1	PE	Y585 PE	0.06 μ g (1:320)	0.32
	CD19	BUV661	UV675	0.12 μ g (1:160)	0.63
	IgD	BV605	V610	0.125 μ g (1:160)	0.63
	IgM	PE-Cy7	Y763-PC7	0.25 μ g (1:80)	1.25
Myeloid cells	F4/80	PE/Dazzle 594	Y610 mcherry	0.25 μ g (1:160)	1.25
	CD11c	BV650	V660	0.25 μ g (1:80)	1.25
	Siglec F (CD170)	BV421	V450 PB	0.13 μ g (1:160)	0.63
	Ly6G	BV510	V525-PB	0.25 μ g (1:80)	1.25
	CD11b	BUV395	UV405	0.12 μ g (1:160)	0.63
	MHC II (IA^b)	AF700	R712- APCA700	0.125 μ g (1:400)	0.25
	cKit (CD117)	APC	R660-APC	0.125 μ g (1:160)	0.63
	FcϵRI alpha	PerCP-Cy5.5	B690 PC5.5	0.125 μ g (1:160)	0.63
Live/Dead	DAPI	-	UV525	3 μ M (1:100)	1

Results

Eosinophilia, neutrophilia, lymphopenia and anemia in p101/p110 δ transgenic mice

We generated double mutant mice by crossing p110 δ ^{D910A} kinase-inactive mutants with either p101, p84 or p110 γ null mice. The hereby resulting offsprings were crossed with each other until homozygous for both alleles. Since homozygous p110 γ /p110 δ and p101/p110 δ mutants would not breed, homozygous experimental animals had to be crossed from parents heterozygous on the p110 δ allele (p101^{-/-}/p110 δ ^{D910A/WT} and p110 γ ^{-/-}/p110 δ ^{D910A/WT} respectively). With this approach homozygous animals were born in mendelian ratio. Opposingly, p84/p110 δ mice could be bred from homozygous parents and did not present any gross phenotype. A schematic representation of the mouse crossing scheme is depicted in Figure 1A.

The hematograms of single and double transgenic mice revealed conspicuous surplus of eosinophilic granulocytes in p101^{-/-}/p110 δ ^{D910A/D910A} and p110 γ ^{-/-}/p110 δ ^{D910A/D910A} mutants (Figure 1B, S1). Eosinophils are usually rare cells in the circulation ($2.6 \pm 1.34\%$ in wild-types, WT, mean \pm SD) but made up to $18.9 \pm 9.9\%$ of leukocytes in the blood of p101^{-/-}/p110 δ ^{D910A/D910A} animals and $7.23 \pm 6.52\%$ in p110 γ ^{-/-}/p110 δ ^{D910A/D910A} mice. Basophil numbers remained unaltered (Figure 1C), and increases in circulating neutrophil counts were present in p101, p110 γ as well as the corresponding p101^{-/-}/p110 δ ^{D910A/D910A} and p110 γ ^{-/-}/p110 δ ^{D910A/D910A} double mutants (Figure 1D). Slightly reduced monocyte numbers in p110 γ ^{-/-}/p110 δ ^{D910A/D910A} mice were found, though the absolute number of monocytes is generally already low under non-stimulated conditions (Figure 1G). However, a more severe problem for p101^{-/-}/p110 δ ^{D910A/D910A} and p110 γ ^{-/-}/p110 δ ^{D910A/D910A} transgenic mice is the substantial leukopenia with lymphocyte numbers dropping to approximately a third of the blood counts of healthy mice (Figure 1E). Instead of . Large unstained cells (LUC) represent a variety of unspecific cells including blasts and were not significantly altered or elevated (Figure 1F).

Furthermore red blood cell count (RBC, Figure 1H), total hemoglobin (Hb, Figure 1I), mean erythrocyte volume (MCV, Figure 1J) and hemoglobin contents per erythrocyte (MCH, Figure 1K) indicate microcytic hypochromic anemia in p101^{-/-}/p110 δ ^{D910A/D910A} mice, but is less pronounced in p110 γ ^{-/-}/p110 δ ^{D910A/D910A} mice (Figure 4G-J). Platelet count and size remained unaffected in all examined strains (Figure 1L&M).

Figure 1. Combined loss of p101 and p110 δ reduces circulating lymphatic cells in parallel with expansion of myeloid lineage

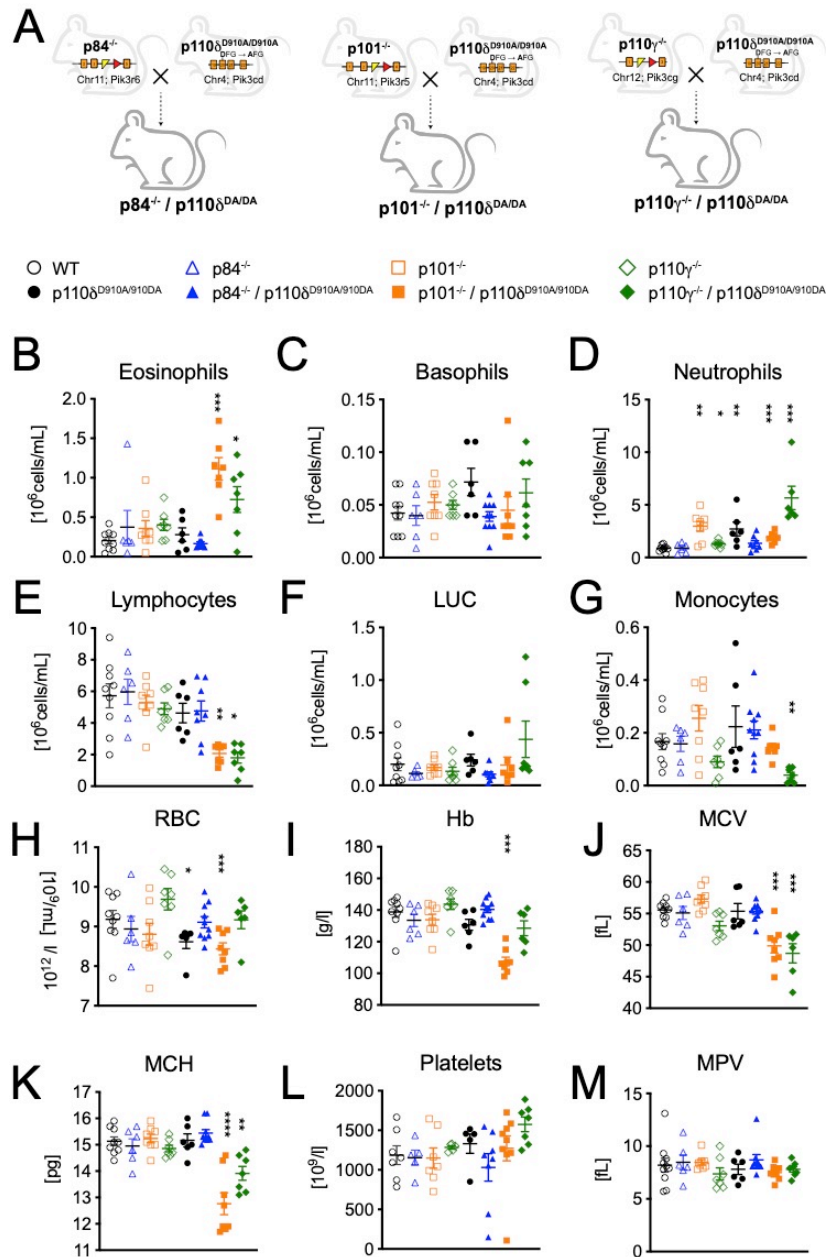


Figure 1. Hematograms of WT and transgenic mouse lines indicate lymphopenia and expansion of granulocytes in p101 $^{-/-}$ /p110 $\delta^{D910A/D910A}$ strain. (A) Mice expressing kinase-inactive p110 δ^{D910A} were crossed with either p110 $\gamma^{-/-}$, p101 $^{-/-}$ or p84 $^{-/-}$ mice. Offspring became heterozygous for both alleles and were further crossed with respective animals lacking PI3K γ subunit p110 γ , p101 or p84 to achieve homozygosity for the first allele. These mice were further crossed with each other to obtain experimental mice that were homozygous for both alleles. Leukocytes in EDTA anti-coagulated full blood were counted using a hemocytometer. Numbers of **(B)** eosinophilic, **(C)** basophilic and **(D)** neutrophilic granulocytes, **(E)** lymphocytes, **(F)** large unstained cells (LUC), **(G)** monocytes, **(H)** red blood cells (RBC) and **(I)** platelets per ml full blood. **(J)** Hemoglobin is indicated in gram/liter. **(K)** Mean corpuscular volume (MCV) and **(L)** Mean corpuscular hemoglobin (MCH) of erythrocytes and **(M)** Mean platelet volume (MPV) are calculated values. All mice subjected to blood analysis were between 8-12 weeks of age. Results are presented as mean \pm SEM of 6-10 mice per genotype. P-values are *: p<0.05, **: p<0.01, ***: p<0.001, ****: p<0.0001.

PI3K γ targeting exacerbates IgE isotype switching in vulnerable mice with inactivated PI3K δ

We next wondered whether the remarkably diminished circulating lymphocyte numbers would affect antibody production and whether p84 and p101 impact the type of antibody being secreted. Therefore we elaborately analyzed the serum immunoglobulin profiles of 8-12 week old mice. Disruption of PI3K δ alone only mildly impacted immunoglobulin production with selective decreases in IgG2a and IgA. Loss of PI3K δ signaling in combination with any PI3K γ complex component however results in dropped total immunoglobulin levels (Figure 2A). p84 $^{-/-}$ /p110 $\delta^{D910A/D910A}$ mice show an intermediate phenotype with significantly reduced IgG1, IgG2A, IgG2b, IgG3, IgA and IgM, while in p101 $^{-/-}$ /p110 $\delta^{D910A/D910A}$ and p110 $\gamma^{-/-}$ /p110 $\delta^{D910A/D910A}$ mice also IgG3 is abnormally lowered (Figure 2C-H). The lack of IgG, IgA and IgM isotypes in the double mutant genotypes was accompanied by substantial elevation of IgE. p84 $^{-/-}$ /p110 $\delta^{D910A/D910A}$ mice show 6-fold, p101 $^{-/-}$ /p110 $\delta^{D910A/D910A}$ 48-fold and p110 $\gamma^{-/-}$ /p110 $\delta^{D910A/D910A}$ 23-fold increase in serum IgE titers (Figure 2B). However, the high IgE secretion could not replenish total immunoglobulins amount summed up in Figure 2A in any case.

Figure 2. Combined PI3K δ and PI3K γ inactivation lead to varying degrees of immunoglobulin deficiency and isotype switching towards IgE

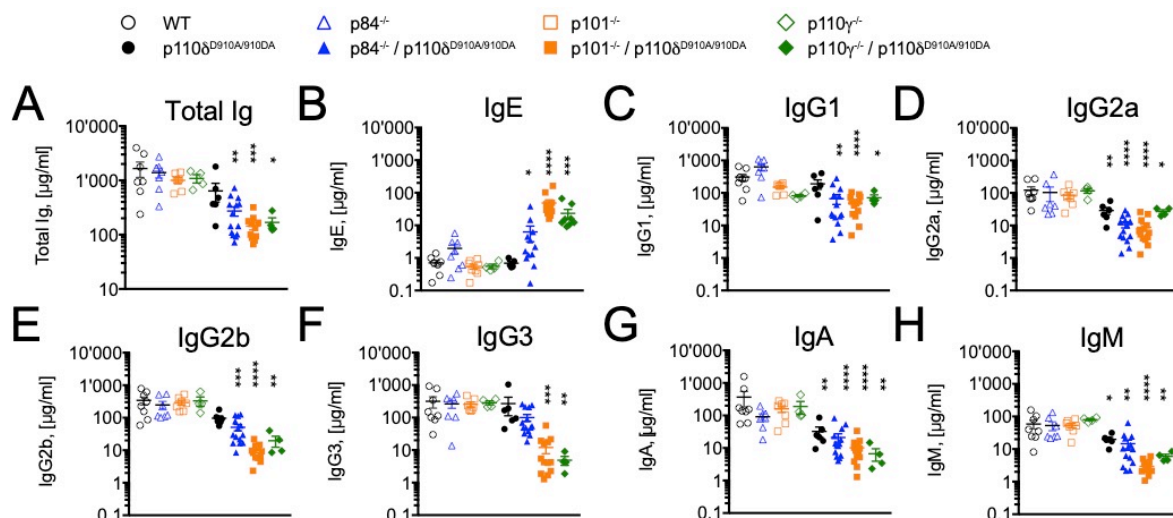


Figure 2. Immunoglobulin isotyping reveal shift towards IgE in double mutant mice. Immunoglobulin isotypes were detected in serum of 8-12 week old WT and transgenic mice. (A) Total Immunoglobulin (Ig) is the sum of all Ig isotypes in (B-H). Each data point on graph represents one animal and lines indicate mean \pm SEM. P-values are *: $p < 0.05$, **: $p < 0.01$, ***: $p < 0.001$, ****: $p < 0.0001$.

Th1 and Th2 cytokines are elevated in p101^{-/-}/p110 δ ^{D910A/D910A} mouse serum

Since Th2 cytokines favor immunoglobulin switching towards IgE we investigated the cytokine concentrations in mouse serum to check, whether differences in Th1/Th2 balance would correlate with immunoglobulin profiles. Indeed, IL-5, a Th2 cytokine and eosinophil maturation factor was elevated in p101^{-/-}/p110 δ ^{D910A/D910A} and p110 γ ^{-/-}/p110 δ ^{D910A/D910A} mice (Figure 3D). IL-4 showed a similar trend, however systemic concentrations were partly below detection limit and the results did not reach statistical significance. We attempted to measure IL-13 and IL-33 as additional Th2 markers, but did not find meaningful differences between genotypes. Regarding pro-inflammatory Th1 cytokines, TNF- α levels were substantially increased in the serum of p101^{-/-}/p110 δ ^{D910A/D910A} as well as p110 γ ^{-/-}/p110 δ ^{D910A/D910A} mice (Figure 3A). IL-6 was also elevated but is seemingly subject to greater variability between animals (Figure 3B). Conversely, p84^{-/-}/p110 δ ^{D910A/WT} show no signs of abnormal Th1 nor Th2 cytokine elevation.

Figure 3. p101 but not p84 disruption increases systemic cytokine concentrations in p110 δ ^{D910A} mutated mice

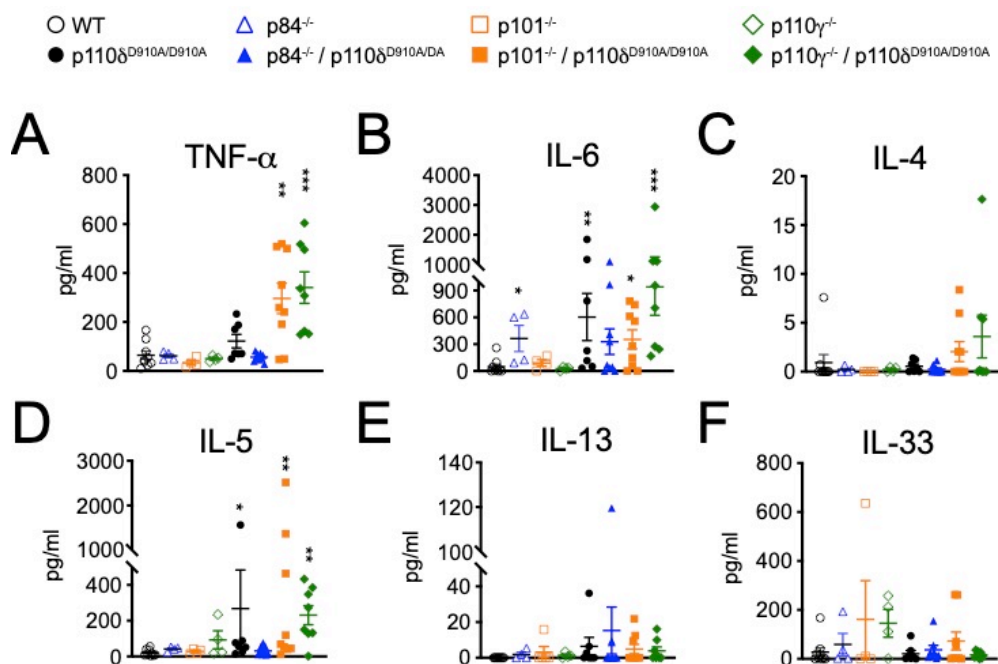


Figure 3. Systemic Th1 and Th2 cytokine concentrations detected in serum. Serum from 8-12 week old mice of indicated genotypes were probed for pro-inflammatory Th1 cytokines TNF- α (A) and IL-6 (B) as well as anti-inflammatory Th2 cytokines IL-4 (C), IL-5 (D), IL-13 (E) and IL-33 (F). N=4 for p84^{-/-}, p101^{-/-} and p110 γ ^{-/-} single knock-outs and N=7-9 for all other genotypes. Results are shown as mean \pm SEM. p-values of Mann-Whitney non-parametric tests are *: p<0.05, **: p<0.01, ***: p<0.001.

p101^{-/-}/p110 δ ^{D910A/D910A} transgenic mice develop colitis

We next checked for disease signs and organ damage corresponding to the elevated cytokine production. Mice devoid of functional p110 γ /p110 δ or p101/p110 δ develop colitis at variable ages. In mice older than 8 weeks we found histological evidence for gut inflammation, most consistently in the colon mucosa (Figure 4A). In H&E stained sections, lamina propria is infiltrated with neutrophilic and eosinophilic granulocytes and the mucosal layer was thickened and hypertrophic. Gut histology of age-matched WT and p84^{-/-}/p110 δ ^{D910A/D910A} are completely healthy without indications for inflammatory activity.

Figure 4. Gut inflammation and signs of distorted lymphatic organ organization in p101^{-/-}/p110 δ ^{D910A/D910A} spleen and thymus

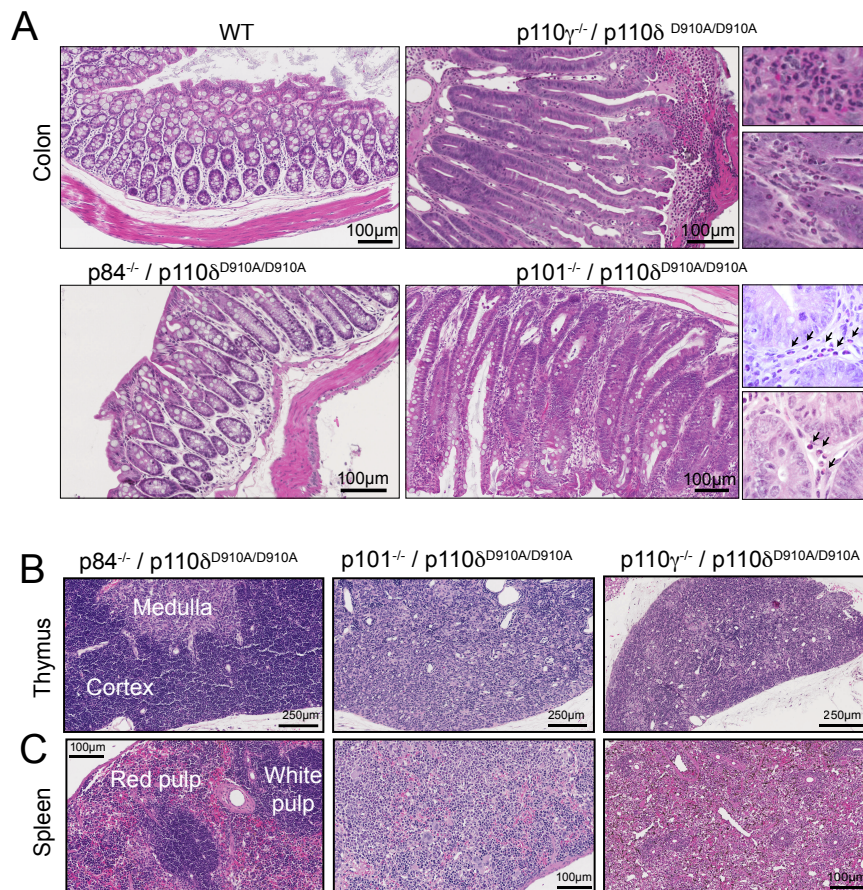


Figure 4. Histology of colon and lymphatic organs. (A) Representative H&E stained colons from 8 week old mice showing normal mucosa in WT and p84^{-/-}/p110 δ ^{D910A/D910A} mice, while p110 γ ^{-/-}/p110 δ ^{D910A/D910A} and p101^{-/-}/p110 δ ^{D910A/D910A} mutants develop colitis with hypertrophic mucosa and infiltrations with eosinophilic granulocytes (arrows). **(B)** Thymus and **(C)** spleen were collected from 8 week old mice and stained with H&E. Normal cortico-medullary organization is visible in p84^{-/-}/p110 δ ^{D910A/D910A} thymus while not identifiable in p101^{-/-}/p110 δ ^{D910A/D910A} and p110 γ ^{-/-}/p110 δ ^{D910A/D910A} thymi. Distinction between white and red pulp is only maintained in p84^{-/-}/p110 δ ^{D910A/D910A} spleen and becomes irregular in the other genotypes

Disorganization of lymphatic tissues in p101^{-/-}/p110 δ ^{D910A/D910A} genotype

More discrepancies between the p84^{-/-}/p110 δ ^{D910A/D910A} and p101^{-/-}/p110 δ ^{D910A/D910A} phenotype concern the macroscopic and microscopic appearance of lymphatic tissues. Histological analysis suggests heavily defective development and organization of thymus and spleen of p101^{-/-}/p110 δ ^{D910A/D910A} and p110 γ ^{-/-}/p110 δ ^{D910A/D910A} mutant mice. In comparison with p84^{-/-}/p110 δ ^{D910A/D910A} animals that have normal thymus size and clearly demarcated cortical and medullary zones, elimination of p101 or p110 γ instead led to thymus atrophy and loss of cortico-medullary organization. The cortex remains depleted of lymphocytes (Figure 4B). Furthermore, the spleens of p101^{-/-}/p110 δ ^{D910A/D910A} and p110 γ ^{-/-}/p110 δ ^{D910A/D910A} mice presented dispersed white pulp and the three normal compartments of the lymphatic tissue, namely periarteriolar lymphocyte sheath (PALS), follicular zones and marginal zone, were not identifiable. The red pulp contains numerous foci of hematopoiesis with cells belonging to the erythroid, myeloid and megakaryocytic lineage (Figure 4C).

Figure 5. Loss of lymphocyte compartment and compensatory upregulation of myeloid lineage p101^{-/-}/p110 δ ^{D910A/D910A} mice

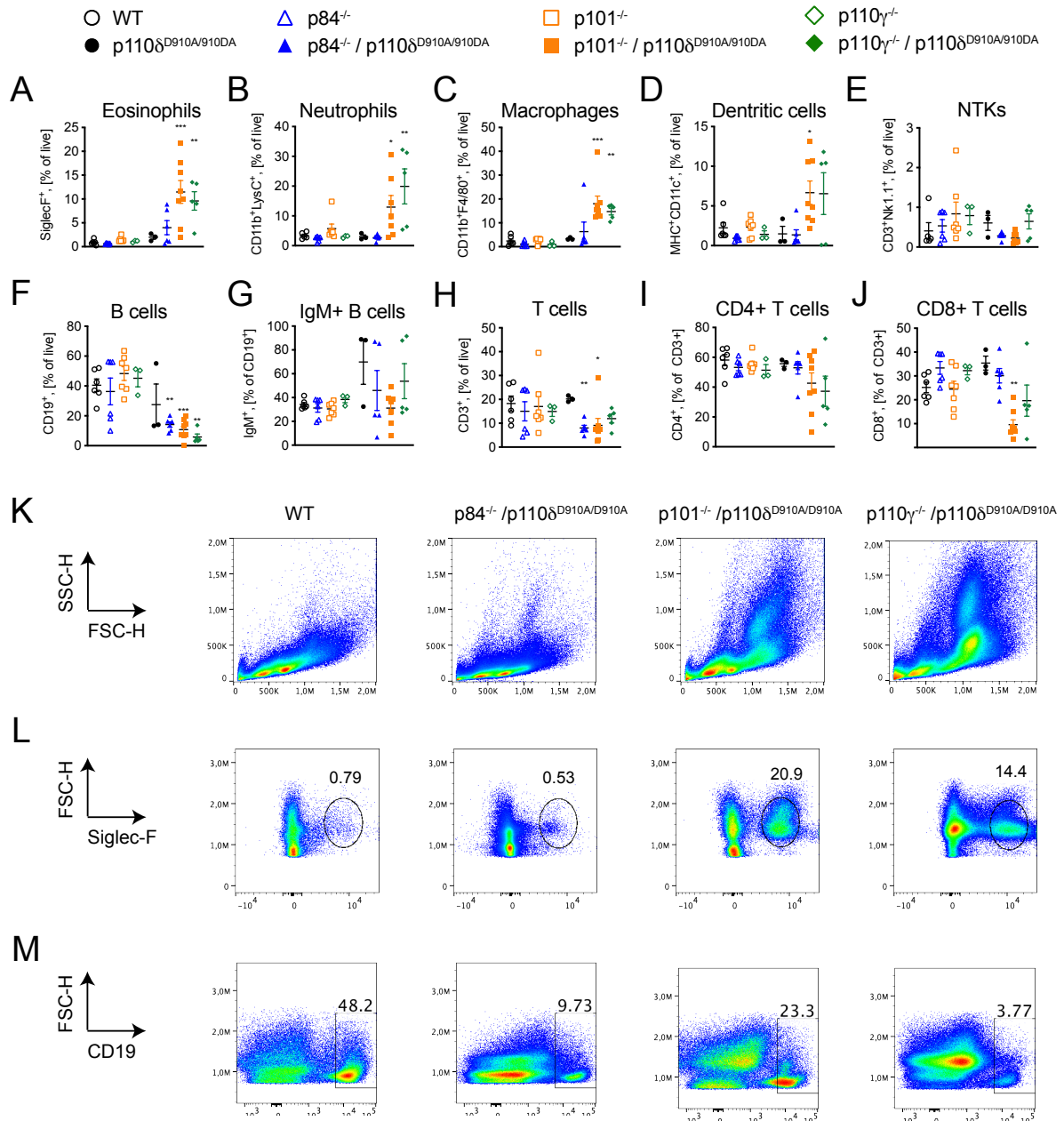


Figure 5. p101^{-/-}/p110 δ ^{D910A/D910A} mice display splenic lymphopenia and expansion of myeloid cells. (A-E) are represented as % of live spleen cells (F) CD19⁺ B cells were further probed for surface IgM expression (G). (H) CD3⁺ T cells were further divided in to (I) CD4⁺ and (J) CD8⁺ subpopulations. All spleens were isolated from 3-4 week old mice. Mean \pm SEM of n=3-8 mice per genotype. P-values are *: p<0.05, **: p<0.01, ***: p<0.001. (K) Expansion of granulated cells in p101^{-/-}/p110 δ ^{D910A/D910A} and p110 γ ^{-/-}/p110 δ ^{D910A/D910A} spleens. (L) Gating of CD3⁺ CD19⁺ SiglecF⁺ eosinophilic granulocytes. (M) Gating of CD19⁺ B cells.

Loss of p101 and p110 δ drives splenic lymphopenia and increase of myeloid cells

For better understanding of the disorganized spleen phenotype we went on further characterizing splenocytes by flow cytometry. Since chronic stressors such as inflammatory bowel disease, infection or other chronic inflammation can influence spleen composition, we chose young mice at 3-4 weeks of age to obtain a picture of the immune state before mice develop additional symptoms. In accordance with the blood counts of 8-12 week old mice, 3-week old p101^{-/-}/p110 δ ^{D910A/D910A} and p110 γ ^{-/-}/p110 δ ^{D910A/D910A} targeted mice have elevated myeloid cell counts also in the spleen. Particularly SiglecF⁺ eosinophilic and CD11b⁺Ly6C⁺ neutrophilic granulocytes were overrepresented, and splenic antigen presenting cells such as CD11b⁺F4/80⁺ macrophages and CD11c⁺MHCII⁺ dendritic cells were also relatively increased (Figure 6A-D). This increase of myeloid cells corresponds with a simultaneous decrease of lymphoid cells, namely B cells (CD19⁺), as well as CD4⁺ and CD8⁺ CD3⁺ T cells (Figure 5F-J). In the p84^{-/-}/p110 δ ^{D910A/D910A} line we found decrease of CD3⁺ cells while CD4/CD8 was maintained (Figure 5H-J), and CD19⁺ B cells with highly variable degrees of surface IgM expression (Figure 5F,G&M).

Discussion

Manipulation of PI3K signaling in leukocytes deeply disturbs normal regulatory mechanisms that ensure proper balance between host defense and tolerance. We recognize different significances of PI3K γ adaptor proteins p101 and p84 in autoimmunity-prone p110 δ^{D910A} mice.

We could clearly reproduce thymus hypotrophy and lymphopenia in p110 $\gamma^{-/-}$ /p110 δ^{D910A} mice as previously described (17), as well as halted thymocyte DN3 to DN4 transition in p101 $^{-/-}$ /PI3K $\delta^{D910A/D910A}$ mutants (30) (supplementary Figure S3). Beyond, we document the Th2 skewed immune signature, consisting of highly elevated immunoglobulin E levels (Figure 2), eosinophilic infiltration in gut mucosa (Figure 4) and increased IL-4 and IL-5 secretion (Figure 3) of p101 $^{-/-}$ /p110 $\delta^{D910A/D910A}$ genotype. p101 $^{-/-}$ /p110 $\delta^{D910A/D910A}$ mice emulate the phenotype of p110 $\gamma^{-/-}$ /p110 $\delta^{D910A/D910A}$ mutants with regard to histology and blood parameters (Figure 1&4), which is firstly in line with the involvement of p101 in thymocyte development and secondly agrees with the concept of homeostatic expansion causing autoimmunity. When applying side-by-side comparison to the immune status of p84 $^{-/-}$ /p110 $\delta^{D910A/D910A}$ mice we came to realize that p84 is far less critical for maintenance of leukocyte homeostasis. p84 $^{-/-}$ /p110 $\delta^{D910A/D910A}$ mutants are spared from thymus anomalies and have normal lymphocyte numbers in the periphery. Still, basal immunoglobulin production is impaired and we observe a class switch bias towards IgE isotype, even though the effect is quantitatively less pronounced than in p101 $^{-/-}$ /p110 $\delta^{D910A/D910A}$ mice. B cell antibody production with and without T cell help both rely on functional PI3K δ . On one side, class switch recombination is suppressed in PI3K δ deficient B lymphocytes. In turn, mice with overshooting PI3K signaling due to PTEN loss experience accumulation of IgM producing B cells and increased expression of activation induced cytidine deaminase (AID) (31). In line with previous reports (29), in our cohort loss of PI3K δ signaling causes slight decreases in IgG2a, IgA and IgM. Additional elimination of p101 or p84 increases IgE secretion and further decreases IgG1 and IgG2b (Figure 2). GPCR derived signals are poorly documented in context of B cell isotype switching, thus it remains unclear what PI3K γ -dependent reaction might favor IgE production. IL-4 provokes expression of the immunoglobulin constant C ϵ - region in germinal center B cells undergoing recombination (32). The sources of IL-4 include Th2 cells and might involve myeloid or stromal cells.

Furthermore, lymphopenia itself is associated with Th2 skewing (18, 33). p84 $^{-/-}$ /p110 $\delta^{D910A/D910A}$ mice have normal circulating lymphocyte numbers but show splenic B and T cell depletion

Project 3. Targeting of PI3K γ Adaptor p101 Deteriorates Th2 Inflammation

(Figure 5). Lymphocyte-autonomous effects unlikely explain this observation because p84 is not expressed in lymphocytes (23). On this basis it is more plausible to attribute B cell depletion in the spleens of p84^{-/-}/p110 $\delta^{\text{D910A/D910A}}$ animals to a lack of lymphocyte-extrinsic survival factors. Beer-Hammer and colleagues found decreased B cell survival when p110 $\gamma^{\text{-/-}}$ /p110 δ^{D910A} bone marrow was adoptively transferred to irradiated WT recipient mice. Proliferation of purified B cells however was not impacted by PI3K $\gamma\delta$ deficiency which led to the conclusion that non-cell-autonomous reasons cause B cell lymphopenia (19). Our results show now that maintenance of splenic lymphocyte populations are partly dependent on myeloid or stroma linked p84 function. However this effect is only exposed on the background of p110 $\delta^{\text{D910A/D910A}}$ mutation which predisposed to B cell apoptosis, as p84^{-/-} genotype itself is insufficient to distort lymphocyte homeostasis.

Of note, in contrast to hyper IgE syndrome (HIES, Job's syndrome) and the inflammatory phenotype of p101^{-/-}/p110 $\delta^{\text{D910A/D910A}}$ genotype, surplus IgE production in p84^{-/-}/p110 $\delta^{\text{D910A/D910A}}$ mice is asymptomatic. We did not observe spontaneous unprovoked onset of inflammation in the gastrointestinal tract, nor did the animals show obvious signs of severe illness, such as diarrhea, weight loss, anemia or infertility. It is currently unclear whether vulnerable antibody production and relative IgE overrepresentation would have consequences during challenge with allergens or infectious agents. p110 $\gamma^{\text{-/-}}$ /p110 $\delta^{\text{D910A/D910A}}$ have previously been subjected to OVA-induced allergic asthma where they remained unaffected from airway inflammation despite high serum IgE levels (20). This reflects the inability of effector lymphocytes, mast cells, eosinophils or neutrophils, to execute destructive actions in mice systemically lacking PI3K γ and PI3K δ signaling. It is difficult to estimate the contribution of p101 in inflammatory effector cells in the current model, since anti-apoptotic signals are most relevant in the neonatal thymus but effector lymphocyte and myeloid cell activation may initiate later in life. We were therefore not able to clearly separate the phenotype of thymocyte intrinsic p101 action from possible effects in antigen-presenting cells (APCs), granulocytes, CD8 T cells and others. Pharmacologic PI3K inhibition in a therapeutic context is usually necessary in adulthood when primary lymphopoiesis is complete. Gene-targeted mouse models with congenital PI3K defects often do not adequately picture this situation. There again, pharmacological tools to study the biological roles of p84 and p101 are not yet available. In this regard the p84^{-/-}/p110 $\delta^{\text{D910A/D910A}}$ mouse represents a complementary model system to learn about the significance of myeloid PI3K γ signaling in humeral immunity.

Acknowledgements

We thank Gael Aurey for help with flow cytometry and Dimitros Tsakiris and Labormedizin Universitätsspital Basel for access to hemocytometer and technical support.

References

1. Hawkins, P. T., and L. R. Stephens. 2015. PI3K signalling in inflammation. *Biochim Biophys Acta* 1851: 882-897.
2. So, L., and D. A. Fruman. 2012. PI3K signalling in B- and T-lymphocytes: new developments and therapeutic advances. *Biochem J* 442: 465-481.
3. Costa, C., E. L. Martin-Conte, and E. Hirsch. 2011. Phosphoinositide 3-kinase p110 γ in immunity. *IUBMB Life* 63: 707-713.
4. Wymann, M. P., K. Björklöf, R. Calvez, P. Finan, M. Thomast, A. Trifilieff, M. Barbier, F. Altruda, E. Hirsch, and M. Laffargue. 2003. Phosphoinositide 3-kinase gamma: a key modulator in inflammation and allergy. *Biochem Soc Trans* 31: 275-280.
5. Ali, K., A. Bilancio, M. Thomas, W. Pearce, A. M. Gilfillan, C. Tkaczyk, N. Kuehn, A. Gray, J. Giddings, E. Peskett, R. Fox, I. Bruce, C. Walker, C. Sawyer, K. Okkenhaug, P. Finan, and B. Vanhaesebroeck. 2004. Essential role for the p110delta phosphoinositide 3-kinase in the allergic response. *Nature* 431: 1007-1011.
6. Okkenhaug, K., and B. Vanhaesebroeck. 2003. PI3K-signalling in B- and T-cells: insights from gene-targeted mice. *Biochem Soc Trans* 31: 270-274.
7. Clayton, E., G. Bardi, S. E. Bell, D. Chantry, C. P. Downes, A. Gray, L. A. Humphries, D. Rawlings, H. Reynolds, E. Vigorito, and M. Turner. 2002. A crucial role for the p110delta subunit of phosphatidylinositol 3-kinase in B cell development and activation. *J Exp Med* 196: 753-763.
8. Aiba, Y., M. Kameyama, T. Yamazaki, T. F. Tedder, and T. Kurosaki. 2008. Regulation of B-cell development by BCAP and CD19 through their binding to phosphoinositide 3-kinase. *Blood* 111: 1497-1503.
9. Hirsch, E., V. L. Katanaev, C. Garlanda, O. Azzolino, L. Pirola, L. Silengo, S. Sozzani, A. Mantovani, F. Altruda, and M. P. Wymann. 2000. Central role for G protein-coupled phosphoinositide 3-kinase gamma in inflammation. *Science* 287: 1049-1053.
10. Sasaki, T., J. Irie-Sasaki, R. G. Jones, A. J. Oliveira-dos-Santos, W. L. Stanford, B. Bolon, A. Wakeham, A. Itie, D. Bouchard, I. Kozieradzki, N. Joza, T. W. Mak, P. S. Ohashi, A. Suzuki, and J. M. Penninger. 2000. Function of PI3Kgamma in thymocyte development, T cell activation, and neutrophil migration. *Science* 287: 1040-1046.
11. Rommel, C., M. Camps, and H. Ji. 2007. PI3K delta and PI3K gamma: partners in crime in inflammation in rheumatoid arthritis and beyond. *Nat Rev Immunol* 7: 191-201.
12. Lucas, C. L., A. Chandra, S. Nejentsev, A. M. Condliffe, and K. Okkenhaug. 2016. PI3K δ and primary immunodeficiencies. *Nat Rev Immunol* 16: 702-714.
13. Weidner, A. S., N. C. Panarelli, J. T. Geyer, E. B. Bhavsar, R. R. Furman, J. P. Leonard, J. Jessurun, and R. K. Yantiss. 2015. Idelalisib-associated Colitis: Histologic Findings in 14 Patients. *Am J Surg Pathol* 39: 1661-1667.
14. Yeung, C. C., D. M. Hockenbery, M. Westerhoff, S. E. Coutre, R. H. Sedlak, R. L. Dubowy, V. Munugalavadla, K. Taylor, and F. Bosch. 2018. Pathological assessment of gastrointestinal biopsies from patients with idelalisib-associated diarrhea and colitis. *Future Oncol* 14: 2265-2277.
15. Patton, D. T., O. A. Garden, W. P. Pearce, L. E. Clough, C. R. Monk, E. Leung, W. C. Rowan, S. Sancho, L. S. Walker, B. Vanhaesebroeck, and K. Okkenhaug. 2006. Cutting edge: the phosphoinositide 3-kinase p110 delta is critical for the function of CD4⁺CD25⁺Foxp3⁺ regulatory T cells. *J Immunol* 177: 6598-6602.
16. Swat, W., V. Montgrain, T. A. Doggett, J. Douangpanya, K. Puri, W. Vermi, and T. G. Diacovo. 2006. Essential role of PI3Kdelta and PI3Kgamma in thymocyte survival. *Blood* 107: 2415-2422.

Project 3. Targeting of PI3K γ Adaptor p101 Deteriorates Th2 Inflammation

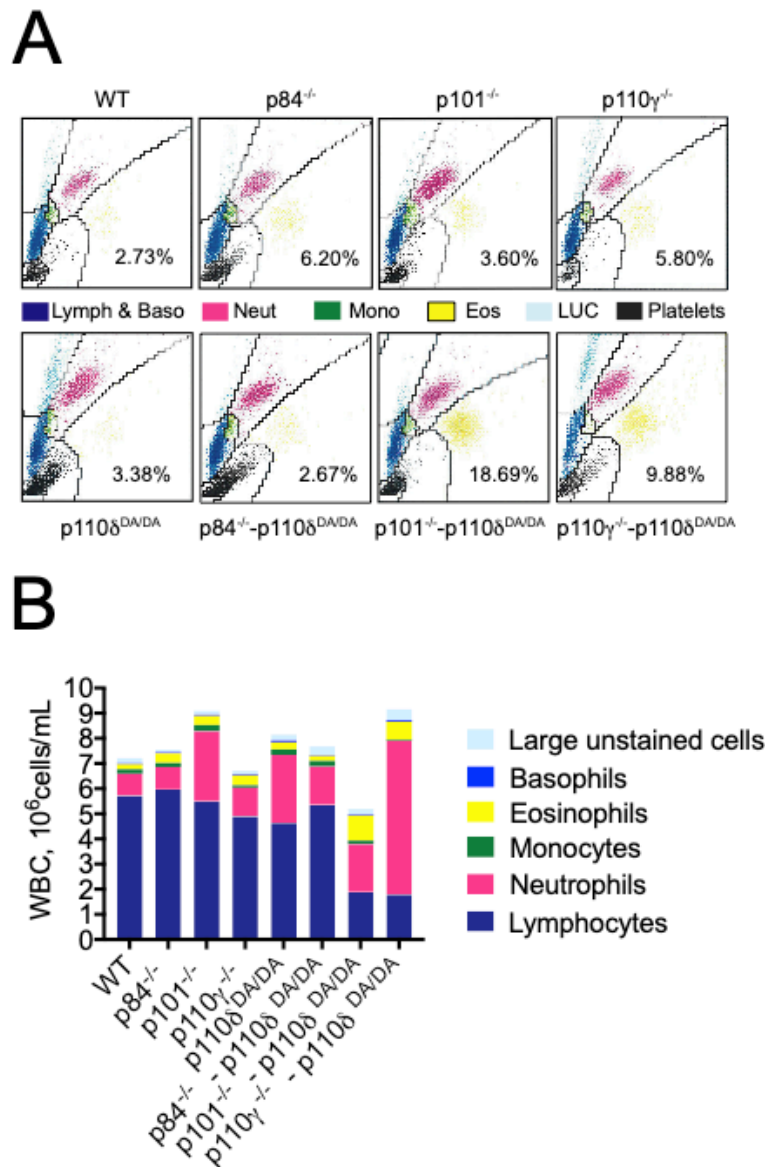
17. Ji, H., F. Rintelen, C. Waltzinger, D. Bertschy Meier, A. Bilancio, W. Pearce, E. Hirsch, M. P. Wymann, T. Rückle, M. Camps, B. Vanhaesebroeck, K. Okkenhaug, and C. Rommel. 2007. Inactivation of PI3K γ and PI3K δ distorts T-cell development and causes multiple organ inflammation. *Blood* 110: 2940-2947.
18. Milner, J. D., J. M. Ward, A. Keane-Myers, and W. E. Paul. 2007. Lymphopenic mice reconstituted with limited repertoire T cells develop severe, multiorgan, Th2-associated inflammatory disease. *Proc Natl Acad Sci U S A* 104: 576-581.
19. Beer-Hammer, S., E. Zebedin, M. von Holleben, J. Alferink, B. Reis, P. Dresing, D. Degrandi, S. Scheu, E. Hirsch, V. Sexl, K. Pfeffer, B. Nürnberg, and R. P. Piekorz. 2010. The catalytic PI3K isoforms p110 γ and p110 δ contribute to B cell development and maintenance, transformation, and proliferation. *J Leukoc Biol* 87: 1083-1095.
20. Mothes, B., K. Bucher, S. Ammon-Treiber, M. Schwab, R. P. Piekorz, E. Hirsch, B. Nürnberg, and S. Beer-Hammer. 2016. p110 γ/δ Double-Deficiency Induces Eosinophilia and IgE Production but Protects from OVA-Induced Airway Inflammation. *PLoS One* 11: e0159310.
21. Bucher, K., F. Schmitt, B. Mothes, C. Blumendeller, D. Schäll, R. Piekorz, E. Hirsch, B. Nürnberg, and S. Beer-Hammer. 2017. Deficiency of PI3-Kinase catalytic isoforms p110 γ and p110 δ in mice enhances the IL-17/G-CSF axis and induces neutrophilia. *Cell Commun Signal* 15: 28.
22. Suire, S., J. Coadwell, G. J. Ferguson, K. Davidson, P. Hawkins, and L. Stephens. 2005. p84, a new Gbetagamma-activated regulatory subunit of the type IB phosphoinositide 3-kinase p110 γ . *Curr Biol* 15: 566-570.
23. Bohnacker, T., R. Marone, E. Collmann, R. Calvez, E. Hirsch, and M. P. Wymann. 2009. PI3K γ adaptor subunits define coupling to degranulation and cell motility by distinct PtdIns(3,4,5)P₃ pools in mast cells. *Sci Signal* 2: ra27.
24. Shymanets, A., Prajwal, K. Bucher, S. Beer-Hammer, C. Harteneck, and B. Nürnberg. 2013. p87 and p101 subunits are distinct regulators determining class IB phosphoinositide 3-kinase (PI3K) specificity. *J Biol Chem* 288: 31059-31068.
25. Deladeriere, A., L. Gambardella, D. Pan, K. E. Anderson, P. T. Hawkins, and L. R. Stephens. 2015. The regulatory subunits of PI3K γ control distinct neutrophil responses. *Sci. Signal.* 8:
26. Rynkiewicz, N. K., K. E. Anderson, S. Suire, D. M. Collins, E. Karanasios, O. Vadas, R. Williams, D. Oxley, J. Clark, L. R. Stephens, and P. T. Hawkins. 2020. G $\beta\gamma$ is a direct regulator of endogenous p101/p110 γ and p84/p110 γ PI3K γ complexes in mouse neutrophils. *Sci Signal* 13:
27. Kurig, B., A. Shymanets, T. Bohnacker, Prajwal, C. Brock, M. R. Ahmadian, M. Schaefer, A. Gohla, C. Harteneck, M. P. Wymann, E. Jeanclos, and B. Nürnberg. 2009. Ras is an indispensable coregulator of the class IB phosphoinositide 3-kinase p87/p110 γ . *Proc Natl Acad Sci U S A* 106: 20312-20317.
28. Jin, J. R., E. Gogvadze, A. R. Xavier, T. Bohnacker, J. Voelzmann, and M. P. Wymann. 2020. PI3K γ Regulatory Protein p84 Determines Mast Cell Sensitivity to Ras Inhibition—Moving Towards Cell Specific PI3K Targeting? *Front Immunol* 11: 585070.
29. Okkenhaug, K., A. Bilancio, G. Farjot, H. Priddle, S. Sancho, E. Peskett, W. Pearce, S. E. Meek, A. Salpekar, M. D. Waterfield, A. J. Smith, and B. Vanhaesebroeck. 2002. Impaired B and T cell antigen receptor signaling in p110 δ PI 3-kinase mutant mice. *Science* 297: 1031-1034.

Project 3. Targeting of PI3K γ Adaptor p101 Deteriorates Th2 Inflammation

30. Janas, M. L., G. Varano, K. Gudmundsson, M. Noda, T. Nagasawa, and M. Turner. 2010. Thymic development beyond beta-selection requires phosphatidylinositol 3-kinase activation by CXCR4. *J Exp Med* 207: 247-261.
31. Omori, S. A., M. H. Cato, A. Anzelon-Mills, K. D. Puri, M. Shapiro-Shelef, K. Calame, and R. C. Rickert. 2006. Regulation of class-switch recombination and plasma cell differentiation by phosphatidylinositol 3-kinase signaling. *Immunity* 25: 545-557.
32. Leberman, D. A., and R. L. Coffman. 1988. Interleukin 4 causes isotype switching to IgE in T cell-stimulated clonal B cell cultures. *J Exp Med* 168: 853-862.
33. Milner, J., J. Ward, A. Keane-Myers, B. Min, and W. E. Paul. 2007. Repertoire-dependent immunopathology. *J Autoimmun* 29: 257-261.

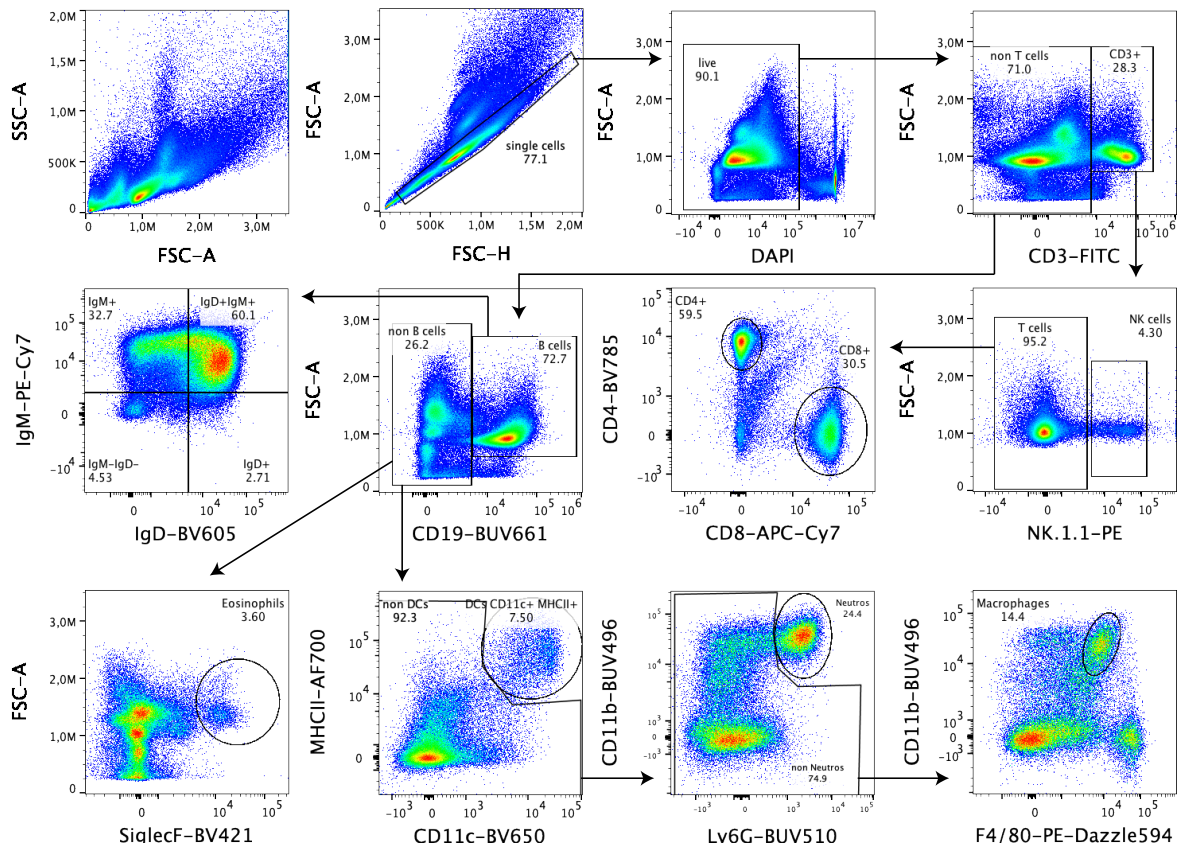
Supplementary information

Supplementary Figure S1. Mouse hematograms



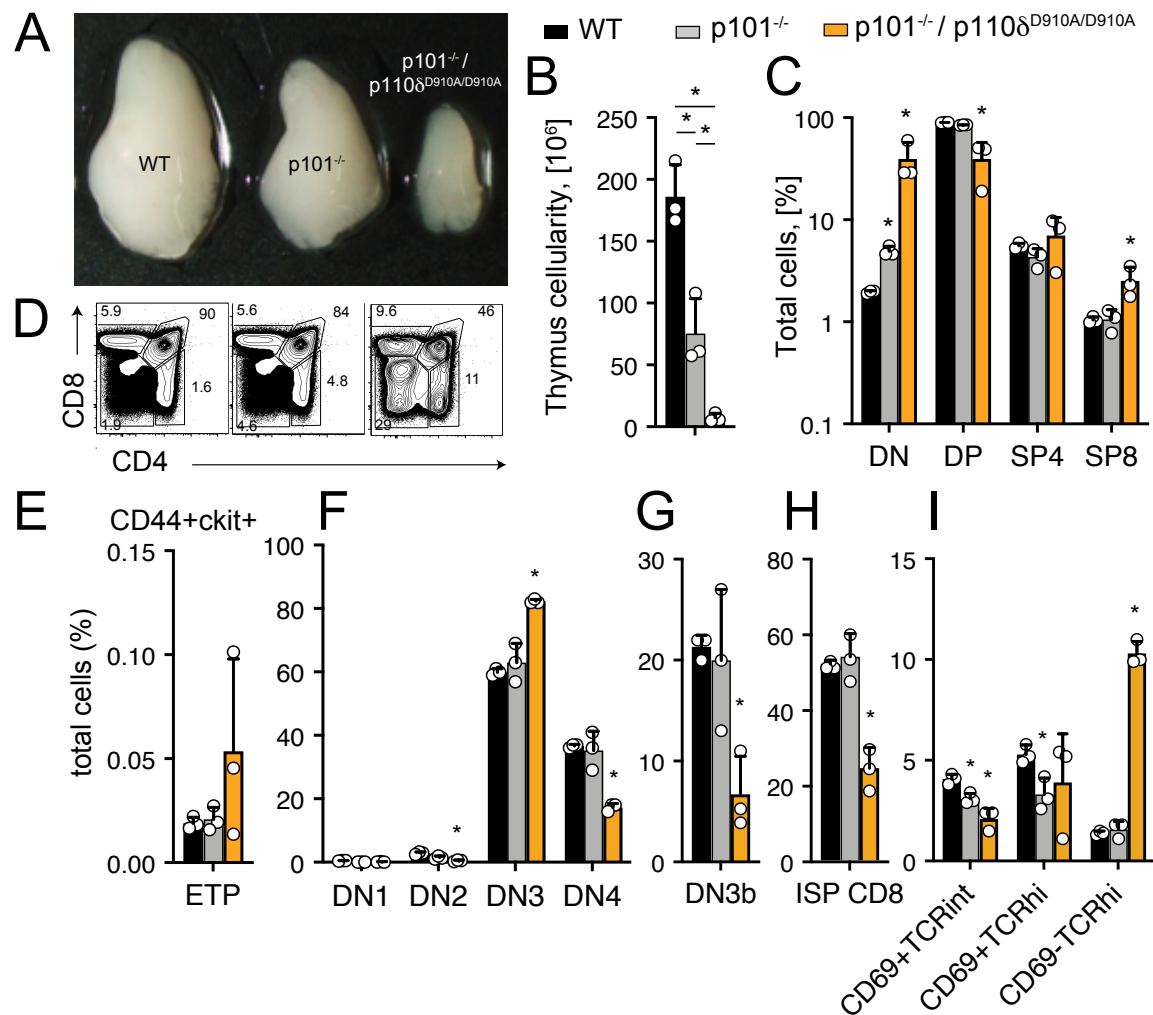
Supplementary Figure S1. Hematograms and WBC count from 8-12 week old mice. (A) Representative scatter dot plots containing lymphocytes & basophilic granulocytes (dark blue), neutrophilic granulocytes (pink), monocytes (green), eosinophilic granulocytes (yellow) and platelets (black). % of eosinophils is the mean value of 6-10 animals from each genotype. **(B)** Representation of absolute white blood cell (WBC) numbers and subtypes. Results come from the same data set as in Figure 1, but utilizing mean values of 6-10 animals per genotype.

Supplementary Figure S2. Splenocyte gating strategy



Supplementary Figure S2. Flow cytometry gating strategy used to characterize spleen lymphocytes. Dead cells were excluded by gating out DAPI stained cells. CD3 expressing cells were further subdivided into NK1.1 expressing natural killer cells and NK1.1 negative T cells. The latter population was subsequently checked for CD4 and CD8 marker. The CD3- population was further gated for CD19 expression to identify B cells, which also carry surface IgM and/or IgD. From the CD3- CD19- gate, SiglecF+ cells were defined as eosinophilic granulocytes, while CD11c+ MHCII+ cells qualified as dendritic cells. Starting from the CD11c- MHCII- cells neutrophilic cells were identified based on CD11b and Ly6G expression. Ly6G- CD11b+ F4/80+ cells were considered macrophages.

Supplementary Figure S3. p101 is involved in thymus growth but additional p110 δ inactivation is required to block DN3 to DN4 transition



Supplementary Figure S3. The role of p101 in thymocyte development and maturation.

(A). Hypomorph thymi from 3 week old p101^{-/-} and p101^{-/-}/p110^{ΔD910A/D910A} littermates compared to age-matched WT animals. (B) Enumeration of thymus cellularity from n=3 mice from each genotype. (C) CD4/CD8 double negative (DN) and double positive (DP) progenitors as well as mature single positive (SP) cells are plotted as % of total thymocytes. (D) Representative FACS plots of CD4 versus CD8 gating. (E) CD4⁻ CD8⁻ DN population contain early T cell progenitors (ETP) or DN1 cells which are defined as CD44⁺ckit⁺CD25⁻. (F) Additional acquisition of CD25 qualify for DN2 stage while reduction of CD44 and ckit mark the transition to DN3. To progress to DN4 stage cells will produce the TCR β -chain and loose CD25 expression (CD25⁻TCR⁺). (G) DN3b comprises a subpopulation with

Project 3. Targeting of PI3K γ Adaptor p101 Deteriorates Th2 Inflammation

CD25⁺CD28⁺ cells. **(H)** Immature single positive (ISP) CD8⁺ are a fraction of SP CD8⁺ cells with low or absent TCR expression (CD8⁺CD4⁻TCR^{lo/-}). **(I)** Cell expressing intermediate and high levels of TCR were further characterized based on CD69 lectin-receptor status. Thymi from n=3 mice per genotype were analyzed. p101^{-/-} and p101^{-/-}/p110 δ ^{D910A/D910A} animals came from the same litter while we used age and sex-matched WT controls. Results are represented as mean \pm SD and * indicates p<0.05 in students t-test.

5. Discussion and concluding remarks

Since the discovery of the second PI3K γ adaptor protein p84, the field has been wondering and speculating about the relevance of having two PI3K γ complexes. In light of the large potential of PI3K γ inhibitors in inflammatory and malignant diseases, more precise understanding of how its enzymatic activity and related signaling pathways are controlled are of obvious medical interest. Mast cells are in the unique situation to exclusively possess the p84/p110 γ dimer and therefore provide an ideal environment to study regulation of p84-dependent cell functions and test pharmacological targeting strategies. Effectiveness of FTIs to halt mast cell degranulation, cytokine expression and migration are routed in the disruption of the Ras/p84/p110 γ complex. FTIs prevent post-translational farnesylation of Ras which is required for proper anchoring in the plasma membrane. Without the farnesyl moiety Ras is not correctly localized to engage with activated G $\beta\gamma$ subunit and stabilize p84/p110 γ . Although we were able to demonstrate effective mast cell inhibition with Ras inhibitors while preserving p101-mediated macrophage activity, these drugs suffer from pleotropic effects that render them unsuitable for clinical use as anti-allergic treatments. We hope that our work originates future development of novel compounds that can achieve selective disruption of p84/p110 γ or p101/p110 γ dimer for cell-type specific PI3K γ manipulation.

The importance of the p101/p110 γ signaling complex in lymphocyte and particularly thymocyte development opposed to the relative restriction of p84/p110 γ dimer in the myeloid lineage becomes more emphasized on the background of autoimmunity-prone p110 δ ^{D910A} mutation. The divergent phenotypes of p101^{-/-} / p110 δ ^{D910A/D910A} and p84^{-/-} / p110 δ ^{D910A/D910A} mice regarding gut inflammation, lymphopenia, immunoglobulin isotype skewing and cytokine secretion strengthen the evidence for non-redundant immune-regulatory roles of p101

and p84. Although using a rather artificial system of autoimmunity, our observations again propose that manipulation of p84 is less at risk to deeply distort the delicate balance of pro- and anti-inflammatory PI3K signaling.

The significance of PI3K γ in obesity and metabolic syndrome is additionally complicated by the fact that beside immunological processes, also metabolic parameters are directly regulated by PI3K γ . By nature, metabolic syndrome affects nearly every cell type in the organism and immense cross-talk between adipose, liver, muscle and immune cells funnel into a vicious cycle driving disease progression. PI3K γ in leukocytes acts as an important molecular switch on inflammation, but in non-hematopoietic compartments, it has supplementary roles in regulation of body mass and energy consumption. Both aspects collectively contribute to progression of insulin resistance. Our investigations propose that p84/p110 γ supervises lipolytic activity in adipose tissue while p101 secondarily influences glucose metabolism via immune-mediated effects.

Figure 3. Proposed positioning of p84 and p101 in metabolic disease progression

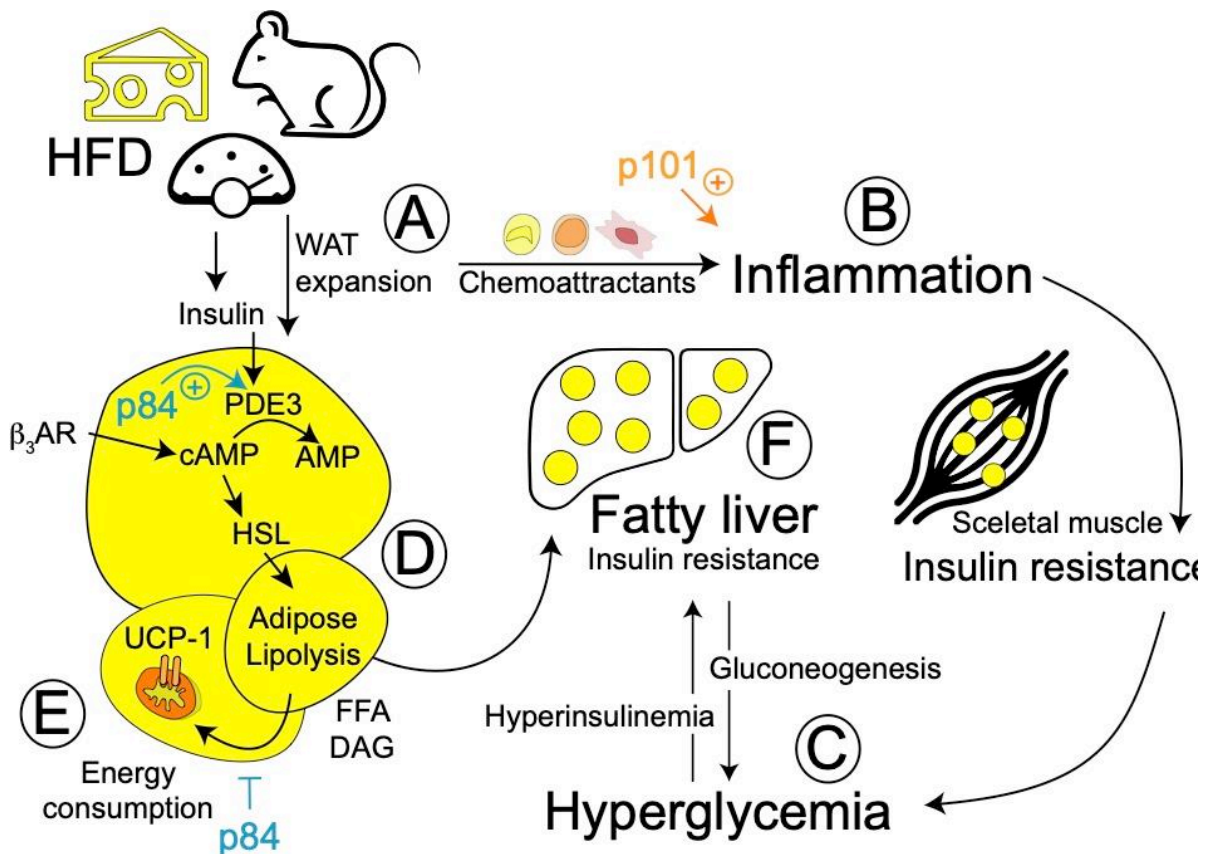


Figure 3. Proposed functions of p84 and p101 in metabolic syndrome and NAFLD. (A) High fat and high caloric diet leads to expansion of WAT and obese body weight. (B) Adipocytes secrete chemoattractants to recruit inflammatory cells to the WAT. p101 contributes to chronic low-grade inflammation by integrating chemokine signaling in WAT leukocytes. (C) Activation of WAT macrophages and other immune cells affect skeletal muscle and insulin resistance and subsequently systemic glycemia. (D) In insulin sensitive WAT, cAMP levels are regulated by PDEs to brake lipolysis and favor lipid storage. In the catabolic state, catecholamines stimulate β_3 AR and increase cAMP-dependent activation of HSL and lipolysis. p84 supports PDE3-mediated cAMP depletion. When adipocytes become insulin resistant and the inhibitory effect of insulin is relieved, stored TAG are hydrolysed into FFA and DAG. (E) p84 has a negative effect on UCP-1 expression in WAT, thus hindering that excess FFA can be consumed by thermogenesis. (F) FFA and DAG are redirected to the liver and fuel lipogenesis in hepatocytes. Systemic hyperinsulinemia additionally stimulates liver lipogenesis, while gluconeogenesis in the fatty liver further aggravates fasting glucose.

The immense efforts put in PI3K inhibitor development in the last decades has just begun to yield effective anti-cancer treatment options for clinical use. Future perspectives in the field will strive for the diversification to immune-pathologies, as some efforts in this direction have already emerged. Especially for chronic conditions that require long-term treatment, drug safety and adversity profiles are of crucial interest, and the experiences made with pan- and isoform selective PI3K inhibitors in the field of oncology are acknowledged as valuable lessons learned. Murine disease models are an important element in the investigation of PI3K targeting in the immune system, since tissue and cell-type crosstalk are insufficiently recapitulated in cell culture models. Transgenic mice lacking p84 and p101 are of great value to dissect the importance of the two distinct PI3K γ complexes and their non-redundant roles in healthy immunity as well as allergic, metabolic and auto-immune disease. Although active compounds that specifically disrupt p84/p110 γ or p101/p110 γ activity remain to be identified or invented yet, continuous progress in this direction will prospectively bear fruit in form of precise pharmacological solutions to fine-tune PI3K γ action in inflammatory and obesity-related disorders.

7. Appendix

7.1. Protocols

BMDM stimulation with GPCR agonists

Materials

- BMDM at day 7 of culture
- GPCR agonist, e.g. C5a, C3a, RANTES, MIP-1a, MCP-1
- Starvation medium = RPMI + 1% FCS + 2mM Gln + 100µg/ml Penicillin/Streptomycin
- 5x sample buffer (2.5 ml 1.25M Tris-HCl pH 6.8, 1g SDS, 2.5 ml beta-mercaptoethanol, 5.8ml 87% glycerol, 5mg Bromophenol blue)
- Styrofoam box, ice, timer, thermoblock

Procedure

- 1) Collect BMDM on day 7 by pipetting up and down several times to detach cells
- 2) Spin down at 900rpm (127xg) and resuspend in starvation medium
- 3) Adjust concentration to 1×10^6 cell/ml
- 4) Plate 1ml cell suspension in 24-well dish
- 5) Starve 2-4h in the incubator (37°C, 5% CO₂)
- 6) Pre-warm styrofoam box in (non-sterile) incubator
- 7) In the meantime: dilute GPCR agonists in starvation medium and warm to 37°C on thermoblock
- 8) Dilute 5x Sample buffer with water to 2x
- 9) After starvation period, check under the microscope if cells are attached
- 10) Place 24-well plate in pre-warmed Styrofoam box
- 11) Aspirate medium and immediately add GPCR agonist diluted in starvation medium
- 12) Stimulate for 2min (*start timer*)
- 13) After 2min, place plate on ice and remove medium by aspiration
- 14) Add 2x Sample buffer to each well
- 15) Collect lysate (*hard to pipette, cutting the tips with scissors helps*) into 1.5ml tubes

16) Boil at 96°C for 7min

17) Spin down, store lysate at -20°C

RNA extraction from WAT

Adapted from Invitrogen user guide for TRIzol reagent

Materials

- TRIzol reagent (Invitrogen, 15596026)
- Chloroform (Scharlau CL2031000)
- Isopropanol (Scharlau AL03211000)
- Ethanol (Scharlau ET00110500), 75%
- RNase-free water
- *Optional: RNase-free glycogen (Invitrogen 10814010)*

Procedure

- 1) Weight between 50-100mg of frozen WAT tissue and place in 2ml screw up tube containing beads (e.g. 1 mm glass beads)
- 2) Add 1ml TRIzol reagent
- 3) Shake in tissue disrupter FastPrep 24 (3rd flood “Medienküche”) at 6m/s for 60s
- 4) Repeat 2 times with 2 minute rests on ice inbetween
- 5) Check if tissue is dissolved properly, otherwise repeat shaking until no visible tissue chunks are left
- 6) Centrifuge lysate for 10 minutes at 12'000xg at 4°
- 7) Transfer the clear supernatant to a new tube (approx. 500µl)
- 8) Incubate 5 minutes to allow complete dissociation of the nucleoprotein complex
- 9) Add TRIzol up to 1ml
- 10) Add 200µl Chloroform and vortex to mix
- 11) Incubate for 3 minutes
- 12) Centrifuge for 15 minutes at 12'000xg at 4°
- 13) You should see a lower red phenol-chloroform phase, an interphase and a clear colorless upper aqueous phase
- 14) Transfer upper phase containing RNA to fresh tube
- 15) *Optional for small starting samples (<10 mg tissue): add 5-10 µg glycerol*
- 16) Add 500µl Isopropanol and incubate for 10 minutes at 4°C

- 17) Incubate for 10 minutes at 4°
- 18) Centrifuge for 10 minutes at 4°
- 19) RNA should precipitate and form a pellet at the bottom of the tube
- 20) Discard the supernatant
- 21) Resuspend pellet in 1ml 75 % Ethanol
- 22) Vortex and centrifuge at 7'500xg at 4° for 5 minutes
- 23) Discard the supernatant and let pellet air dry for 5-10 minutes
- 24) Resuspend in 20µl RNase-free water
- 25) Dissolve at 55°C on Thermoblock for 5-10 minutes
- 26) Measure concentration on Nanodrop
- 27) Proceed with RT-PCR

WAT lysis for Western blot analysis

Materials

- WAT lysis buffer: 20mM Tris-HCl pH=8,5% glycerol, 138 glycerol, 2.7 mM KCl, 1% NP-40, 5mM EDTA cOmplete Protease inhibitor cocktail (Roche 11697498001)
- PhosSTOP Phosphatase inhibitor cocktail (Roche 4906845001)
- 1 mm glass beads for tissue disruption (Sigma Z273619)
- 2ml screw up tubes (Starstedt Ref. 72.693)
- 5x sample buffer (2.5 ml 1.25M Tris-HCl pH 6.8, 1g SDS, 2.5 ml beta-mercaptoethanol, 5.8ml 87% glycerol, 5mg Bromophenol blue); dilute 1:5 with ddH₂O before use
- BCA protein assay (Pierce Cat#23225)
- BSA standard (e.g. from Pierce, Cat #23209, concentration 2mg/ml)
- Non-binding 96-well plate (Greiner BioOne 650901)

Procedure

WAT collection and snap freezing

- 1) euthanize mouse with CO₂ (4l/min)
- 2) open abdominal cavity to remove intra-abdominal fat pad:
 - *epididymal fat pad = largest visceral WAT*
 - *in obese mice the peri-renal fat pad (behind kidney) can be collected as well*

- *if the animal is obese I make 2 aliquots for each fat pad*
- 3) collect separate samples from subcutaneous fat (I only take inguinal fat)
- 4) snap freeze WAT aliquots in 2ml screw up tubes in liquid nitrogen
- 5) can be stored at 80°C from here or be lysed immediately

WAT lysis

1. Pre-cool centrifuge to 4°C
 2. Lyse approx. 100µg WAT in 600ul RIPA buffer supplemented with protease and phosphatase inhibitors. Combine in a 2ml screw up tube containing glass beads.
 3. Disrupt the tissue in lysis buffer and glass beads on Fast Prep 24 (located on 3rd floor, medium kitchen) at 6m/s for 60 seconds.
 4. Let sit on ice for 10 minutes
 5. Spin at 16'000 x g at 4°C for 10 minutes
 6. Collect supernatant under fat cake and transfer to fresh 1.5ml tube
 7. *Optional: repeat centrifugation to achieve more complete lipid removal*
 8. Proceed with BCA assay according to manufacturer's protocol to determine protein concentration
 9. Adjust concentrations of the remaining lysate for Western blot analysis and add sample buffer (SB)
 10. Boil at 96°C for 7 minutes shaking
- 6) denatured lysate with SB can be stored at -20°C until loading on
- A) SDS-PAGE: load 10-30 µg total protein per lane
 - B) WES Simple Western plate: dilute sample to 0.4µg/µl in WES 0.1x Sample buffer (provided in the kit) and add fluorescent marker as described in the kit instructions
- 7) keep remaining lysate and freeze at -80°C until further use

WAT digest and adipocyte isolation

Materials

- euthanized mouse of desired genotype
- histology equipment: tweezers, scissors, scalpel, 70% EtOH
- DMEM (serum free) + Penicillin/Streptomycin 0.1kU μ g/ml
- DMEM complete
 - DMEM (Sigma D6421)
 - 2mM L-glutamine
 - 10% FCS (Amimed)
 - Penicillin/Streptomycin 0.1kU μ g/ml
- Krebs-Ringer Hepes pH 7.4
 - store 10x stock at -20°C: 14.6 g NaCl, 0.7 g KCl, 0.12 g NaH₂PO₄, 0.58 g MgSO₄, 0.764 g CaCl₂, 11.9 g Hepes in a final volume of 200 mL water
 - supplement 100mL 1x buffer with 0.0168 g NaHCO₃ + 0.099 g glucose + 1 g BSA
- Collagenase D (Roche 11088866001)
 - stock is 100mg/mL in PBS (freezer R)
 - prepare dilution of 2mg/mL in Krebs-Ringer Hepes + 1% BSA
- Optional: Cell strainer (BD Falcon Cat #352350, 70 μ m)

Procedure

- 1) remove white adipose tissue from euthanized mouse
 - collect intraperitoneal fat: epididymal fat pad, visceral/mesenterial; perirenal
- 2) put in DMEM (serum free) on ice
- 3) mince and digest with Collagenase 2mg/mL
- 4) ratio of tissue to Collagenase solution 1:1
 - a) option 1: in 15mL Falcon tube in 37°C water bath
 - b) option 2: in 1.5mL Eppendorf tube on Thermoblock at 37°C
- 5) digest for 30min at 37, with gentle shaking every 5min

- 6) oil drops in the solution indicate cell death, digestion should be stopped before this happens
- 7) optional: filter through 70um mesh (adipocyte diameter ~30-50um, but overnutrition can result in much larger cells)
- 8) rinse filter with additional 15mL of DMEMc
- 9) if no filtration step is applied, add 15mL of DMEMc to stop digestion
- 10) centrifuge at 100g (500rpm) for 5min
- 11) shake vigorously for 5min to completely liberate stromal cells from the adipocyte fraction
- 12) centrifuge again at 100g (500rpm) for 5min
- 13) discard oil drops (top) if necessary
- 14) keep mature adipocyte fraction (white ring in top layer)
- 15) gently collect with 1mL pipette and transfer to 1.5mL tube
- 16) bottom fraction is stromal fraction

Adipocyte stimulation in vitro

Materials

- DMEM complete (10% FCS, PEST 0.1kU μ g/ml, L-Gln 2mM)
- Forskolin (Adenylyl Cyclase activator)
- Mirabegron (β 3-selective adrenaline receptor agonist)
- Salbutamol (β 2-selective adrenaline receptor agonist)
- cOmplete Protease inhibitor cocktail (Roche 11697498001)
- PhosSTOP Phosphatase inhibitor cocktail (Roche 4906845001)
- RIPA buffer: 50mM Tris HCl, PH 7.4, 150mM NaCl, 1% Triton X-100 (or NP-40), 0.5% Sodium deoxycholate, 0.1% SDS, 1mM EDTA (0.5M stock)
- BCA protein assay (Pierce Cat#23225)
- BSA standard (e.g. from Pierce, Cat #23209, concentration 2mg/ml)
- Non-binding 96-well plate (Greiner BioOne 650901)

Procedure

- 1) use approx. 30 μ g adipocytes per condition
- 2) distribute packed cells to 1.5ml tubes on ice
- 3) stimulate for 20min at 37°C with gentle shaking:
- 4) prepare stimulation in DMEMc and prewarm to 37°C
- 5) use 0.5mL per condition
- 6) add medium + stimulant to 1.5ml tubes with packed cells
- 7) vortex briefly and place on thermoblock preheated to 37°C
- 8) after 20min place short spin (5s, short button)
- 9) place tubes on ice and remove medium with a 25G syringe
- 10) lyse cells immediately
- 11) cell lysis: use RIPA + Protease inhibitory cocktail + Phosphatase inhibitors
- 12) dissolve tablet in distilled water to make 10x stock solution (Phosphatase inhibitors)
or 25x stock (Protease inhibitor)
- 13) mix with RIPA buffer before lysis
- 14) use 300 μ l lysis buffer per tube
- 15) vortex vigorously and place tubes on ice for 30min
- 16) precool centrifuge to 4°C
- 17) spin at max speed (16'000g) for 10min
- 18) collect clear fraction between pellet and solidified lipids and transfer to fresh tube
- 19) *Optional: repeat centrifugation step: spin at max speed (16'000g) for 10min*
- 20) Transfer 300 μ l to fresh tube
- 21) take 2x 10 μ l lysate for BCA protein quantification (duplicates)
- 22) to the remaining 240 μ l add 60 μ l 5x SB and boil at 96°C for 7min

Glucose tolerance test (GTT) & insulin tolerance test (ITT)

Materials

- Glucose 40% (sterilized, 1ml aliquots stored at -20°C)
- Human recombinant Insulin (Actrapid, Novo Nordisk, gift from Daniel Zemann/Donath Diabetes Group), stock at 100 IU/ml, dilute in PBS
- Scalpel for tail vein incision (Cutfix B.Braun Nr.11)
- Heparinized Capillary Tubes (Fisherbrand Cat. # 11719435)
- Glucose measurement strips (Abbott Freestyle Lite)
- Glucometer (Abbott Freestyle Freedom Lite)

Procedure

GTT on day 1

- 1) At t = -6 h: weight all animals, register toe clipping code numbers and transfer animals to clean new cage without food; with water available at libitum. Animal caretakers can perform this step in the morning (usually 7 am).
- 2) Using the determined body mass (step 1), calculate glucose or insulin amount to be injected
 - a) GTT: Glucose: 1 g/kg body weight
 - b) ITT: Insulin 1 IU/kg body weight for HFD animals
 - c) Insulin 0.75 IU/kg body weight for Chow diet animals
- 3) Prepare dilutions of glucose and insulin in PBS. Planned injection volume is 10 μ l/g body weight for i.p. injections. Max. injection volume is 20 μ l/g.
- 4) 4) At t = -1 h: draw first blood sample to determine baseline serum glucose. Place mouse in tube restrainer. Clean tail with Henryschein cosmetic alcohol swabs (or similar) to sterilize skin. Use one of the two methods to collect tail blood samples:
- 5) A small tail vein incision ca. 0.5 – 1 cm from the base of the tail will be made.
- 6) For the "base" bleed, glucose will be measured as described in 5), and 22 μ l of blood will be collected for an insulin determination to monitor the effect of obesity in

various genotypes. Collect 22 μ l blood with heparinized glass capillary, transfer to 1 mL Eppendorf tube and spin at 900xg (3100 rpm) for 10 minutes. Collect plasma and transfer to fresh tube; store at -80°C until analysis.

- 7) Collect $\sim 1\mu\text{L}$ blood with glucose strip and measure immediately on Glucometer (Abbot FreeStyle or similar). Measure twice. If values differ >2 mM, measure a third time and ignore the outlier.
- 8) Release mouse from restrainer, ensure that blood flow has stopped and put back to cage (where possible: perform follow-up bleeds without restrainer).
- 9) At $t = 0\text{h}$: For i.p. injection sterilize skin with cosmetic alcohol swap. Inject glucose or insulin bolus using 27G needle. Injection volume is $10 \mu\text{l/g}$ (max. $20 \mu\text{l/g}$) using solutions prepared in step 2.
- 10) At time points 30, 60, 90 and 120 min post injection blood samples from the tail are collected for glucose measurement: Gently remove the scar tissue (scab) from the tail using a soft tissue (Kleenex). Use cosmetic alcohol swabs to sterilize skin. Collect $\sim 1\mu\text{L}$ blood and measure as described in step 5).
- 11) supply cages with food (as before tolerance tests), put mice to rest until ITT test on the next day.

ITT on day 2

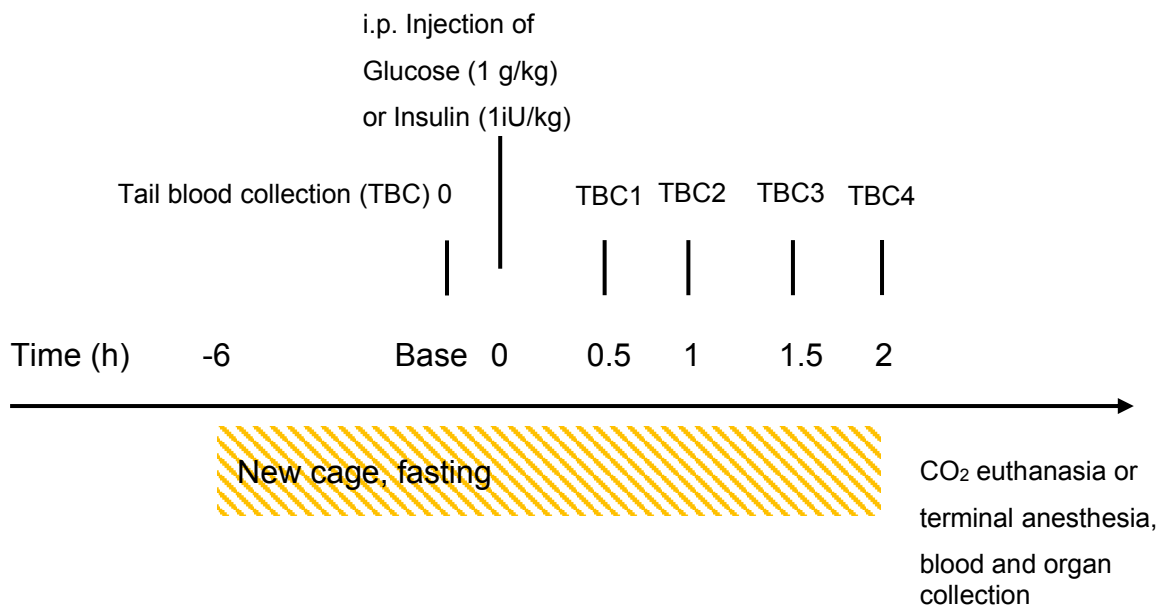
- 12) Perform ITT starting with step 1.
- 13) Supply mice with food and put them to rest until the next day

Organ collection on day 3

- 14) Terminate experiment by euthanasia (CO_2 , 4 Lt/min). Collect blood by heart puncture. Transfer $5\mu\text{l}$ of full blood to fresh tube for Hb1a analysis (see separate protocol).
- 15) Let remaining blood clot at room temperature

- 16) Spin at 900xg (3100rpm) for 10 minutes; aliquot serum in 2 Eppendorf tubes and store at 80°C until analysis
- 17) Perform peritoneal lavage to collect peritoneal (immune) cells for FACS analysis (see separate HbA1c measurement protocol)
- 18) Collect organs (adipose tissue, liver, etc.) for histology and molecular analysis
- 19) Weight all collected organs
- 20) fix one lobe of epididymal and one lobe of subcutaneous WAT in 10% PFA; proceed according to WAT paraffin embedding protocol
- 21) fix one lobe of liver in 4% PFA and preserve one lobe in O.C.T for frozen sections (see liver embedding protocol)
- 22) snap freeze aliquots of 50-100mg WAT and liver for RNA and protein extraction in liquid nitrogen; store at -80°C

Flow Scheme Glucose and Insulin Tolerance Tests (GTT, ITT)



Protocol for serum glucose determination following glucose or insulin challenge

WAT paraffin embedding

Materials

- 10 % Paraformaldehyde (PFA, Sigma 158127)
- 70% Ethanol
- Tissue Loc Cassettes (ThermoScientific 58955)
- Paraffin Type 6 (ThermoScientific 8336)
- Reusable plastic casting molds for paraffin blocks

Protocol

1) Place one piece of WAT (100-500mg) in 15ml Falcon tube with 5ml 10% PFA

For bigger WAT lobes (HFD fed mice) one may switch to 50ml tubes and 10ml PFA)

2) Incubate on rotator at 4°C for 72 hours

3) Discard PFA and add 5-8ml of 70% Ethanol

4) Incubate 48 hours at 4°C on rotator

5) Transfer tissues to labeled cassettes

6) Wash cassettes with tissue inside 3 times 30 minutes with PBS

7) Transfer to embedding machine, apply program 1 (settings below)

8) The following day, prepare paraffin blocks on Microm EC350-1

9) Let blocks solidify on cooling plate; store at room temperature afterwards

Liver paraffin and O.C.T embedding

Materials

- O.C.T. Compound (Tissue-Tek, Sakura Finetek Ref 4583)
- Plastic embedding mold (Polysciences 18646A, 18646B)
- 100% Ethanol and dry ice in Styrofoam box to cool blocks
- Roti© -Histofix 4%, pH 7 (Roth P087.1)
- Tissue Loc Cassettes (ThermoScientific 58955)
- Paraffin Type 6 (ThermoScientific 8336)
- Reusable plastic casting molds for paraffin blocks

Protocol

- 1) Prepare Styrofoam box with dry ice and a thin layer (<1cm) of 100% ethanol
- 2) Separate liver lobes: biggest for Paraffin; second biggest for fresh frozen in O.C.T;
rest for snap freezing in liquid nitrogen
- 3) Apply a drop of O.C.T compound to labeled plastic mold
- 4) Place second biggest lobe in the plastic mold; make sure no bubbles are at the interface between organ and O.C.T compound
- 5) Cover organ with O.C.T and place mold in ethanol cooled with dry ice
- 6) Let solidify until O.C.T turns from transparent to opaque and white; store at -80°C
- 7) Place biggest liver lobe in 4% PFA (Histofix) for 5 days, rotating at 4°C
- 8) After 5 days, discard PFA and transfer liver to labeled cassettes
- 9) Wash cassettes with tissue inside 3 times 30 minutes with PBS
- 10) Transfer to embedding machine, apply program 1 (settings below)
- 11) The following day, prepare paraffin blocks
- 12) Let blocks solidify on cooling plate; store at room temperature afterwards

Tissue embedding with paraffin

Program 1 of Tissue processor Tissue-Tek VIP5Jr

Step	Reagent	time	Temperature	P/V	mix
1	50% Ethanol	45 minutes	Room temperature	on	slow
2	70% Ethanol	45 minutes	Room temperature	on	slow
3	80% Ethanol	45 minutes	Room temperature	on	slow
4	95% Ethanol	45 minutes	Room temperature	on	slow
5	100% Ethanol	60 minutes	Room temperature	on	slow
6	100% Ethanol	60 minutes	Room temperature	on	slow
7	100% Ethanol	60 minutes	40°C	on	slow

8	Xylene	60 minutes	40°C	on	slow
9	Xylene	60 minutes	45°C	on	slow
10	Xylene	60 minutes	45°C	on	slow
11	Paraffin	45 minutes	60°C	off	slow
12	Paraffin	60 minutes	60°C	on	slow
13	Paraffin	60 minutes	60°C	on	slow
14	Paraffin	120 minutes	60°C	on	slow

Oil Red O staining

Materials

- Oil Red O (ORO) stock solution, 0.5% in Isopropanol (Sigma O1391)
- Isopropanol 60%
- ddH₂O
- O.C.T. mounting medium (Medita 81-0771-00)
- Coverslips (Menzel-Gläser #1, 24x60 mm)
- OCT sections on microscope slides (Important: use Superfrost PLUS Menzel-Slides, Art.No J1800AMNZ; appropriate section thickness 8-12µm for liver; sections can be fresh or stored at -80° for up to 3 years)

Procedure

- 1) Prepare ORO working solution: mix 18ml of ORO stock solution with 12ml ddH₂O, let sit at 4° for 5-10 minutes , filter and use within 6 hours
- 2) If freshly cut sections are stained, let dry at room temperature for minimum 15 minutes to ensure proper adhesion to the microscope slide
- 3) If frozen sections are used, let equilibrate at room temperature for 10 minutes
- 4) Let slides sit in 60% Isopropanol for 5 minutes
- 5) Incubate in ORO working solution for 10 minutes
- 6) Dip in 60% isopropanol for 3 seconds
- 7) Dip in ddH₂O for 3 seconds
- 8) mount with O.C.T. mounting medium and coverslip

Toluidine blue staining

Protocol from Ana Xavier

Materials

- Paraffin embedded tissue sections (4µm) on glas slides, ready to stain
- Toluidine blue O (Sigma 198161), 0.5% working solution in 0.5N HCl
- HistoClear
- Ethanol, 100, 90, 80, 70 and 30% working solutions
- Xylene
- 0.5N HCl
- MonoQ H₂O
- Cytoseal XYL mounting medium (Microm 8312-4)
- Coverslips (Menzel-Gläser #1, 24x60 mm)

Procedure

Incubate slides in

- 1) HistoClear 1 hour or overnight
- 2) HistoClear 20 minutes
- 3) 100% Ethanol 5 minutes
- 4) 100% Ethanol 5 minutes
- 5) 90% Ethanol 2 minutes
- 6) 80% Ethanol 2 minutes
- 7) 70% Ethanol 2 minutes
- 8) 30% Ethanol 2 minutes
- 9) MonoQ H₂O 5 minutes
- 10) 0.5% Toluidine blue 30 seconds
- 11) 0.5N HCl 1 minute
- 12) MonoQ H₂O 10 minutes (change once)
- 13) 30% Ethanol 30 seconds
- 14) 70% Ethanol 30 seconds
- 15) 80% Ethanol 30 seconds
- 16) 90% 30% Ethanol
- 17) 100% Ethanol 30 seconds
- 18) 100% Ethanol 30 seconds
- 19) Xylene 20 minutes
- 20) Xylene 20 minutes
- 21) Let dry under the hood
- 22) Put 3 drops of Cytoseal XYL on each slide and mount the coverslip

Quantitative image analysis

Quantification of nuclei and lipid vacuoles from H&E stained liver sections

Software: Fiji (Version 2.1.0/1.53c), StarDist 2D plugin

Procedure

- 1) Acquire microscopy images of H&E stained liver sections. I used 10x magnification overview images for nucleus and vacuole quantification.
- 2) Save as .lif files
- 3) To train StarDist 2D we utilized 192x192 pixel sized image crops from representative areas of the tissues
- 4) Those annotated image crops are stored in:
CAMIS>teamfolder>Julie>Results>Obesity>Histology>HFD>H&E HFD liver>Julie_forDL
 - a. groundTruthLipids (54 crops with lipid vacuoles annotated)
 - b. groundTruthNuclei (50 crops with cell nucleus annotated)
- 5) StarDist 2D Models were generated separately for vacuole and nucleus detection
 - a. 20200917_Julie_RGB_jointly-2D-32-rays_lipid_model_nsm0-3_prob0-54
 - b. 20200904_Julie_RGB_jointly-2D_32-rays_Number2_model_nms0-3_prob0-455
- 6) To batch process images we generated a cell counting script for Fiji that analyzes all .lif files selected and returns number and area in a .csv file. The StarDist models and Fiji script can be found on:
CAMIS>teamfolder>Julie>Results>Obesity>Histology>FromLoic

Quantification of Oil Red O staining

- 1) Use 20x magnification when analyzing ORO stained liver sections
- 2) Open as 8 bit image: Image>Type>8 bit
- 3) Set threshold: Image>Adjust>Threshold
 - a. Test on several images to select optimal values to differentiate stained and unstained regions
- 4) Measure
 - a. Analyze>Set Measurements>check “Area”, “Integrated density”, “Limit to threshold” and “Display label”
 - b. Analyze>Measure
- 5) Batch processing: Process>Batch>Macro
 - a. Select input and output
 - b. Enter following code (with adjusted threshold settings):

```

run("8-bit");

//run("Threshold...");

//setThreshold(70, 225);

setOption("BlackBackground", false);

run("Convert to Mask");

run("Measure");

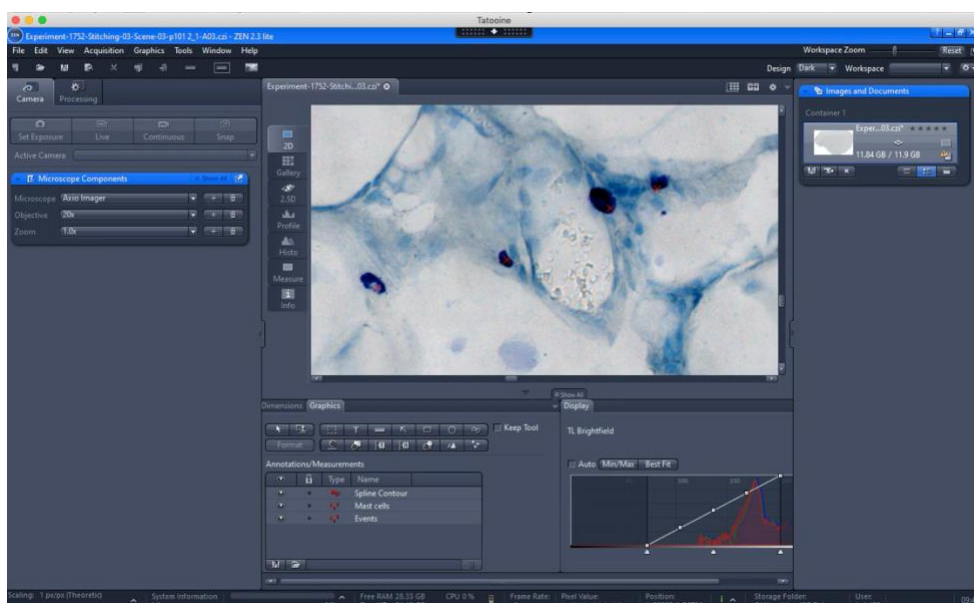
```

c) Press process

Quantification of Toluidine blue stained mast cells

Software: Zeiss ZEN 2.3 (blue edition)

- 1) Use slide scanner Zeiss Axio Imager Z2 Scanning microscope to acquire large tissue sections
- 2) Use stitched & fused images for quantification of mast cells
- 3) Open image in ZEN 2.3
- 4) Adjust brightness under *Display* until borders of the tissue become clearly visible
- 5) Select under *Graphics > Spline (Contour)*
- 6) Draw outline of the whole tissue area; μm^2 will be displayed
- 7) Select *Graphics > Points > Events*
- 8) Zoom into the image and mark dark blue granulated cells
- 9) When all cells are marked, click on *Select*
- 10) Number of events will be displayed
- 11) Note area and number of events in a excel sheet and calculate number of mast cells/ mm^2



FACS analysis of mouse splenocytes

Materials

- Mouse spleen
- RPMI
- PBS
- Nylon mesh 100 μ m, Sefar 3053-0201-100-00
- BD cell strainer 70 μ m
- Optional: Red blood cell lysis buffer (eBioscience 00-4333-57)
- FcBlock (CD16/CD32; Clone 2.4G2, BD Biosciences 553142), diluted 1:50 in PBS
- Antibody cocktail (see FACS antibody list)

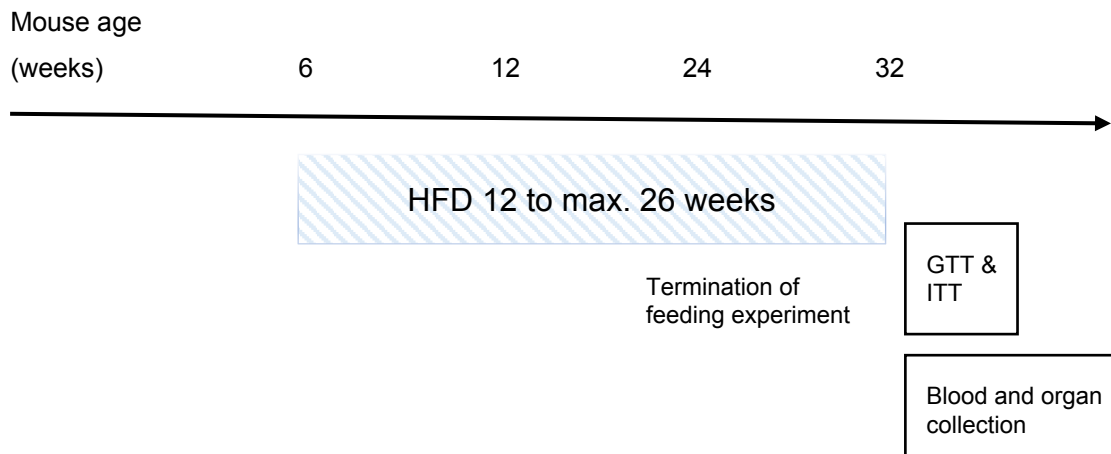
Procedure

- 1) Disrupt spleen with two tweezers
- 2) Smash between two layers of Nylon mesh using the rubber end of a syringe pestle
- 3) Rinse with RPMI and filter through 70 μ m cell strainer
- 4) Count cell number on Casy counter
- 5) Centrifuge for 5 minutes at 300 x g to collect cells
- 6) Optional: Decant and add 3ml RBC lysis buffer
- 7) Incubate for 3 minutes (longer lysis might damage leukocytes)
- 8) Add 12ml PBS and spin for 5 min at 300 x g
- 9) Decant and resuspend in fresh PBS
- 10) Collect 2-5x10⁶ cells per staining by centrifugation (300 x g, 3min)
- 11) Add 100 μ l FACS antibody mix in PBS
- 12) Incubate for 20 minutes in the dark on ice
- 13) Spin the cells for 1 minute at 900 x g and wash with 1mL PBS
- 14) Spin again, remove supernatant and resuspend in 250 μ L FACS buffer
- 15) Mix by pipetting and vortex before acquiring the sample on the Cytotflex

Table 1. FACS antibody mix for mouse peritoneal cells and splenocytes

	mAb	Fluorochrome	Cytoflex laser	Concentration/Dilution	Volume in 100 μ L
Lymphoid cells	CD3	FITC	B525 FITC	0.25 μ g (1:200)	0.5
	CD8	APC-Cy7	R763 APCA750	0.06 μ g (1:320)	0.32
	CD4	BV785	V763	0.12 μ g (1:160)	0.63
	Nk1.1	PE	Y585 PE	0.06 μ g (1:320)	0.32
	CD19	BUV661	UV675	0.12 μ g (1:160)	0.63
	IgD	BV605	V610	0.125 μ g (1:160)	0.63
	IgM	PE-Cy7	Y763-PC7	0.25 μ g (1:80)	1.25
Myeloid cells	F4/80	PE/Dazzle 594	Y610 mcherry	0.25 μ g (1:160)	1.25
	CD11c	BV650	V660	0.25 μ g (1:80)	1.25
	Siglec F (CD170)	BV421	V450 PB	0.13 μ g (1:160)	0.63
	Ly6G	BV510	V525-PB	0.25 μ g (1:80)	1.25
	CD11b	BUV395	UV405	0.12 μ g (1:160)	0.63
	MHC II (IA^b)	AF700	R712-APCA700	0.125 μ g (1:400)	0.25
	cKit (CD117)	APC	R660-APC	0.125 μ g (1:160)	0.63
	FcϵRI alpha	PerCP-Cy5.5	B690 PC5.5	0.125 μ g (1:160)	0.63
Live/Dead	DAPI	-	UV525	3 μ M (1:100)	1

Flow Scheme High Fat Diet (HFD)



Standard operating Procedure for high fat diet (HFD) feeding

- start HFD* with 6-week-old, healthy mice
- *for example, F3282 Mouse Diet, High Fat, calories >60% in fat, soft pellets; Bio-Serv, Frenchtown, NJ.
- Body weight is documented weekly

→ At end of HFD → GTT, ITT, euthanasia and organ & tissue collection

Table 2. Mouse food nutritional profile

	Chow	High Fat
Protein (%)	18.5 %	20.5 %
Fat (%)	4.5 %	36 %
Fiber (%)	4.5 %	0 %
Carbohydrates (%)	54 %	35.7 %
Water (%)	12 %	7.8%
Energy (kJ/g)	16.1 kJ/g	22.97 kJ/g

7.2. Antibodies

Table 2. Antibodies for Western blot

Mouse Anti-total-Akt	Cell Signaling, Cat# 2920S, clone 40D4
Rabbit Anti-Phospho-Akt Ser 473	Cell signaling, Cat# 4058, clone 193H12
Rabbit Anti-Phospho-Akt Thr308	Cell signaling, Cat# 4056, clone 244F9
Rabbit Anti-total MAPK	Sigma Aldrich, Cat# M7927, polyclonal
Mouse Anti-Phospho-MAPK p44p42	Sigma Aldrich, Cat# M8159, clone MAPK-YT
Rabbit Anti-HSL (total)	Cell Signaling, Cat# 4107, polyclonal
Rabbit Anti-HSL pSer660	Cell Signaling, Cat# 4126, polyclonal
Rabbit Anti-HSL pSer565	Cell Signaling, Cat# 4137, polyclonal
Rabbit Anti-HSL pSer563	Cell Signaling, Cat# 4139, polyclonal
Rabbit Anti-Perilipin 1	Cell Signaling, Cat# 9349, polyclonal
Mouse Anti-PI3Kgamma (Russian)	Alexis, clone H1
Rabbit Anti-p84 (Anti-p87)	Rabbit serum, epitope N-terminus of p84 (aa 1-162)
Rabbit Anti-p101	Cell Signaling Cat# 5569, clone D32A5
Mouse Anti-GAPDH	Sigma-Aldrich Cat# G8795, clone GAPDH-71.1
Mouse Anti-alpha Tubulin	Sigma-Aldrich Cat# T9026, clone DM1A
Mouse Anti-beta Actin	Sigma Aldrich, Cat# A5441, clone AC-15
Goat Anti-Rabbit IgG-Peroxidase	Sigma Aldrich, Cat# A6154, polyclonal
Goat Anti-Mouse IgG-Peroxidase	Sigma Aldrich, Cat# A4416, polyclonal

Table 3. Antibodies for FACS

Specificity	clone	Fluorochrome	Producer, Cat #
CD3	145-2C11	FITC	Biologend 100306
CD8	YTS156.7.7	APC-Cy7	Biologend 126620
CD4	GK1.5	BV785	Biologend 100453
Nk1.1	S17016D	PE	Biologend 156503
CD19	1D3	BUV661	BD 612971
IgD	11-26c.2a	BV605	Biologend 405727
IgM	RMM-1	PE-Cy7	Biologend 406514
F4/80	BM8	PE-Dazzle 594	Biologend 123146
F4/80	BM8	APC/Cy7	Biologend 123118
CD11b	M1/70	BUV395	BD 563553
CD11b	M1/70	PE	BD 553311
CD11b	M1/70	APC	BD 553312
CD11b	M1/70	FITC	Biologend 101206
CD11c	Clone N418	BV650	Biologend 117339
SiglecF (CD170)	S17007L	BV421	Biologend 155509
SiglecF (CD170)	S17007L	APC	Biologend 155507
Lys6G	1A8	BV510	Biologend 127633
Ly6C	HK1.4	PE-Cy7	Biologend 128217
MHC-II (IA ^b)	M5/114.15.2	AF700	Biologend 107622
c-Kit	2B8	APC	Biologend 105812
FceRI alpha	MAR-1	PerCP-Cy5.5	Biologend 134319
FceRI alpha	MAR-1	PE	eBioscience 12-5898-83
CD34	SA376A4	PE	Biologend 152203
Arginase 1	A1exF5	APC	ThermoFosher 17-3697-82

7.3. Primer for qPCR

Table 4: Primer for quantitative RT-PCR

gene	forward primer	reverse primer	primer #
Arg1	CTC CAA GCC AAA GTC CTT AGA G	AGG AGC TGT CAT TAG GGA CATC	Mm_Arg1_f #1534 Mm_Arg1_r #1535
IL-1b	GCA ACT GTT CCT GAA CTC AAC T	ATC TTT TGG GGT CCG TCA ACT	MmIL1beta_f#806 MmIL1beta_r#807
IL-1b	GCA ACT GTT CCT GAA CTC AAC T	TCT TTT GGG GTC CGT CAA CT	MmIL1beta_f#806 Mm_IL-1beta reverse#1627
IL-1RA	GTG TCC TGT TTA GCT CAC CCA	CCA GAT TCT GAA GGC TTG CAT C	Mm_IL1RA_f#1547 Mm_IL1RA_r#1548
IL-1RA	AAA TCT GCT GGG GAC CCT AC	TCT TCT AGT TTG ATA TTT GGT CCT TG	Mm_IL-1Ra_for_#1635 Mm_IL-1Ra_rev#1636
IL-4	CGA GGT CAC AGG AGA AGG GA	GCA CCT TGG AAG CCC TAC AG	MmIL4_f2 #1278 MmIL4_r#816
IL-5	GAA TCA AAC TGT CCG TGG GG	CCA CAC TTC TCT TTT TGG CGG	Mm_IL-5_for3#1586 Mm_IL-5_rev3#1587
IL-6	ACA ACC ACG GCC TTC CCT ACT T	CAC GAT TTC CCA GAG AAC ATG TG	MmIL6_f#818 MmIL6_r#819

IL-6	TCC TAC CCC AAT TTC CAA TGC TC	TTG GAT GGT CTT GGT CCT TAG CC	Mm_IL-6_for_#1632 Mm_IL-6_rev_#1633
IL-10	ACT TTA AGG GTT ACT TGG GTT GC	CCT GGG GCA TCA CTT CTA CC	Mm_IL10_f1549 Mm_IL10_r1550
IL-12b	TCG CAG CAA AGC AAG ATG TG	TGG AGA CAC CAG CAA AAC GA	Mm_IL12_f1545 Mm_IL12b_r1546
IL-13	ATG GCC TCT GTA ACC GCA AG	CCT CAT TAG AAG GGG CCG TG	Mm_IL-13_f#1536 Mm_IL-13_r#1537
IL-33	TGA GAC TCC GTT CTG GCC TC	CTC TTC ATG CTT GGT ACC CGA T	Mm_IL-33_for#1582 Mm_IL-33_rev#1583
MGL-1	TGA GAA AGG CTT TAA GAA CTG GG	GAC CAC CTG TAG TGA TGT GGG	Mm_MGL-1_f#1540 Mm_MGL-1_r#1541
MRC-2	TAC AGC TCC ACG CTA TGG ATT	CAC TCT CCC AGT TGA GGT ACT	Mm_MRC-2_f1_1543 Mm_MRC-2_r1_1544
MCP-1	CCC CAA GAA GGA ATG GGT CC	GGT TGT GGA AAA GGT AGT GG	MmMCP1_f#831 MmMCP1_r#832
TNF-a	ATC CGC GAC GTG GAA CTG	CGA AGT TCA GTA GAC AGA AGA	MmTNFalpha_f#837 MmTNFalpha_r2#839

TNF-a	CCC CAA AGG GAT GAG AAG TT	CTC CTC CAC TTG GTG GTT TG	Mm_TNFa_For#1628 Mm_TNFa_rev#1629
MIP-1a	TTT TGA AAC CAG CAG CCT TTG	TCT TTG GAG TCA GCG CAG ATC	MmMIP1alpha_f#833 MmMIP1alpha_r#834
MIP-1a	TTC TCT GTA CCA TGA CAC TCT GC	CGT GGA ATC TTC CGG CTG TAG	Mm_MIP1a(CCL3)_for#1630 Mm_MIP1a(CCL3)_rev#1631
H-PGDS	TAG GCA ATT ATG TAA CCT GGG C	ATC CAG GCA GAA ATG GCA GG	Mm_h-PGDS_for2_1561 Mm_h-PGDS_rev2_1562
COX-2	CCA CTT CAA GGG AGT CTG GA	AGT CAT CTG CTA CGG GAG GA	Mm_COX2_for2_1563 Mm_COX2_rev2_1564
p101	GAC ATC CTA CAG GAA GTC CTT CTC	TCA GCG CAA TGC CTG TCC AT	Mmp101-qP c3 #1345 Mmp101-qP r4#428
P101e3	GCT GTG TCT GAA CTG CTG GA	CAG GAG GAT GAG GAA GTG GC	Mm_p101_e3_f1555 Mm_p101_e3_r1556
P101	AAG CCC TGG GAA ACT CCA CA	GAG AAG GAC TTC CTG TAG GAT GTC	Mmp101-qP c2#426 Mmp101-qP r6 1346
p110g	CCC TGG TGA TCG AGA AAT GC	GTC TTG GCG CAG ATC ATC AC	MmPI3Kg-qP c2#434 MmPI3Kg-qP r6 #1340

p84	ATA GAG CAG GTG GCT AGC GA	CAG AAG GTC ACC GAC ACA GTG	Mmp87-qP c1#416 Mmp87-qP r6#1348
P84e4	AGA GCT CAA CAC CCC AAA CC	TCC TGG GTT TCT CTC CAC CT	Mm_p84_e3_f1565 Mm_p84_e4_r1566
P84e4	AGC TGG ACT TCC AGA GGA GT	GAG ACC ATC TCC ACA TGC CC	Mm_p84_e3_f1567 Mm_p84_e4_r1568
GAPDH	CTG CAC CAC CAA CTG CTT AG	CCA TCC ACA GTC TTC TGG GTG	GAPDHc#357 Mm_GAPDH_r2 #1281
18S	CCT GGA TAC CGC AGC TAG GA	GCG GCG CAA TAC GAA TGC CCC	18Sc359 18Sr#360
FceRI	TAG CAC TGC TGT TCA TGT CTC	GAG TTC ATT TGA AGG TGA TTG TT	MmFceRIa_f#840 MmFceRIa_r#841
F4/80	CTT TGG CTA TGG GCT TCC AGT C	GCA AGG AGG ACA GAG TTT ATC GTG	Mm_F4/80_for_1611 Mm_F4/80_rev_1612
UPC-1	CCT GCC TCT CTC GGA AAC AA	TCT GGG CTT GCA TTC TGA CC	Mm_UPC1_for1_1623 Mm_UPC1_rev1_1624
UPC-2	GGA AAA TCG AGG GGA TCG GG	GGA GTT CTG GAG GCT GCT TT	Mm_UPC2_for1_#1625 Mm_UPC2_rev1_#1626
Tph1	GAG TGG GTG AGT GGG ATA GC	GTT GAT CCC GTC CTT GCT GG	Mm_Tph1_for1_1621

			Mm_Tph1_rev1_1622
ELANE	GCG GAT CTT CGA GAA TGG CT	TTG GCG TTA ATG GTA GCG GA	Mm_ELANE_for1_1617 Mm_ELANE_rev1_1618
MPO	GCT GGA GAG TCG TGT TGG AA	GAG CAG GCA AAT CCA GTC CT	Mm_MPO_for2_1615 Mm_MPO_rev2_1616
KC/CXCL1	CCT ATC GCC AAT GAG CTG C	TCT TGA GTG TGG CTA TGA CTT CG	Mm_KC_f2_1279 MmKC_r3_1280
PPARg	CAA GAA TAC CAA AGT GCG ATC AA	GAG CTG GGT CTT TTC AGA ATA ATA AG	Mm_PPARg_for_#1637 Mm_PPARg_rev_#1638

7.4. Gene maps of transgenic mouse strains

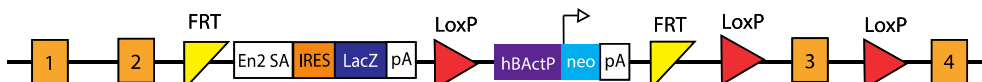
		Pyrat number and name
p84 targeted mouse lines		
Pik3R6 genomic locus		Line 1278 – P84-xF2L
full cassette		Line 1282 – P84-xF2L-R
↓ x FLP recombination		
after FLP		Line 1280 – P84-xFxL
↓ x Cre recombination		
after FLP & CRE		Line 1283 – P84-xFxL-R

p101 targeted mouse lines

Pik3R5
genomic locus

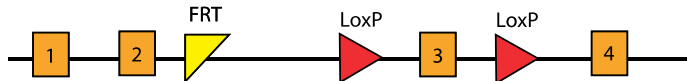


full cassette



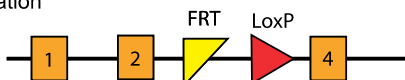
↓
x FLP recombination

after FLP



↓
x Cre recombination

after FLP & CRE



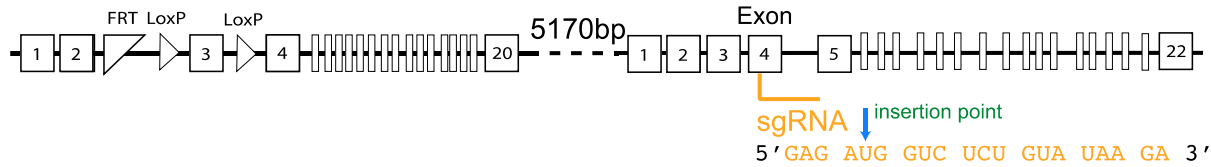
Line 1284 – P101-FLP-R

Line 1285 – P101-FLP-R-Cre

<p>MGI:2443588 p101; Pik3R5 Chr11:68'432'125 - 68'497'849 bp</p>	<p>MGI:2144613 p84; Pik3R6 Chr11:68'503'019 - 68'552'698 bp</p>	
<p>Exon</p> <p>5170bp</p> <p>FRT LoxP LoxP</p> <p>sgRNA 5' TTT GTA GGA TCT GTT CCA GG 3'</p>		
<p>WT CATCCTCCTGGAACAGATCCTACAAAAGACCCAAGAGGTGAGGGTGAAGCAGACACTGATGAGCAC 125bp deletion p101 D125 CATCCT-----</p> <p>WT AGATAGAATTGACATTGTAAAGGCAGGACTTAGGTCAGCTCTGTGGCTCCTGTCTGCTCTGCTCCT p101 D125 -----</p> <p>WT GCATGGAATGTCCTATCCTGTCTGTGTAACACACAGCGGGTCCCGTGTGGAC p101 D125 GCATGGAATGTCCTATCCTGTCTGTGTAACACACAGCGGGTCCCGTGTGGAC</p>	<p>Line 1572 - p101^{D125} /p84^{xF2L}</p>	<p>Line 1572 - p101^{ACA} /p84^{xF2L}</p> <p><i>Cave: p101 was still expressed in BMDM</i></p>
<p>WT CATCCTCCTG--GAACAGATCCTACAAAAGACCCAAGAG -- p101 ACA CATCCTCCTACAGAACAGATCCTACAAAAGACCCAAGAG</p>		

MGI:2443588
p101; Pik3R5
 Chr11:68'432'125 - 68'497'849 bp

MGI:2144613
p84; Pik3R6
 Chr11:68'503'019 - 68'552'698 bp



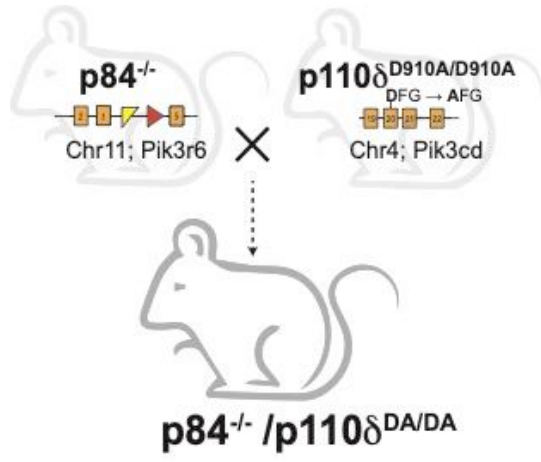
p84 WT ATGTG **GAGATGGTCTCTGCACAA** - GAAGGTG
 |||
p84 A ins ATGTG **GAGATGGTCTCTGCACAA** **A**GAAGGTG

Line 1571 - p101^{FLP}/p84^{Ains}

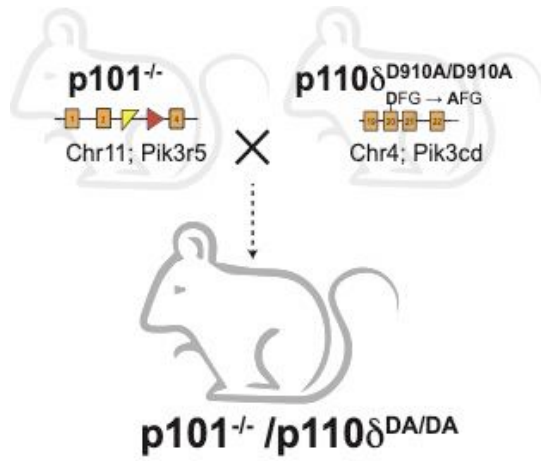
p84 WT ATGTG **GAGATGGTCTCTGCACAAGA** AGGTGGAGAGAAA
 |||
p84 D25 ATGTG **GAGA** ----- **D 25 ncl** ----- GAAA

Line 1571 - p101^{FLP}/p84^{D25}

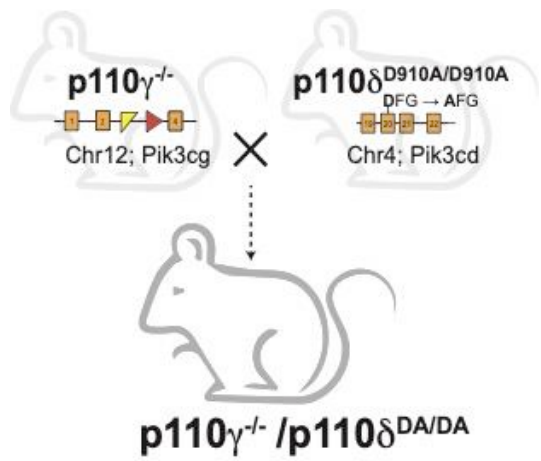
PI3K γ /PI3K δ double mutant mice



Line 1286 - p84^{-/-} / p110 δ ^{DA/DA}



Line 1287 - p101^{-/-} / p110 δ ^{DA/DA}



Line 1458 - p110 γ ^{-/-} / p110 δ ^{DA/DA}

7.3. Curriculum vitae

Julie Ruili Jin

Born Oct 6, 1990 in Ottignies-Louvain-La-Neuve, Belgium

Nationality: Chinese

Languages

German (native), English (fluent), French (fluent), Mandarin Chinese (native speaker, basic writing)



Education

- Since 2023 Resident physician in Internal Medicine, St. Claraspital Basel
- 2021 – 2023 Resident physician in Internal Medicine, Kantonsspital Aarau
- 2021 PhD degree (Dr. phil.), Faculty of Science, University of Basel
- 2020 MD degree (Dr. med) , Medical Faculty, University of Basel
- 2016-2019 Krebsliga Stipend, Project «Phosphoinositide 3-Kinase γ : Adaptor Subunit-Dependent Activation in Inflammation and Allergy», MD-PhD candidate at the Department of Biomedicine in Basel, Cancer- and Immunobiology (Prof. Wymann)
- 2010-2016 Medical degree (Staatsexamen) from University of Basel, Switzerland
- 2015 Practical year (Wahlstudienjahr):
- Internal medicine, Kantonsspital Aarau (3 months)
 - Anesthesiology, Inselspital Bern (1 month)
 - Internal medicine, Universitätsspital Basel (1 month)
 - Emergency department, Universitätsspital Zürich (1 month)
 - Heart surgery, Universitätsspital Zürich (1 month)
 - Anesthesiology, Luzerner Kantonsspital in Sursee (1 month)
- 2013-2014 Master Thesis in Medicine at the Department of Biomedicine in Basel, Immunonephrology (Prof. Schifferli)
- 2006-2009 Matura at Gymnasium Oberwil, BL, Switzerland, Major Biology and Chemistry

Publications

- Cumpelik, A., Gerossier, E., **Jin, J.**, Tsakiris, D., Dickenmann, M., Sadallah, S., Schifferli, J. A. and Zecher, D. (2015), Mechanism of Platelet Activation and Hypercoagulability by Antithymocyte Globulins (ATG). *American Journal of Transplantation*.
- **Julie R. Jin**, Elena Gogvadze, Ana R. Xavier, Thomas Bohnacker, Jan Völzmann, Matthias P. Wymann (2020), PI3K γ Regulatory Protein p84 Determines Mast Cell Sensitivity to Ras Inhibition – Moving towards Cell Specific PI3K Targeting? *Frontiers in Immunology*.

Grants & accomplishments

- Krebsliga full stipend for MD-PhD studies (2016-2019), *competitive* (11 grants)
- Karger Award 2016 (2nd price) for Master thesis («Anti-Thymozyten Globulin-medierte Mikrovesikelfreisetzung von Thrombozyten»)

Posters & Presentations

- Immunomeeting 2017, Basel: Seminar “ PI3K γ adaptor subunits regulate cellular outputs in inflammation and allergy”
- DBM PhD retreat 2018, Einsiedeln: Poster “ Blocking mast cell activation with Ras inhibitors – moving towards cell-specific PI3K γ targeting”
- DBM PhD retreat 2019, Schwarzenburg: Poster “Leukocyte Phosphoinositide 3-Kinase γ relies non-redundantly on regulatory proteins p101 and p84 to shape innate and adaptive immunity”
- Immunomeeting 2019, Basel: Seminar “Targeting allergy and Inflammation via PI3K complexes”
- Immuno PhD Club 2019, Basel: Seminar “PI3K signaling in inflammation”
- SMPA conference 2019, Geneva: Poster “The Role of Leukocyte Phosphoinositide 3-Kinase γ Shaping Innate and Adaptive Immunity”
- University of Luzern, Introduction to medicine lecture series 2019: Lecture “Basics of Immunology”
- Immunomeeting 2020, Basel: Seminar “Obese and inflamed: How PI3K γ drives adiposity and insulin resistance”
- Immuno PhD Club 2020, Basel: Seminar “PI3K γ regulation in obesity, glycemia and lipid metabolism”
- DBM monthly seminar 2021, Basel: Seminar “One kinase, many paths to obesity and metabolic derailment”

Teaching

- 2021 Tutor for 2nd year medical students in TSCR (topics digestion and metabolism), University of Basel
- 2019 Lecturer «Basics of Immunology» for master's program of Clinical Sciences at the University of Lucerne
- 2016-19 Assistant Biochemistry practical course of 1st year medical students, University of Basel

Experiences

- 2020 Immuno-PhD Book Club «Janeway's Immunobiology», DBM Basel
- 2019 Summer School EPFL «Shaping the Future of (Bio-)Medicine» in Bellinzona, Switzerland
- 2018 Volunteer for the Red Cross Basel-Land, German lessons and integration of refugee families in Switzerland (Program «Salute»)
- 2017 Organization committee Swiss and European MD-PhD conference in Basel (SMPA & EMPA joint meeting)
- 2017 Organized graduation ceremony (Staatsfeier) for medical graduates in Basel
- 2010-2016 Board member medical student association (FamBa)
- 2010 Mandarin Chinese Class at the Shanghai International Studies University, China (3 months)
- 2008 English Summer school at the University of Sheffield, UK (1 month)

8. Acknowledgements

I want to thank my supervisor and mentor Matthias Wymann for encouraging me to follow the science, think critically and strive for excellence. Thanks to my secondary advisors and PhD committee, Gennaro De Libero and Pius Lötscher for supporting my studies. I thank all my lab colleagues in the Wymann group for scientific inspirations, hands-on assistance at the bench and empathic after-work exchange. I learned a lot from you all and enjoyed the academic environment and personal connections during my PhD studies.

I appreciate all the fantastic infrastructure people of DBM Mattenstrasse. A PhD wouldn't be feasible without the support of animal caretakers, IT, microscopy and FACS core facility, histology etc.

Thanks to the Immuno-PhD Club and the Janeway Book Club that made the PhD process more communal and less lonely, especially during a pandemic.

I am grateful to my parents who taught me persistency and hard work but also encouraged my creative sides and supported me to follow my own ideas. You contributed endlessly to my accomplishments. Thanks to my brother who keeps animating, inspiring, challenging, and uplifting me.

Thanks to Jonas for never doubting my career and life choices, and devotedly and enthusiastically supporting my dreams. You always have my back. Thank you Benji for being the most joyful PhD companion.